AD/A-006 107

SHORT-PULSE SWITCHES FOR AIRBORNE HIGH-POWER SUPPLIES

Richard J. Thome

Magnetic Corporation of America

Prepared for:

Air Force Aero Propulsion Laboratory

January 1975

UNCLASSIFIED

SECURITY CLASSIFICATION OF THIS PAGE (When Data Entered)

REPORT DOCUMENTATION PAGE		READ INSTRUCTIONS BEFORE COMPLETING FORM
1. REPORT NUMBER AFAPL-TR-74-88	2. GOVT ACCESSION NO.	3. RECIPIENT'S CATALOG NUMBER AD/A-006107
4. TITLE (and Subtitle) SHORT PULSE SWITCHES FOR AIRBORNE HIGH POWER SUPPLIES		5. TYPE OF REPORT & PERIOD COVERED FINAL JUN 72 - JUN 74 6. PERFORMING ORG. REPORT NUMBER
7. AUTHOR(s) Richard J. Thome		8. CONTRACT OR GRANT NUMBER(s) F33615-72-C-2098
9. PERFORMING ORGANIZATION NAME AND ADDRESS Magnetic Corporation of America 179 Bear Hill Road Waltham, Massachusetts 02154		10. PROGRAM ELEMENT, PROJECT, TASK AREA & WORK UNIT NUMBERS Project #3145 (Aerospace Power); Task #314532 (Power Conditioning)
11. CONTROLLING OFFICE NAME AND ADDRESS Air Force Aero Propulsion Laboratory AFAPL/POD-1 Wright-Patterson Air Force Base, Ohio 45433		12. REPORT DATE January 1975 13. NUMBER OF PAGES 148
14. MONITORING AGENCY NAME & ADDRESS(if different from Controlling Office)		15. SECURITY CLASS. (of this report) Unclassified 15a. DECLASSIFICATION/DOWNGRADING SCHEDULE

16. DISTRIBUTION STATEMENT (of this Report)

Approved for public release; distribution unlimited.

17. DISTRIBUTION STATEMENT (of the abstract entered in Block 20, if different from Report)

18. SUPPLEMENTARY NOTES

19. KEY WORDS (Continue on reverse side if necessary and identify by block number)

High power switch
Rotary switch
High current density brush
Filamentary brush

20. ABSTRACT (Continue on reverse side if necessary and identify by block number)

Switching systems for use with pulsed inductive energy storage systems were investigated with the goal of designing for a peak current interrupt capability of 20,000 A at a repetition rate of 5 pps with a voltage following interruption of 100 kV. A charge time of 190 msec or more was desired with switch losses limited to 5,000 j/pulse for a total pulse train length of 300 pulses. Both linearly actuated and rotary devices were considered with means for incorporating an applied magnetic field and cryogenic (continued)

DD FORM 1 JAN 73 1473 EDITION OF 1 NOV 65 IS OBSOLETE

UNCLASSIFIED

SECURITY CLASSIFICATION OF THIS PAGE (When Data Entered)

Block 20.
cooling in the switch design. A design is given for a prototype linearly actuated switch for evaluation of the field and cooling effects and for a rotary switch based on high performance filamentary brushes designed for operation at 3,000 A/in^2. Test results were obtained in the program with filamentary brushes operating at this overall current density. Current densities in the filaments were as high as 9,000 A/in^2.

NOTICE

When Government drawings, specifications, or other data are used for any purpose other than in connection with a definitely related Government procurement operation, the United States Government thereby incurs no responsibility nor any obligation whatsoever; and the fact that the government may have formulated, furnished, or in any way supplied the said drawings, specifications, or other data, is not to be regarded by implication or otherwise as in any manner licensing the holder or any other person or corporation, or conveying any rights or permission to manufacture, use, or sell any patented invention that may in any way be related thereto.

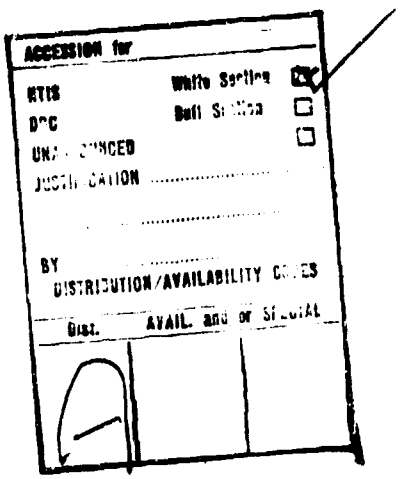

Copies of this report should not be returned unless return is required by security considerations, contractual obligations, or notice on a specific document.

FOREWORD

This report was prepared by Magnetic Corporation of America, 179 Bear Hill Road, Waltham, Massachusetts 02154, under the U.S. Air Force Contract No. F33615-72-C-2098, June 1, 1972. The contract was initiated under project number 3145 (Aerospace Power), task 314532 (Power Conditioning).

The work was administered under the direction of the Air Force Aero Propulsion Laboratory, Wright-Patterson Air Force Base, Ohio 45433. J. Turner (AFAPL/POD-1) served as Technical Monitor for this program and R. L. Verga as Technical Area Manager, Power Conditioning Branch of AFAPL/POD-1.

This report describes work performed during the period June, 1972 to February, 1975. The project engineer was R. J. Thome who was assisted in the theoretical and experimental phases of the program by J. V. Minervini and J. M. Tarrh. W. Mann, D. Sutton and M. Granfield made substantial contributions to report preparation. The report was submitted in draft form in September, 1974.

This technical report has been reviewed and is approved.

P. E. Stover
Chief, Power Distribution Branch

ABSTRACT

Switching systems for use with pulsed inductive energy storage systems were investigated with the goal of designing for a peak current interrupt capability of 20,000 A at a repetition rate of 5 pps with a voltage following interruption of 100 kV. A charge time of 190 msec or more was desired with switch losses limited to 5,000 j/pulse for a total pulse train length of 300 pulses. Both linearly actuated and rotary devices were considered with means for incorporating an applied magnetic field and cryogenic cooling in the switch design. A design is given for a prototype linearly actuated switch for evaluation of the field and cooling effects and for a rotary switch based on high performance filamentary brushes designed for operation at 3,000 A/in^2. Test results were obtained in the program with filamentary brushes operating at this overall current density. Current densities in the filaments were as high as 9,000 A/in^2.

TABLE OF CONTENTS

APPENDICES

LIST OF ILLUSTRATIONS

LIST OF TABLES

SECTION I.

INTRODUCTION

The main purpose of this program was to investigate possible switching arrangements for use with pulsed inductive energy storage systems. The design goals for the switch are outlined in the following table:

Table I.

Switch Design Goals

Peak current	2×10^4 A
Repetition rate	5 pps
Voltage after interruption	100 KV
Recovery time	$\leq$ 40 μ sec
Charge time	$\geq$ 190 msec
Pulse train length	300 pulses
Switch loss per pulse	$\leq$ 5000 J

During the program, means were considered for utilizing an applied magnetic field and cryogenic cooling in the switching process. This is justified since, in the pulsed system, the magnetic field is available because it is the means whereby the inductive element stores its energy and the cryogens are available, since it is likely that the energy storage coil system would be superconducting or cryogenically cooled copper or aluminum. The choice among the latter would be determined by mission requirements such as energy level and discharge time as well as repetition rate, charge time and pulse train length.

Section II presents overall system and switching concepts and begins with a description of inductive energy storage system operation including a typical switch support subsystem. The latter is an auxiliary circuit which helps open the switch by providing an artificial current zero in the switch and by controlling the rate of change of current in the vicinity of current zero.

Basic switch characteristics are discussed next and include the advantages of using a vacuum environment for the switch contacts and the potential advantages for cryogen and magnetic field usage. From a weight and volume standpoint, it is concluded that cryogens may be used to absorb switch losses and to reduce switch losses. In addition, they may be used to cryovacuum pump the switch to assure a hard vacuum. The magnetic field may be used to increase the effective arc resistance (and thus help to extinguish the arc) and to induce arc motion. The latter is shown to have a potentially large effect on contact life by reducing the maximum temperature of the contact surface.

Several switching alternates are then presented. These include:

1) linearly actuated switch with single contact pair

2) linearly actuated switch with multiple contact pairs in parallel

3) two-terminal rotary switch in parallel with linearly actuated arc interrupter

4) three-terminal rotary switch with arc chute.

Alternate 1) is an advanced vacuum interrupter using cryogenic cooling and an applied magnetic field. A prototype test unit of this type is discussed in Section III. The switch features: a) liquid nitrogen cooling of its stationary and moveable leads, b) cryovacuum pumping through provision for liquid nitrogen and liquid helium cooling of its vapor condensation shields, and c) removeable contacts to allow investigation of the magnetic field effects on arcs drawn between specially shaped electrodes. The requirements for a test circuit are then presented together with an outline of the necessary parameter variations to achieve a test to the full current, voltage and recovery time requirements of this program, in successive increments of higher current and voltage.

The second alternate listed above is also a linearly actuated device, but would utilize multiple pairs of contacts in parallel. Estimates indicate that this would be lighter and require less actuation power than a single contact pair device, however, techniques would have to be developed to reliably extinguish multiple parallel arcs simultaneously without restrike.

Alternates 3) and 4) both utilize rotary devices. This is the subject of Section IV., in which the dependence of rotary switch size on current density in a brush system is discussed. The ability of the brush system to withstand arcing is also indicated as a problem area requiring investigation. A rotary switch design is presented assuming that the arcing problem may be nullified and assuming brush current densities of about 3000 A/in.^{2}. The latter is very high relative to operational current densities for standard brushes, but was achieved in tests performed under this program with filamentary brushes.

The filamentary brush concept consists of using many fine metallic filaments in contact with a moving surface for the purpose of transferring current. Tests were performed using Niobium-Titanium alloy filaments heat sunk in a copper matrix. Overall brush current densities of 3000 A/in.^{2} were achieved with voltage drops of about 1 mV/A. Current densities in brush filaments attained 9300 A/in.^{2}. This is a significant development and further testing would be highly desirable to develop a better understanding of brush characteristics and to attempt to optimize material.

In Section V, a conceptual design for an integrated system is presented. In this system the main switch is mounted in the bore of an energy storage solenoid so as to use the magnetic field produced by the inductor. The switch is cryogenically cooled and shares a common vacuum with the dewar for the energy storage coil. The switch used is the multiple contact pair type assuming that the development problems associated with this switch may be nullified. However, the integrated switch-coil-dewar system is valid for any switch using an applied field and cryogenic cooling.

SECTION II.

OVERALL SYSTEM & SWITCHING CONCEPTS

The purpose of this section is to present some of the basic effects and characteristics to be incorporated in the switch designs given in Sections III., IV. and V. This section will begin with a description of energy storage system operation, including a switch support subsystem which aids in opening the main switching element. A discussion is then presented which concludes that the switch should be based on metallic contacts in a vacuum environment because of the high voltage requirement and low loss constraint in this program.

The possible utilization of cryogens in switch operation is discussed next and it is concluded that potential areas of application include: (1) absorption of switch losses, (2) reduction of switch losses and (3) cryovacuum pumping. Since it is likely that cryogens will be available in support of the energy storage element, it is natural to incorporate them into the switch design.

The utilization of an applied magnetic field in the switching process is discussed next because the field is generated by the energy storage element and may be made available to the switch in an integrated system design. It is concluded that it is feasible for the field to move an arc with significant speed and thus (1) reduce the maximum temperature experienced by the contacts and (2) create a "back emf" which appears as an increased arc resistance. In addition, the presence of a transverse field increases arc resistance even if motion is absent by impeding charged particle motion across field lines.

The section proceeds to a discussion of switch dissipation, constraints on actuation time and the use of multiple switches. It is concluded that the multiple switches in parallel carrying a total of 20,000 A offer the following advantages relative to a single switch:

allowable operating time: $\frac{\text{single switch}}{\text{multiple switches}} \sim 0.2$

average power required for actuation: $\frac{\text{single switch}}{\text{multiple switches}} \sim 100$

weight of actuating linkage: $\frac{\text{single switch}}{\text{multiple switches}} \sim 10$

weight of switch components: $\frac{\text{single switch}}{\text{multiple switches}} \sim 1$

The multiple switch arrangement offers a higher probability of achieving a low-weight, low-loss main switch, however, the problems associated with simultaneously extinguishing parallel arcing contacts must be solved.

The section closes with a discussion of alternates which may meet the inductive energy storage system switching function and a summary of advantages and disadvantages.

1. INDUCTIVE ENERGY STORAGE SYSTEM OPERATION

For the pulse repetition rates and energy levels of interest in this study, it is reasonable to assume that the system would utilize an energy storage element which is completely charged and discharged for each pulse. A simplified circuit diagram for such a system is shown in Figure 1. To initiate operation, the switch S is closed and, assuming a high impedance load, the energy storage inductor, L, is charged. When a pre-determined current through L is attained, the switch S is opened and the energy stored in L is discharged into the load. The purpose of the capacitor, C, is to limit the rate of voltage rise across the load when the switch opens and the purpose of the switch support subsystem is to help open the switch.

If the switch is mechanical in nature and involves mechanical separation of contacts in some form, an arc would be drawn as the contacts separated and the switch support subsystem would have to provide conditions which would help extinguish the arc before a substantial amount of energy were dissipated. For the arc to extinguish it is necessary for the rate of energy removal from the arc to exceed the rate at which the rest of the system can supply energy to the arc for a sufficient length of time. Since the rate of energy dissipated in the arc at any instant is the voltage drop across it times the current which it carries, a reasonable (though not necessarily sufficient) goal for the switch support subsystem is to provide an artificial net current zero in the switch. In addition, it is desirable for the rate of change of current at the time of the current zero to be as low as possible to maintain a "low power" condition as long as possible and for the rate of voltage rise after arc interruption to be as low as possible to allow maximum recovery of breakdown strength.

Figure 2 is a simplified circuit diagram of a system that can be used to produce a current zero in the main switching element S_1. Coil L_1 is the energy storage coil and P_1 is the main power supply for the system. Coil L_2 is a non-linear inductor that makes use of a saturable core. Its characteristics are such that it exhibits a high inductance when its core is in the unsaturated condition and a very low inductance when saturated. Capacitor C_2 is used to limit the rate of voltage rise across L_1 following the interruption of current through S_1.

The sequence of events that would occur in a normal charge-discharge cycle is as follows. With switch S_2 open, S_1 is closed causing current i_1 to flow in the circuit composed of P_1, L_1, L_2 and S_1. Very shortly after the closure of S_1, L_2 switches from its unsaturated to its saturated condition. The charge circuit is then effectively composed of P_1, L_1 and S_1. Once the desired level for the i_1 has been reached, the following sequences of events can take place to force a zero current condition in S_1 and allow it to revert to its open circuit condition.

First, assuming that capacitor C_1 had previously been charged to an appropriate level, and with switch S_1 still closed, switch S_2 could be closed. Capacitor C_1 and inductor L_1 would then form a resonant circuit in series with switches S_1 and S_2. Assuming C_1 had initially been charged

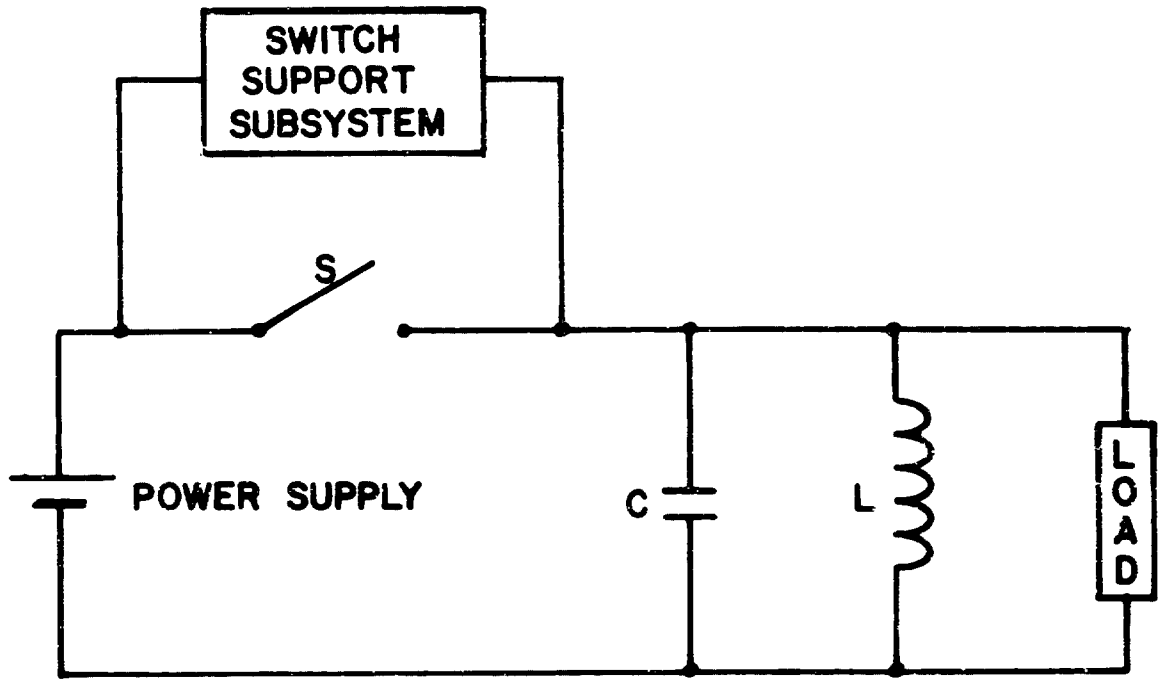

Figure 1. Typical inductive energy storage system in which the storage element is completely charged & discharged for each pulse delivered to the load.

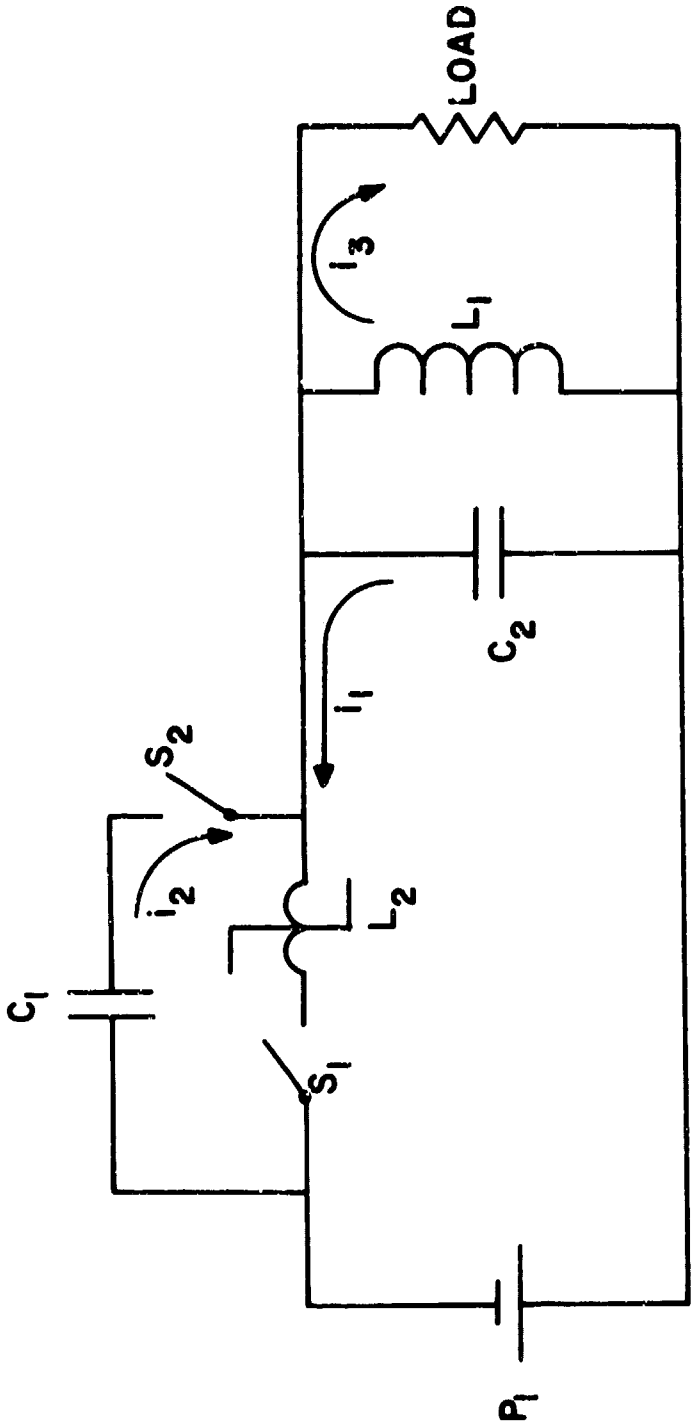

Figure 2. Illustration of an inductive energy storage system using a simple switch support subsystem to provide an artificial current zero in the switch S_1.

in a fashion to force a current in the direction of the arrow shown for i_2, the current in this series resonant circuit would initially be very high and change at a very rapid rate since the surge impedence of the resonant circuit and its frequency would be determined by the saturated inductance of L_2. As a consequence, C_1 would very rapidly charge with a voltage of a polarity opposite to its initial charge. Following this, it would again discharge through S_1, only this time i_2 would be flowing in a direction opposite to that of i_1. This would have the effect of reducing the net current through S_1. Just prior to the moment that this current reaches zero, inductor L_2 would come out of its saturated condition and assume its unsaturated high inductance value. This switch in inductance would drastically slow down the rate of change of current through S_1 just as it was about to reach zero. Assuming that S_1 could be opened at the instant this current reached zero, i_1 would then be divided into branches flowing into C_1, C_2 and the load. The rate of voltage rise across S_1 would then be determined by the frequency of the damped parallel resonant circuit composed of L_1, C_1, C_2 and the load. Assuming S_2 remained closed throughout the cycle, all of the energy in this circuit would eventually be delivered to the load.

As described above, an additional power supply would be necessary to charge C_1 for each operation of S_1. An alternate mode of operation would be to have switch S_2 open either part way up or at the peak of the discharge voltage wave. The advantage of this mode of operation would be the elimination of a separate power supply to charge C_1 except for the initial cycle of a pulse train.

If S_2 were opened part way up the voltage wave then C_1 could be a high capacitance, low voltage capacitor. This would have the effect of slowing down the rise time of the voltage wave immediately following the current zero through S_1 while minimizing the physical size of C_1. The disadvantage of this mode of operation is that S_2 must now open while it has a high current flowing through it. The losses entailed in this switching operation must then be added to those attributed to the losses through S_1 during the charge period and opening operation.

If S_2 were opened at the peak of the voltage wave, then (1) there will be no switching loss since S_2 will be carrying no current at this time; and (2) the capacitance of C_2 could be minimized, conceivably to zero, since the rise time of the voltage wave would be determined essentially by C_1.

Clearly this latter mode of operation will yield the lighter overall system weight provided switch S_1 can regain its dielectric strength fast enough.

The above discussion illustrated operation of the energy storage system and of a switch support subsystem which could produce an artificial current zero and exercise control over the rate of change of current at the time of current zero. The section which follows will discuss basic features to be incorporated into the design of the switch.

2. BASIC SWITCH CHARACTERISTICS

a. Vacuum vs. Gas

Figure 3 depicts a portion of a pulse train for a repetitively pulsed system. Assuming t_c, the time of charge, to be 190 milliseconds, t_p to be 200 milliseconds, and I_o to be 20,000 amperes, the rms current during a pulse train is a minimum of 11,250 amperes. If all of the switching losses occur only during the charging period, the maximum allowable closed resistance for the switch S_1 would be 208 microhms for a peak voltage drop of just in excess of four volts. Clearly this requirement eliminates all but metallic type contacts.

The selection of metallic type contacts requires that mechanical motion take place in opening and closing the switch. If the losses entailed in the switch during opening are to be kept to a minimum, it is mandatory that the switch very rapidly regain its open circuit dielectric strength. To accomplish this, the contacts should part as rapidly as possible in a medium that has a very high dielectric strength. Further, it is important that any arcing that takes place in the switch do so at a minimum in voltage drop and time duration.

Figure 4 is a plot of the breakdown voltage versus contact spacing for a set of contacts in air and in vacuum. Figures 5 and 6 are plots of arcing voltage versus current for copper contacts in vacuum. Figure 7 is a plot comparing the times required for contacts switched in vacuum and various gas media to regain their dielectric strength following a current break. As is evident from these curves, switching in a vacuum: requires a relatively small space to withstand voltages in excess of 100,000 volts; can be accomplished at relatively low arcing potentials out to approximately 8,000 amperes; results in a time delay from current zero to full open circuit dielectric strength which is short, relative to delays necessary in gaseous media. These comparisons indicate that a vacuum environment is desirable around the switch contacts.

b. Cryogen Utilization

This section will consider effects which are intimately connected with the use of cryogens in the switching system. This consideration is natural since the inductive energy storage element will most likely be cryogenically cooled, hence, cryogens will already be available in the system. Specifically, interest will center on effects which may be useful in specially designed vacuum interrupters, either linear or rotary.

Figure 8 is an illustration of a standard vacuum switch. It consists of a stationary and a movable contact encased in an evacuated container. As the contacts part, an arc is drawn across the gap. A current zero then occurs, either naturally in an AC application or artificially in a DC case, and the arc plasma deionizes and condenses on the vapor shield. The rate of change of current near current zero and the rate of voltage rise after the arc breaks must be slow enough to allow the deionization and condensation process to occur and prevent the arc from re-striking.

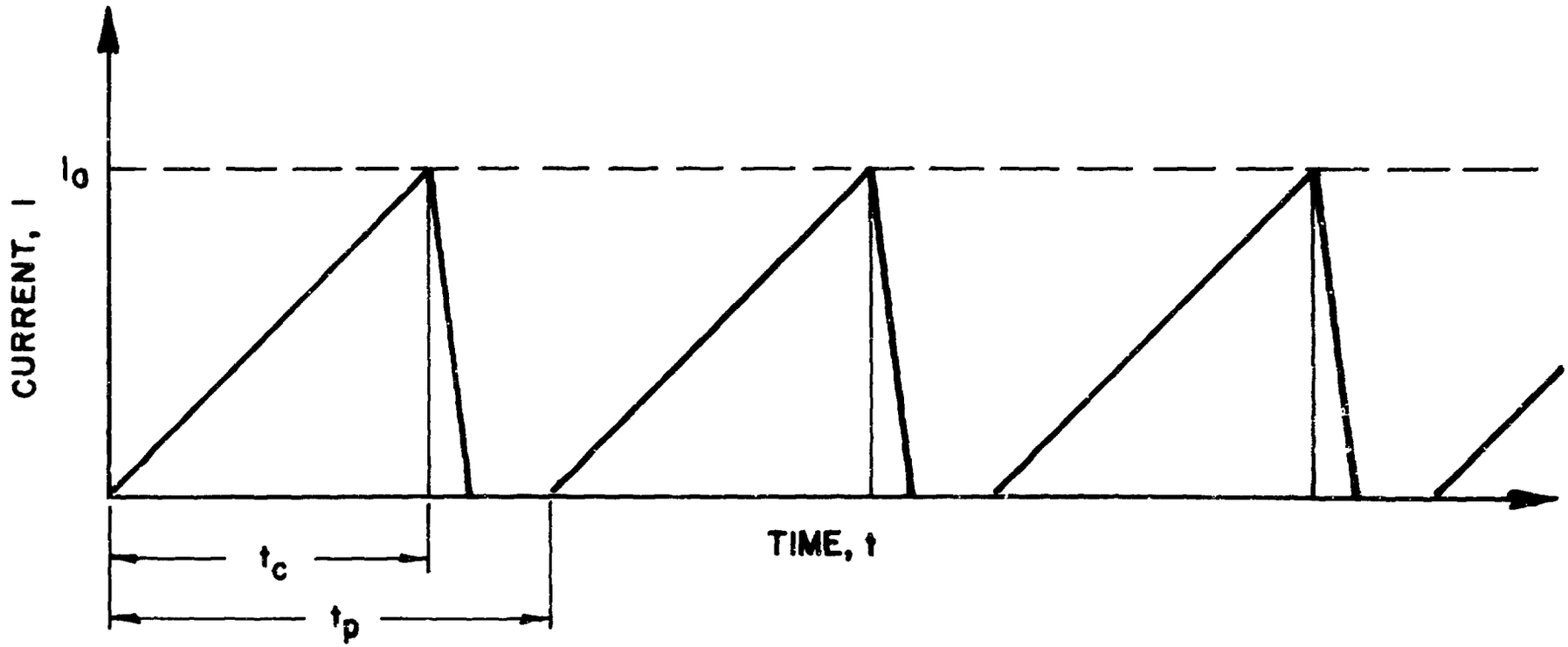

Figure 3. Pulse train illustrating current vs. time in energy storage circuit.

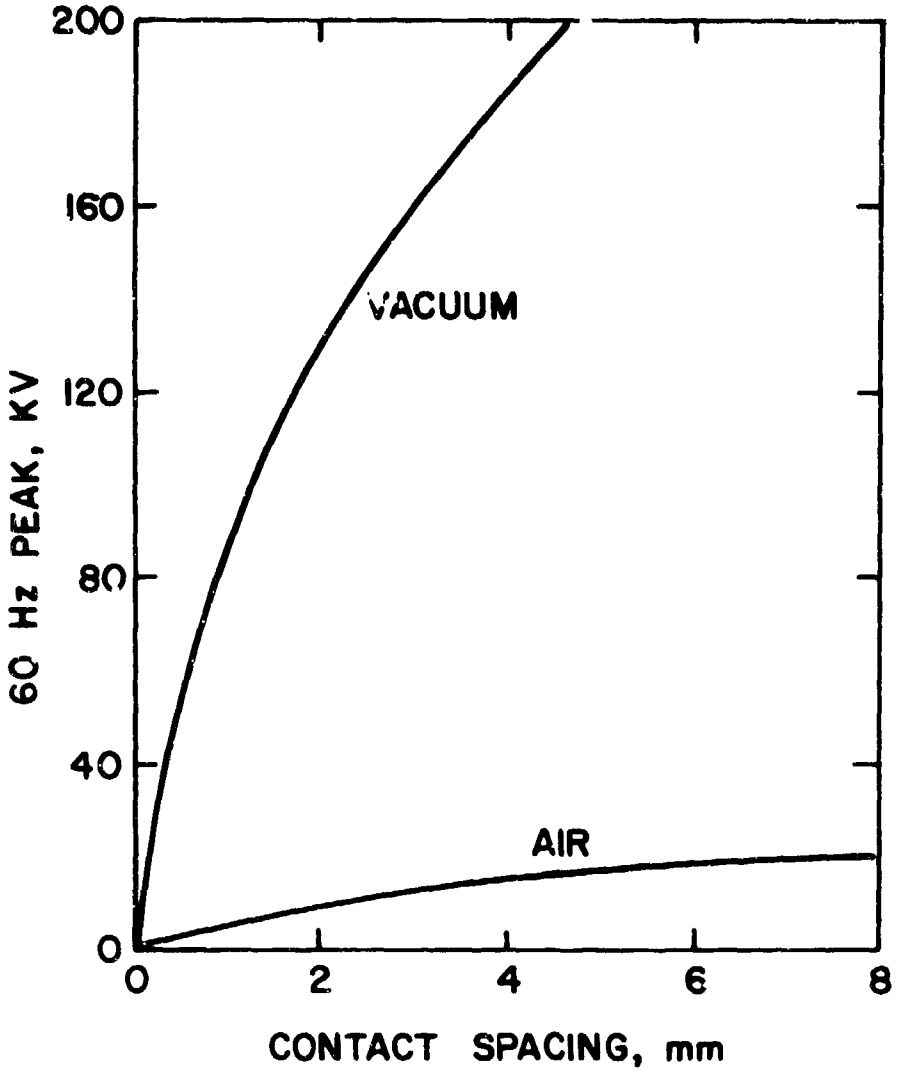

Figure 4. Breakdown voltage of vacuum and of air for one pair of 9.5-mm-diameter tungsten contacts.

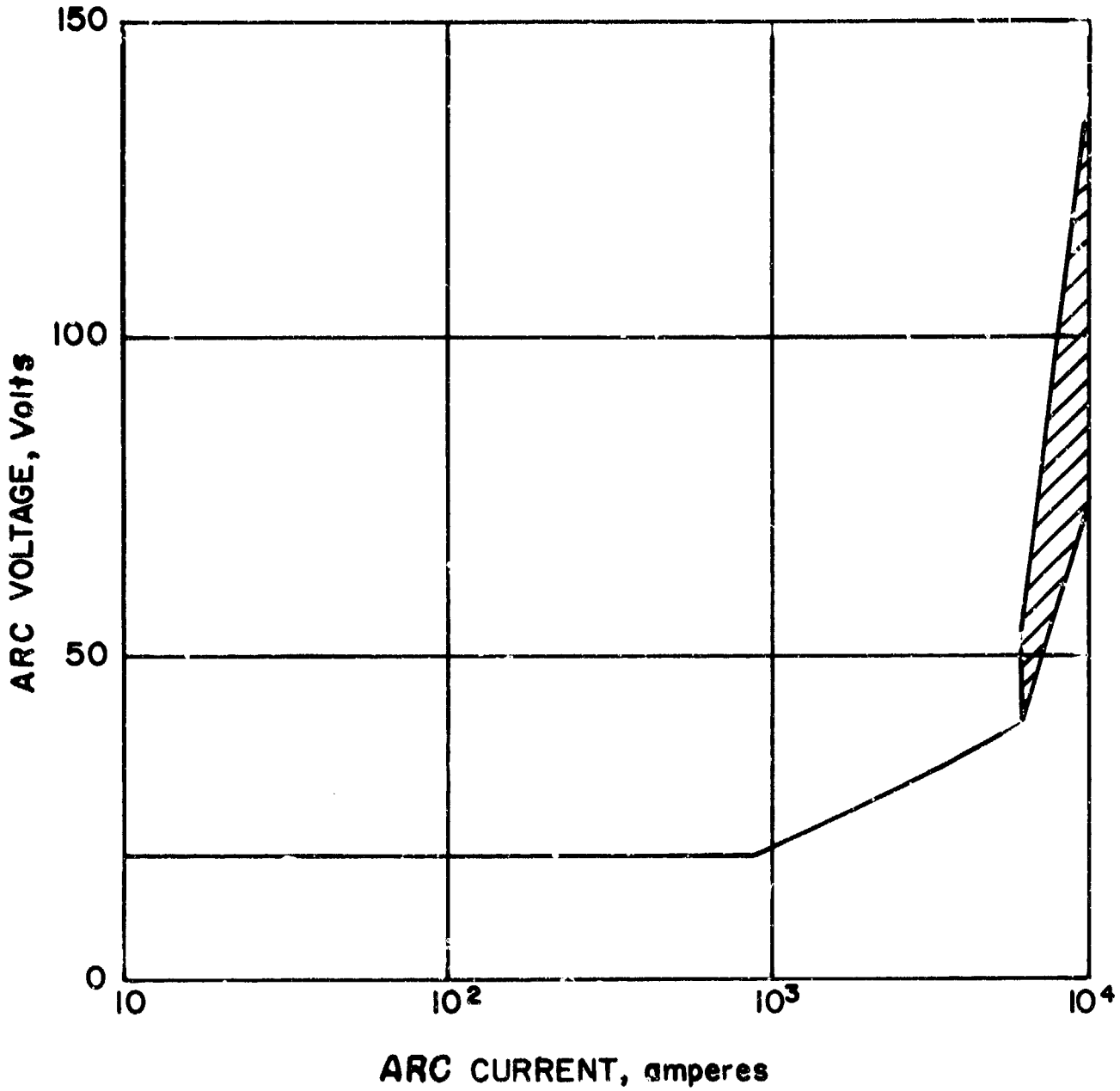

Figure 5. Typical arcing voltage vs. arcing current for vacuum arcs.

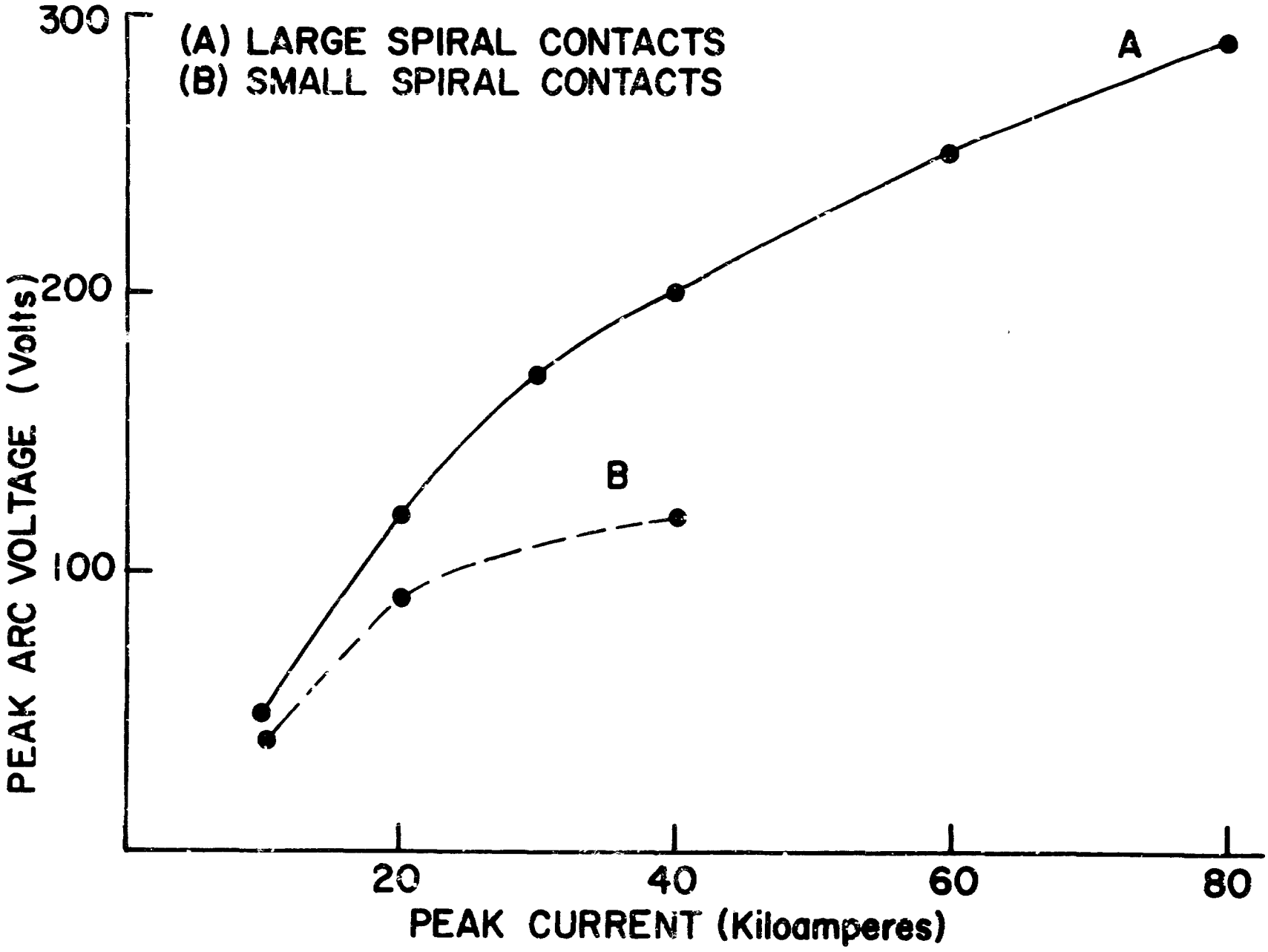

Figure 6. Typical vacuum switch voltage drop as a function of current while arcing.

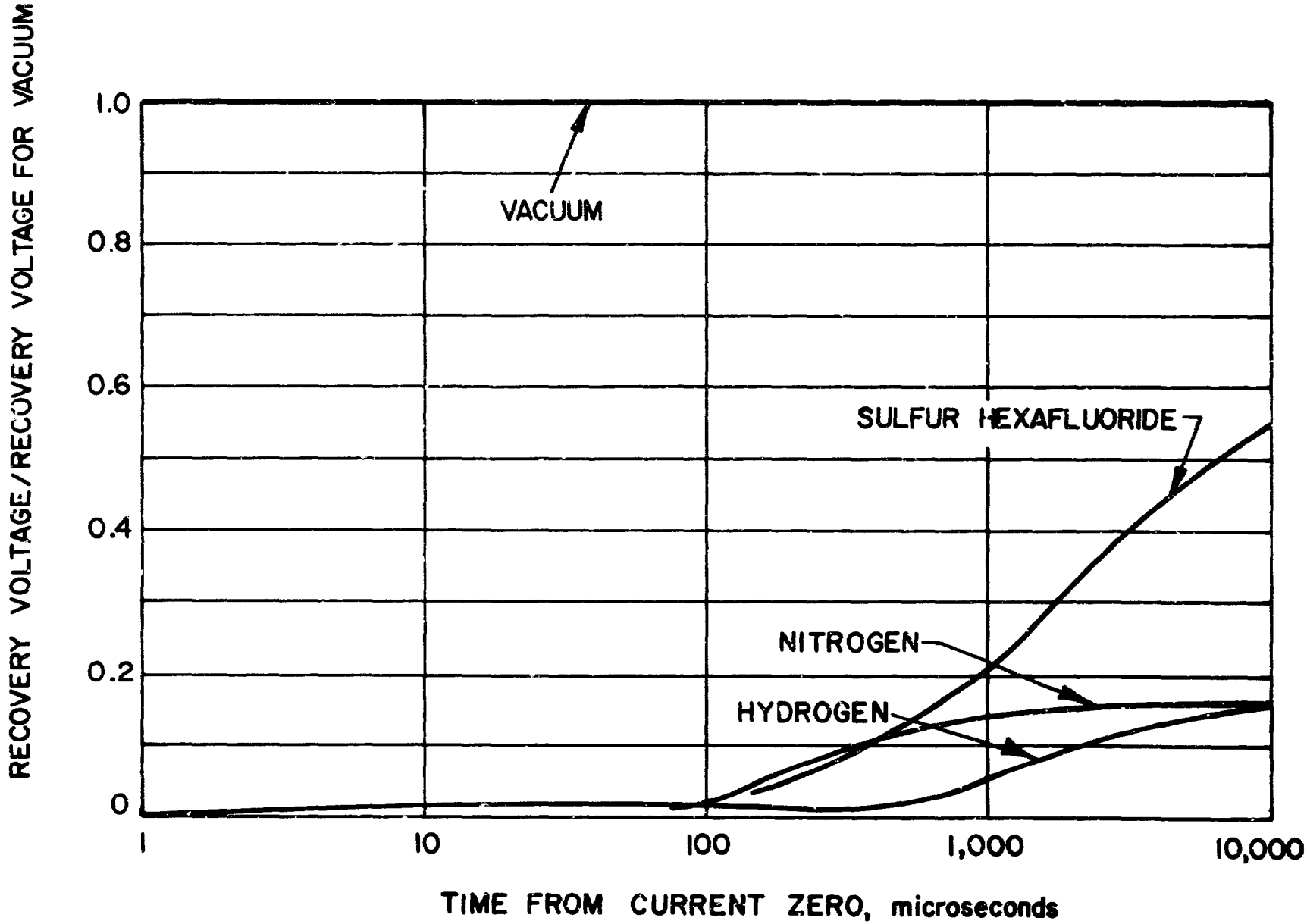

Figure 7. Relative recovery strength for vacuum and various gases.

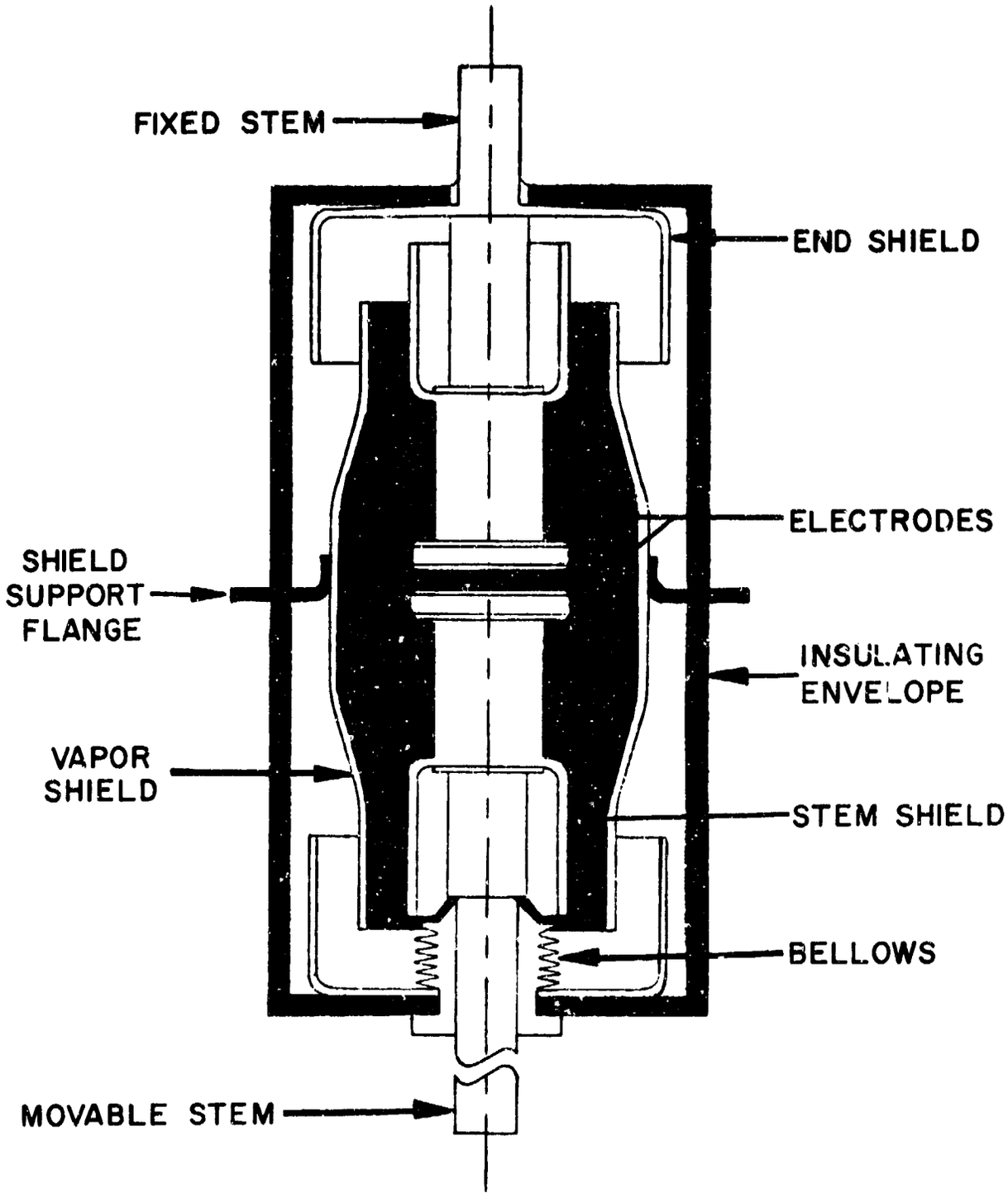

Figure 3. Typical vacuum interrupter schematic diagram.

When an arc strikes between the contacts, the energy it dissipates is partially absorbed in heating the contacts and partially transferred from the arc to its surroundings by radiation. A possible application of cryogenics would be to lower the temperature of elements such as the vapor condensing shield and thus attempt to cool the arc more effectively by radiation heat transfer. The latter is proportional to the difference in the fourth powers of the temperatures of the arc and shield, or

$$Q \propto (T_a^4 - T_s^4)$$

where: T_a = arc temperature

T_s = shield temperature

Since the arc temperature is of the order of 10^4 °K, this relationship indicates that changing T_s from room temperature (300 °K) to <u>any</u> lower temperature has negligible effect; consequently, increasing radiative heat transfer from the arc is <u>not</u> an area likely to be improved in this manner. Cryogenic cooling may have other advantages, however.

A switch operating with a loss per pulse of 5,000j at the rate of 5pps represents a power loss of 25 KW which must be removed from the switch components. The second area to be considered then, is the use of cryogens to support these losses. This would be accomplished by providing thermally conducting paths from the switch contacts and shields to the cryogen taking proper consideration of electrical insulation requirements. Figure 9 shows the liquid liters of cryogen necessary to support switch losses if the switch is heat sunk directly to the liquid cryogen. A similar plot for cryogen weight is shown in Figure 10. Curves are shown for liquid hydrogen, liquid nitrogen and liquid helium. If the energy storage coil were superconducting, the helium would be available and the nitrogen may or may not be available depending on whether the dewar utilized a helium vapor cooled shield or a nitrogen jacket. If the energy storage coil used a cryogenically cooled normal conductor, the cryogen would probably be either liquid nitrogen or liquid hydrogen. For a switch loss per pulse of 5,000j, the graphs indicate cryogen requirements which are summarized in the following table.

Table II.

Liquid Cryogen Requirements to Support
Switch Losses of 5,000j/pulse for 300 pulses
(Assuming Latent Heat of Vaporization Only)

Cryogen	LN_2	LH_2	LH_e
Volume (liters)	9.3	48	552
Weight (Kg)	7.5	3.4	69

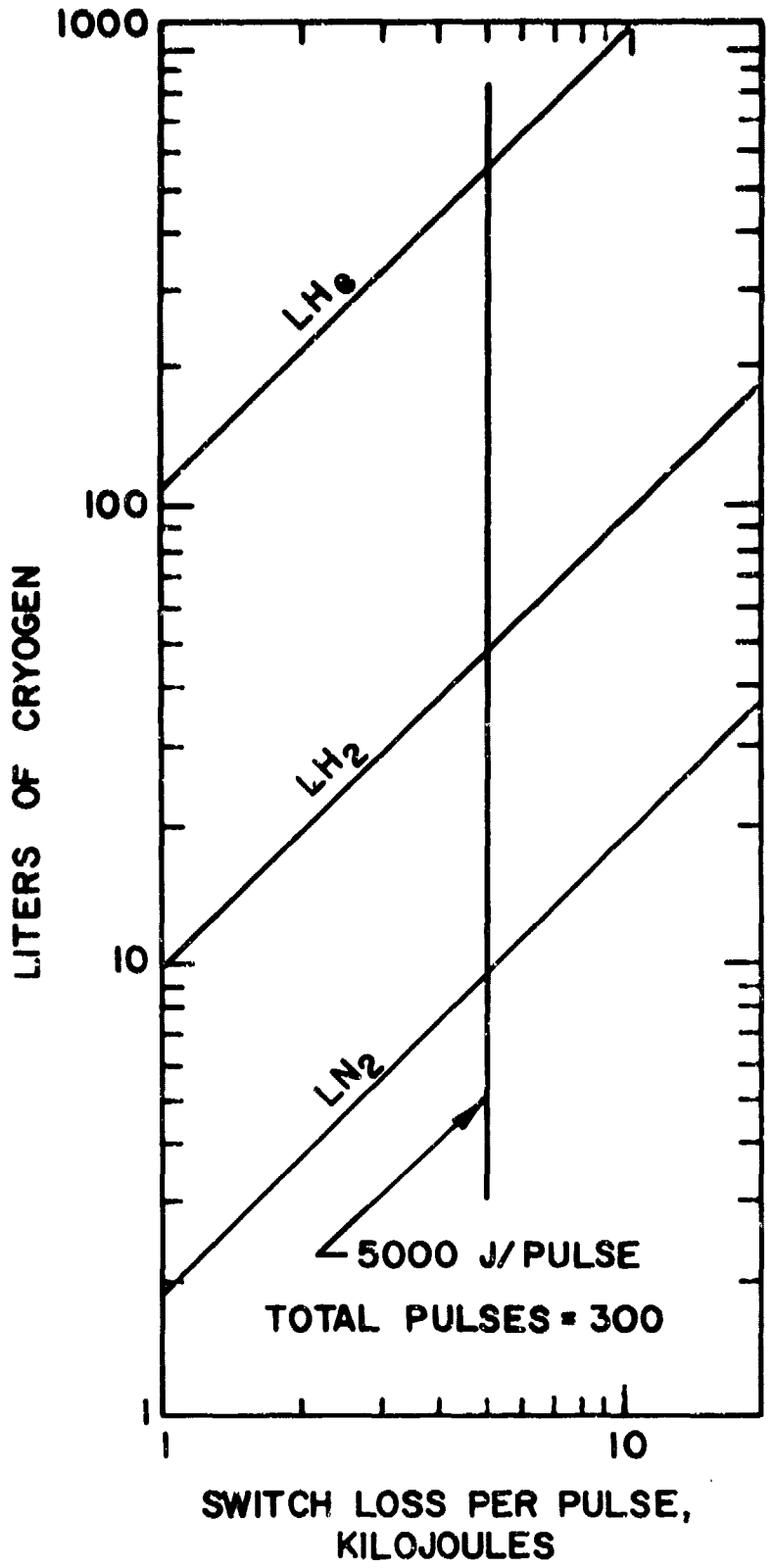

Figure 9. Liquid liters of cryogen necessary to support switch losses (estimates based on heat of vaporization only).

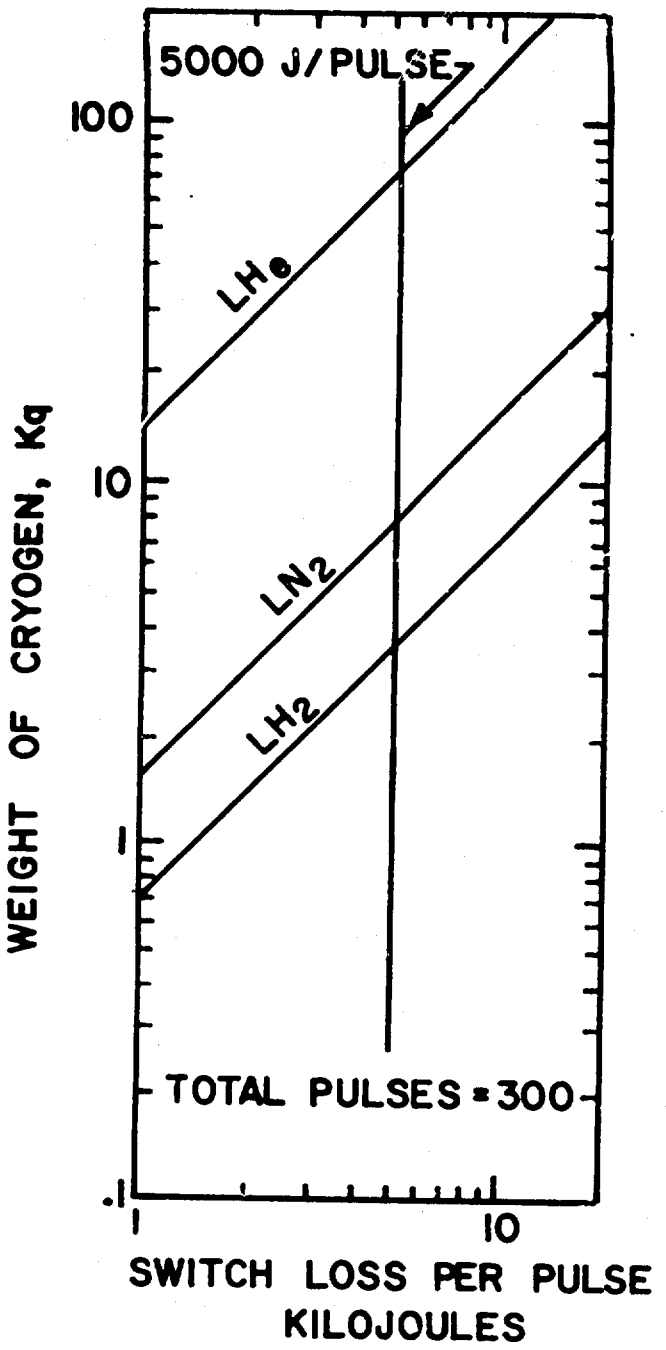

Figure 10. Weight of cryogen necessary to support switch losses (estimates based on heat of vaporization only).

This table indicates that liquid nitrogen is a suitable candidate as a direct heat sink since both the weight and volume required are low. Liquid hydrogen exhibits a lower weight, but a higher volume when compared with the nitrogen. Liquid helium is basically unsuitable because both weight and volume are high. Thus far, only the latent heat of vaporization of the cryogen has been considered. In an integrated system, it is most likely that certain switch components would be cooled by cryogen boiloff from the losses generated in the energy storage coil during operation. For example, the lead to each contact could be surrounded by a heat exchanger through which the cryogen boiloff is passed. To gain an insight into the adequacy of this concept, the following table was prepared.

Table III.

Energy Absorbed by Vaporized Cryogen in Raising Its Temperature from 100°K to 300°K

Cryogen	N_2	H_2	H_e
Energy Absorbed in Raising Temperature of Vapor from 1 liquid liter from 100°K to 300°K (j/ℓ)	1.69×10^5	2.05×10^5	1.29×10^5
Liters to support losses of 5,000j/pulse for 300 pulses (ℓ)	8.9	7.3	11.6
Energy Absorbed per Unit Mass (j/g)	209	2,660	1,060
Mass per liquid liter (g/ℓ)	808	77	125
Boiling Point at 1 atm (°K)	78	20	4.2

The table indicates that sufficient heat capacity is available in the boiloff from each of the three cryogens under consideration. For purposes of illustration, heat exchanger inlet and outlet temperatures of 100°K and 300°K were chosen. Considerably less cryogen would be necessary if the inlet temperature were closer to the boiling point of the cryogen or if the outlet temperature were higher than room temperature (300°K). The quantity of cryogen necessary for heat exchanger inlet temperatures other than 100°K may be estimated with the use of Figure 11. In any case, the estimates verify the feasibility of utilizing the boiloff cryogen in a heat exchanger around individual switch components to remove switch losses during operation.

A configuration which will be considered in more detail in a later section combines the above concepts by utilizing a heat exchanger around each switch lead to cool the contacts and by using a vapor condensing shield which is heat sunk directly to liquid cryogen. In an integrated system, the latter would be the liquid nitrogen used in the nitrogen jacket of the dewar for the energy storage coil and the former would utilize helium vapor which was boiled off by a superconducting energy storage coil when pulsing.

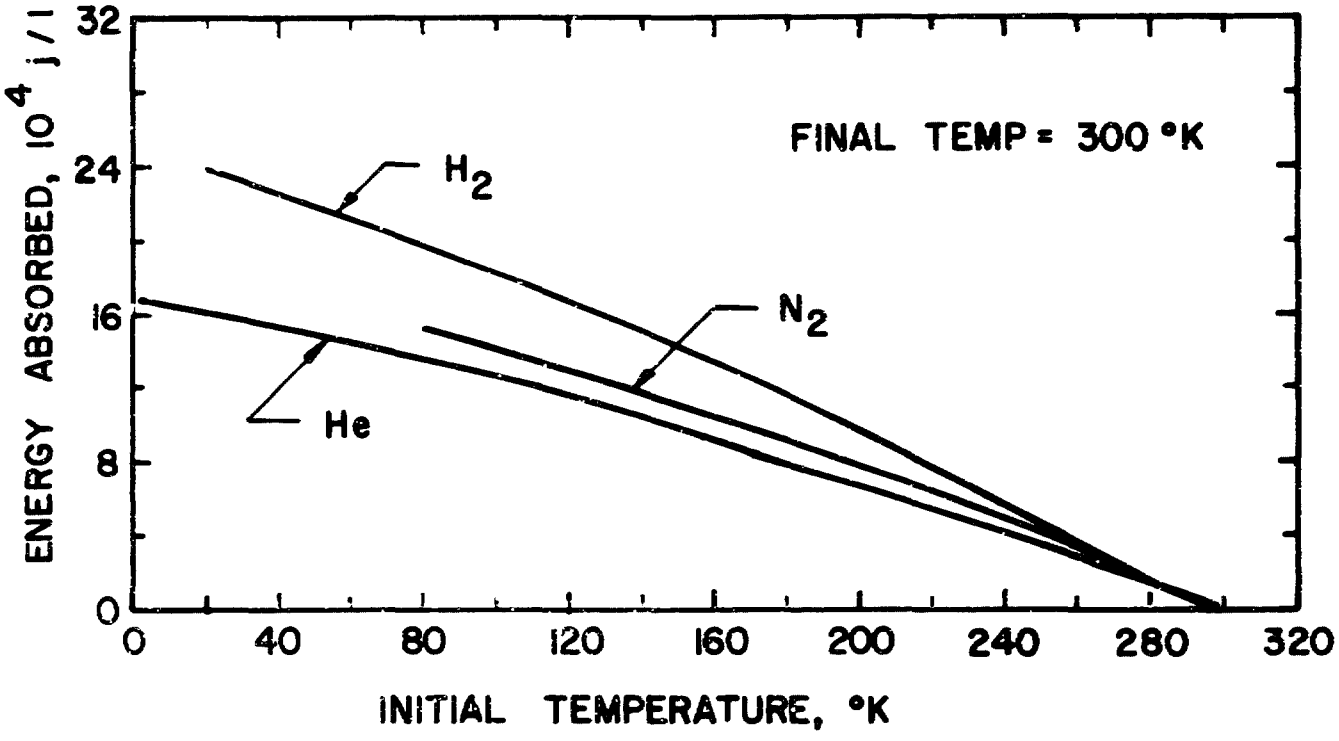

Figure 11. Energy absorbed in raising temperature of vapor produced by one liquid liter from initial temperature, T, to final temperature, 300°K.

The third effect to be considered is the possibility of decreasing switch losses when closed by cooling the switch and thus decreasing its resistance. Typically, the resistivity of metals is a strong function of temperature while the resistivity of the alloys is not. Thus, it may be expected that substantial decreases in lead resistance may be had by cooling since they will most likely be copper (or aluminum for weight purposes).

This is illustrated in Figure 12 which is a plot of the resistivity of copper and of aluminum as a function of temperature. The temperatures of liquid nitrogen, hydrogen and helium at one atmosphere pressure are also shown. Note that little decrease in resistivity occurs below the temperature of liquid hydrogen. For a conductor of given size carrying a given current, the DC power dissipation is directly proportioned to its resistivity. Consequently, the ratio of the resistivity of the material at temperature T to its resistivity at room temperature is also the ratio corresponding to power dissipation relative to the two temperatures. The following table was prepared for copper and aluminum and illustrates the temperature dependence of the DC power dissipation for a conductor of fixed size and fixed current relative to dissipation at room temperature.

Table IV.

Ratio of DC Power Dissipation At Temperature, T, to DC Power Dissipation at Room Temperature for Copper & Aluminum

Temperature, T (^{o}K)	Aluminum	Copper
300	1.0	1.0
250	0.9	0.9
200	0.68	0.7
150	0.42	0.45
100	0.23	0.24
78	0.14	0.15
20	0.03	0.01

The above table clearly indicates the advantages of reduced temperature for the purpose of reducing losses generated in aluminum or copper, current carrying, switch components. From another standpoint, the power dissipation may be held constant and component size decreased with temperature. A temperature reduction to the vicinity of that of liquid nitrogen (78 - 100^{o}K) is attainable relatively easily and will be utilized in the switch designs to be discussed later.

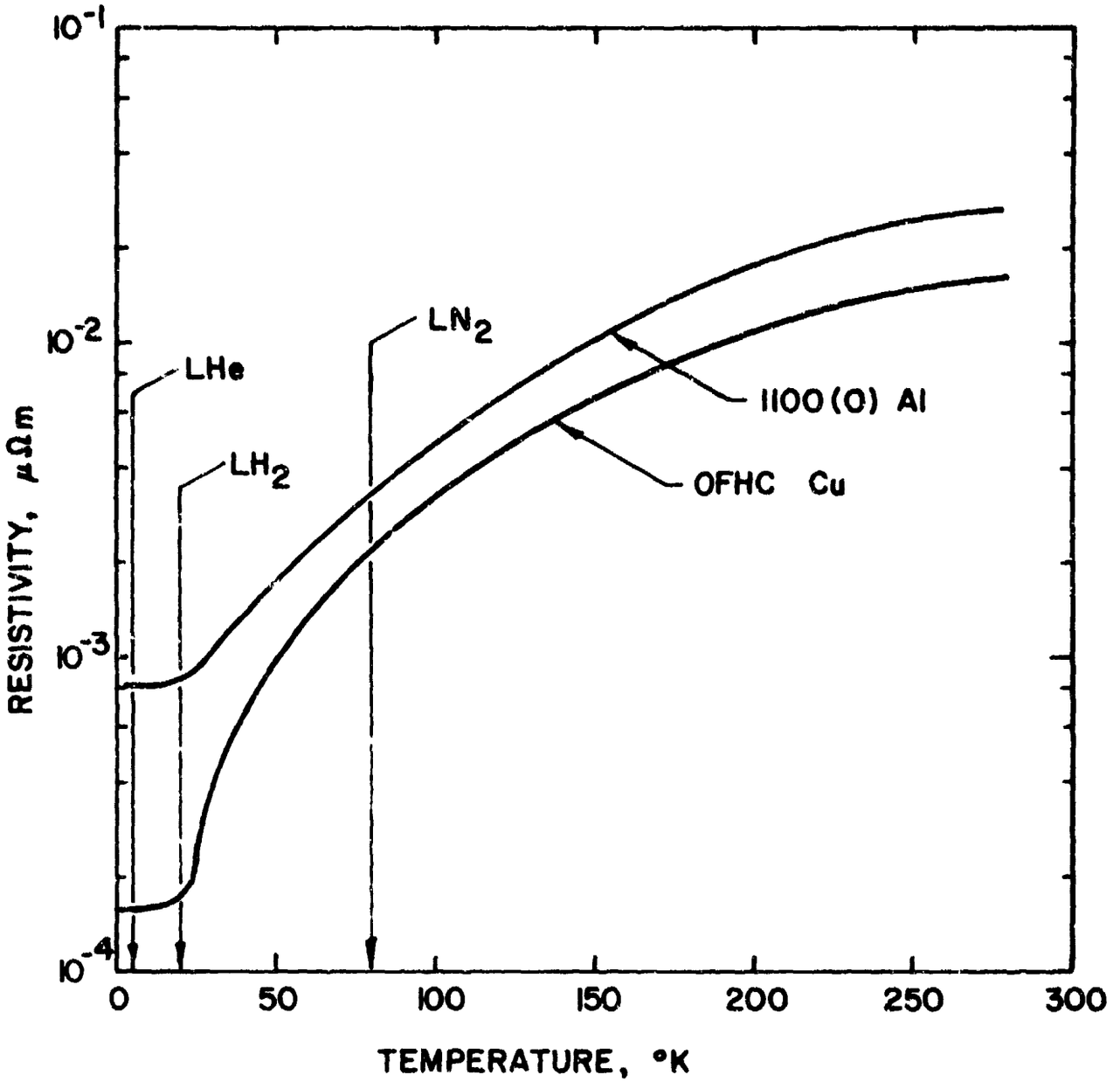

Figure 12. Resistivity of Cu and Al as functions of temperature.

At this point, it should be noted that contact resistance is essentially independent of temperature and primarily dependent on contact pressure as shown in Figure 13. As shown, the switch resistance approaches a lower limit as contact pressure increases. The conclusion to be drawn from this figure and the above table is that significant decreases in switch resistance are possible if cryogenic cooling is provided and contact pressure is sufficiently high.

The fourth cryogenic effect which could be used in a specially designed vacuum interrupter to enhance performance is that of cryovacuum pumping. Standard vacuum interrupters are subjected to complex procedures of baking, outgassing and vacuum pumping prior to sealing. After sealing, the vacuum degrades very slowly by external diffusion of the light elements, principally helium and hydrogen, into the vacuum space and by internal diffusion in which trace impurities embedded in component materials find their way to the surface and into the vacuum. These processes occur over the long term as indicated by the upper curve[1] in Figure 14. The lower curve also indicates the self-pumping action of the vacuum switch. The vacuum contact, particularly if made of high purity tungsten, when interrupting acts similar to a tungsten vapor ion pump and getters all possible contaminants (even helium). Such action requires many interruptions, however, and a high performance unit as required by this program may not survive the first attempt at interruption if trace impurities diffuse into it while it lies dormant.

A possible solution exists in the use of cryovacuum pumping in combination with the proper getter material. This technique involves the capture and retention of mass on low temperature surfaces by both cryocondensation and cryosorption. Molecules are pumped by physical absorption on synthetic zeolite materials, commonly called molecular sieves, which are physically bonded to liquid helium cooled panels.[2] Figure 15 shows the helium sticking coefficient for a molecular sieve as a function of temperature and indicates the essentially perfect capture efficiency of the getter material at the temperature of liquid helium.[3] System pressures in the 10^{-12} Torr range have been recorded[4] by utilization of these techniques.

The use of cryovacuum pumping in an integrated energy storage coil and vacuum switch system would be accomplished by having the switch vacuum space automatically cryo-pumped by the helium container for the energy storage coil when the system is cooled down. All traces of impurities are thus removed from the switch prior to firing regardless of the length of time the switch was inoperable.

This concept will be incorporated into the conceptual, integrated system design to be presented in a later section.

This section has discussed several areas in switch design in which the utilization of cryogens may prove effective. These include: absorption of switch losses, reduction of switch losses and cryovacuum pumping. Since cryogens will be available in support of the energy storage element, it is natural to incorporate them into the switch design wherever applicable.

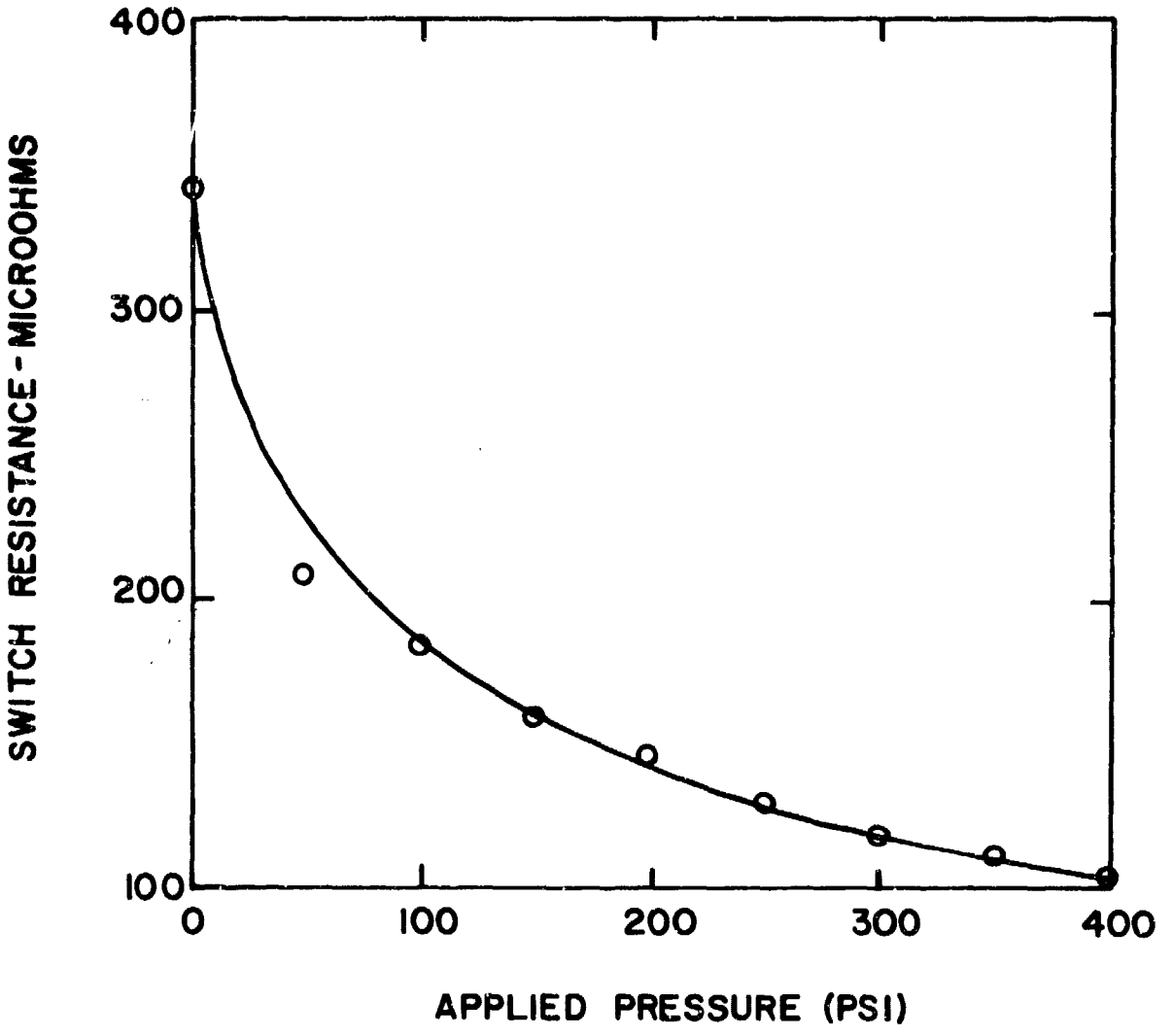

Figure 13. Switch contact resistance as a function of contact pressure for a typical vacuum interrupter. (1)

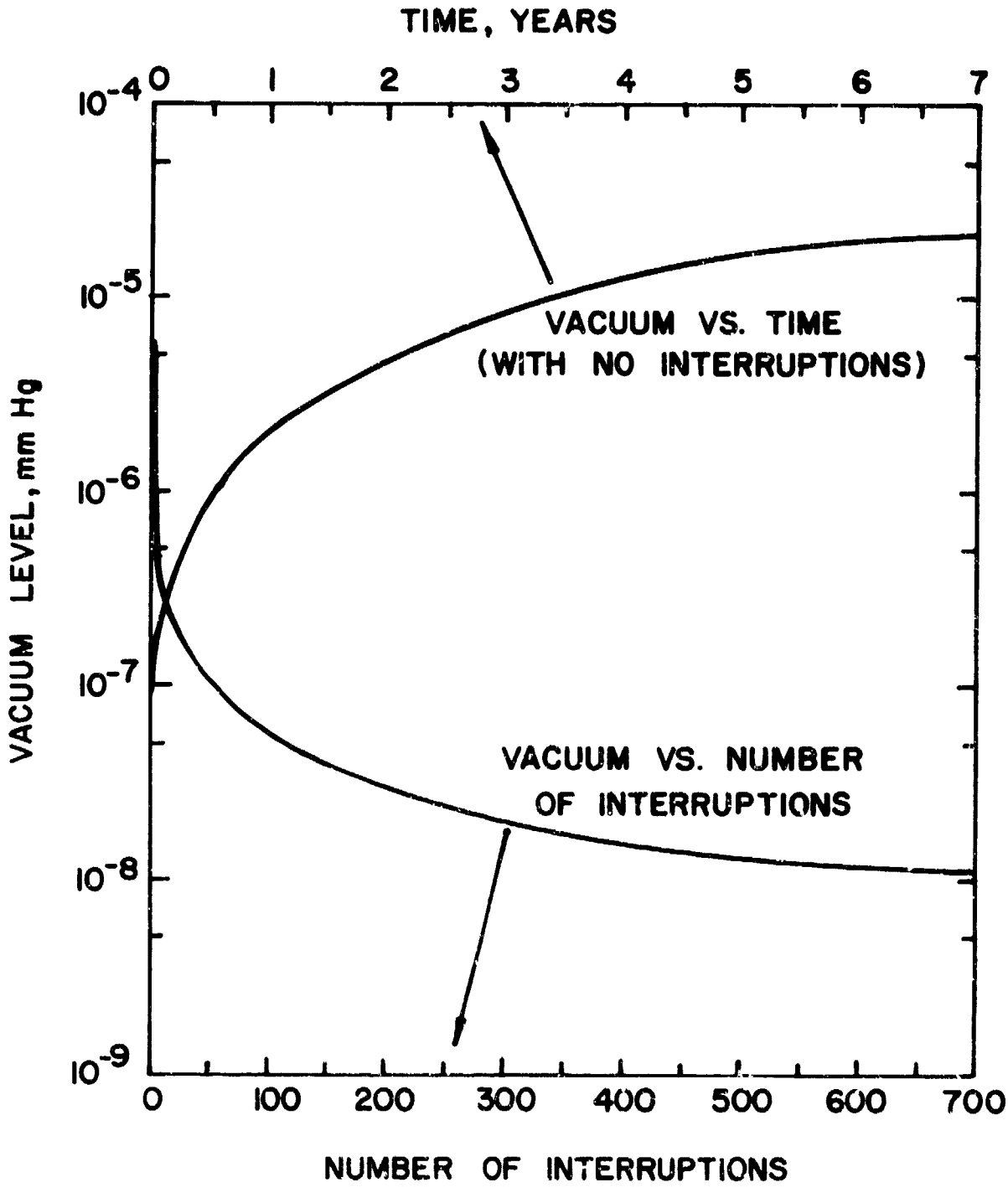

Figure 14. Vacuum level within a typical vacuum interrupter as a function of time (with no interruptions) and as a function of number of interruptions.

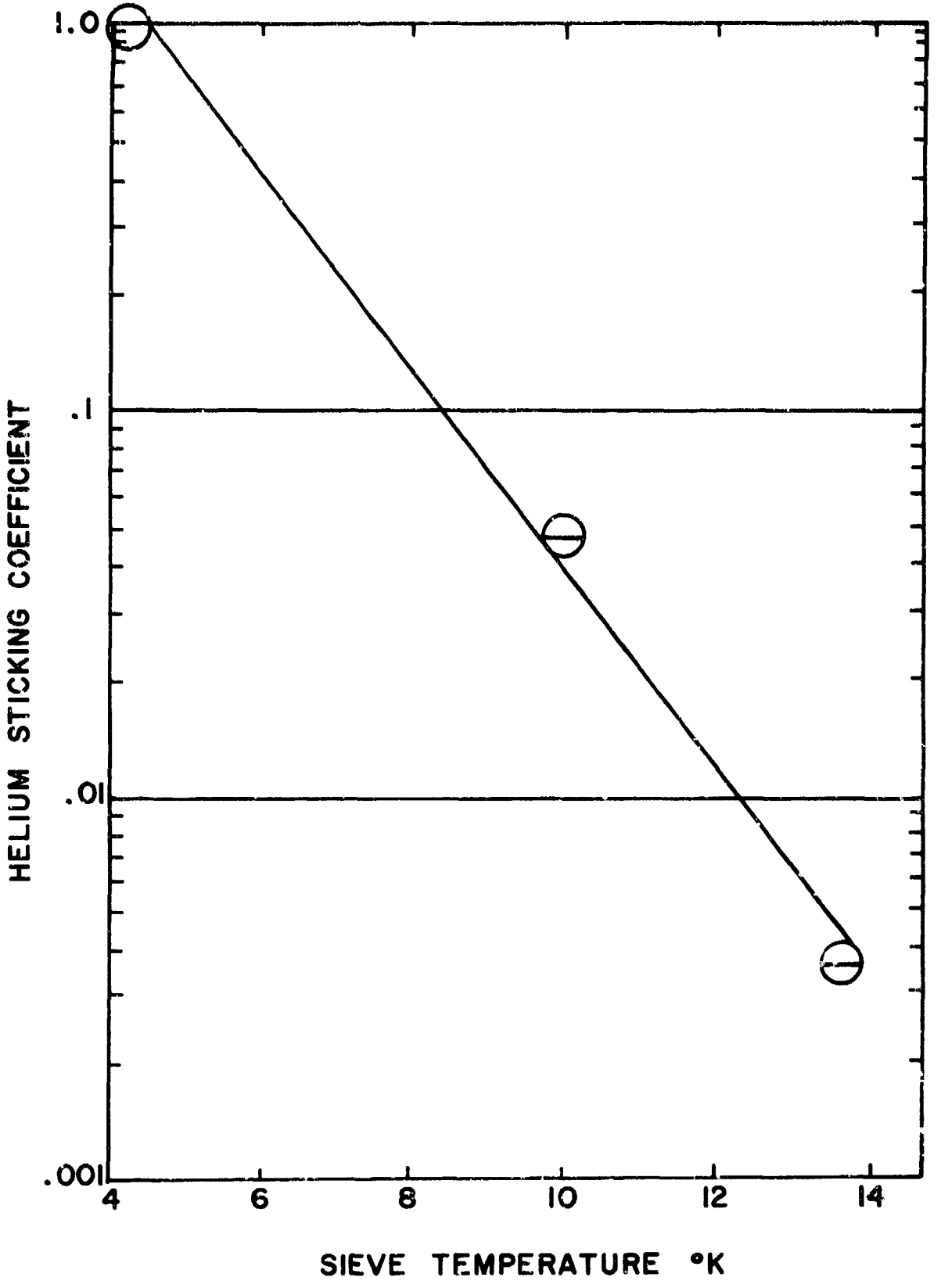

Figure 15. Cryosorption pumping of helium by molecular sieve.[3]

c. Magnetic Field Utilization

The inductive energy storage element in the system creates a magnetic field which can be available, in an integrated system design, to aid in the switching process. This section will discuss those areas in which the utilization of the magnetic field may be advantageous.

(1) Magnetically Induced Arc Motion

When the contacts part in a standard vacuum interrupter and an arc forms, it can take one of two very different forms. One form consists of a large number of separate and coexistent streamers which terminate over a large area of the electrodes available to them. Generally speaking, this type of vacuum arc occurs with currents less than 6-10 kiloamps and results in negligible contact damage provided it is extinguished in a few milliseconds. For larger currents the arc resembles a high pressure arc in that the total current flow is concentrated over a much smaller area of the electrodes. Such an arc can result in severe damage to both anode and cathode because the heat generation rates are not only higher, but the contact area over which the arc is spread is usually smaller.

In both cases the arc tends to move over the contact surfaces due to local effects such as field and thermal concentrations on surface imperfections or machined ridges, or due to local variations in readily ionizable material. The speed of the arc relative to the contacts under such circumstances may be as high as 10 m/sec.[5] Such motion helps prevent excessive local heating of the contacts.

The arc motion is often enhanced (see Appendix I) by applying a magnetic field in the vicinity of the arc. One method for doing this is shown in Figure 16. In this situation the return circuit for the current through the switch is placed parallel to, and as close as possible to, the switch. The arc current interacts with the field to yield a force in the $\overline{I} \times \overline{B}$ direction. The force is in the plane of the circuit, directed outward and of magnitude:

$$F = \frac{\mu_o g I^2}{2\pi d}$$

This force would tend to move the arc across the face of the electrodes; then when the outward side of the gap is reached, the arc would increase in length. The result may be advantageous in four ways:

1) the forced motion does not allow the arc to continuously heat the same portion of the electrode surfaces;

2) the forced lengthening of the arc increases its resistance;

3) the interaction of the moving arc with the magnetic field results in a "back emf" which appears as an increased arc resistance; and

4) the presence of the field transverse to the arc increases its resistance (see Appendix I, Figure 76).

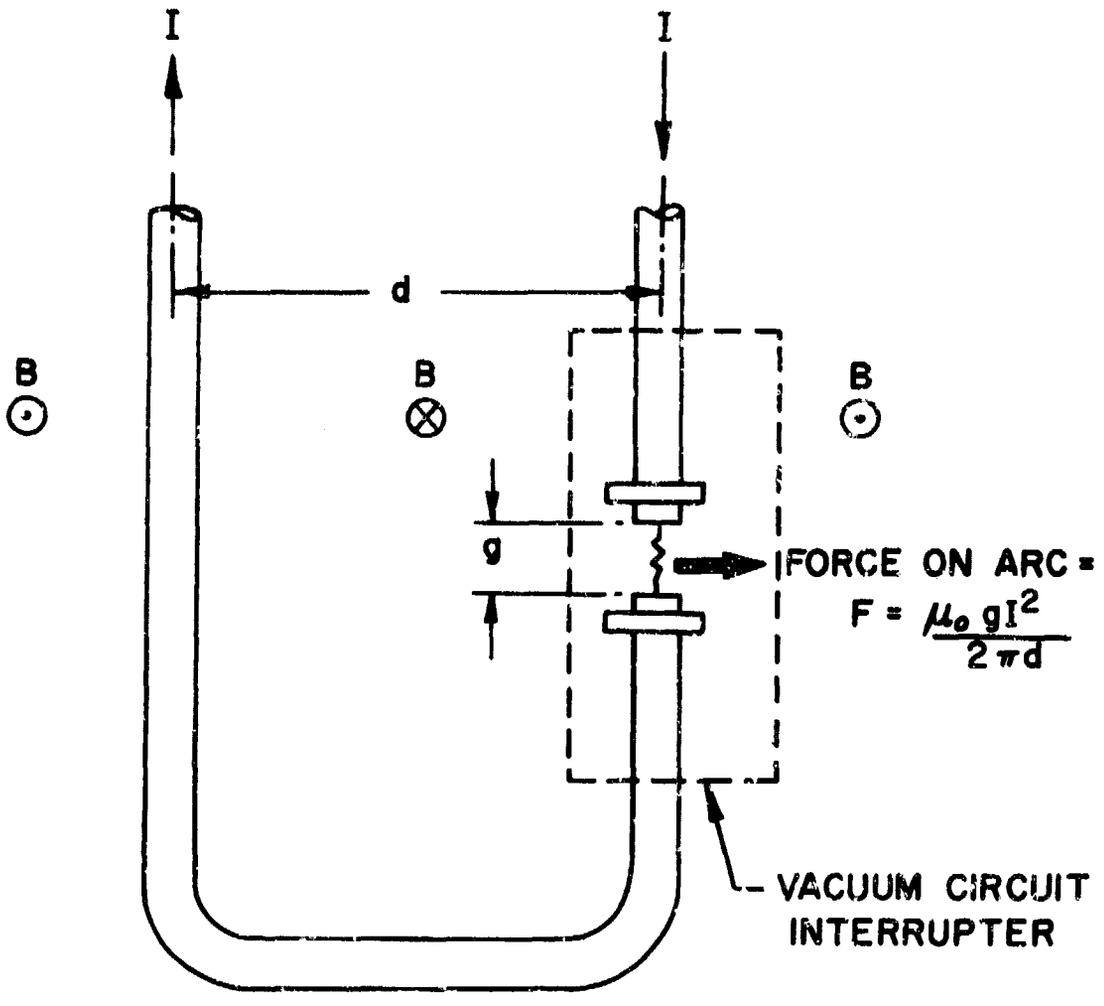

Figure 16. Return circuit configuration to produce $\bar{I} \times \bar{B}$ effect on arc.

The latter effect arises from the force exerted on the moving charged particles which tends to inhibit their motion across field lines. All four effects help to extinguish the arc. For a given current, the speed with which the arc passes over the face of the electrode may be estimated if it is assumed that the effect is governed by the inertia of the arc plasma. With this assumption, the time required to traverse the width of the electrode may be estimated by:

$$t = \frac{\pi a}{I} \sqrt{\frac{w \rho d}{\mu_o}}$$

where:

a = arc diameter

I = circuit current

w = electrode diameter

d = distance between return circuit and switch

ρ = density of plasma

$\mu_o = 4 \times 10^{-7}$ H/M.

This time could be shortened by applying an additional magnetic field across the gap in the direction of the field from the return current. This is often done with standard interrupters by using an auxiliary set of field coils. The time for arc traverse across the electrodes would then be reduced to:

$$t = \sqrt{\frac{w \rho \pi^2 a^2 d}{\mu_o I^2 + 2\pi d I b_o}}$$

where:

B_o = magnetic flux density produced by auxiliary coils.

In such a configuration, however, auxiliary coils provided for the switch represent a weight component chargeable to the switch. This is unnecessary in an energy storage system since the design of a special interrupter could utilize the energy storage coils as the field coils for the switch with no additional system weight and with enhanced switch characteristics.

Estimates of the arc speed as a function of arc current and applied field are given in Figure 17. These estimates are based on data for arcs in air (See Appendix I) and probably represent a lower limit when applied to arcs in vacuum. The plot indicates that an applied field of 2 W/m^2 would produce arc velocities in excess of 850 m/sec and 1500 m/sec for arc currents of 5,000a and 20,000a respectively. If these arcs were 1 cm long, their respective back emfs would be in excess of 15 v and 30 v.

Note that 2 W/m^2 is a reasonable lower limit for the fields which may be expected in the bore of an energy storage coil. The field from the energy storage coil is not constant, however, it is at or near its maximum when the arc is drawn and does not decay to zero until after the arc is extinguished. This is another point in favor of the integrated switch, energy storage coil, and dewar system.

(2) Effects of Arc Motion on Contact Life

The motion of the arc across the face of the contact has a strong influence on the life of the contact. The faster the motion, the smaller the local heating of the contact. This section will illustrate the effects of the speed of the heat source on contact temperature and, therefore, justify the use of an external field to induce arc motion.

The case of an arc or heat source of width 2b moving with velocity u relative to a stationary surface is shown in the upper sketch of Figure 18. From a mathematical standpoint, the problem is more easily solved by transferring the reference frame to the moving arc as shown in the lower sketch. In dimensionless form, the solution for the temperature rise on the slab surface as a function of speed and distance along the contact may be shown to be: (6)

$$\Theta = \frac{1}{2\pi U} \left\{ Ye^{Y} \left[K_0(Y) + K_1(Y)\right] - Ze^{Z} \left[K_o(Z) + K_1(Z)\right] \right\}$$

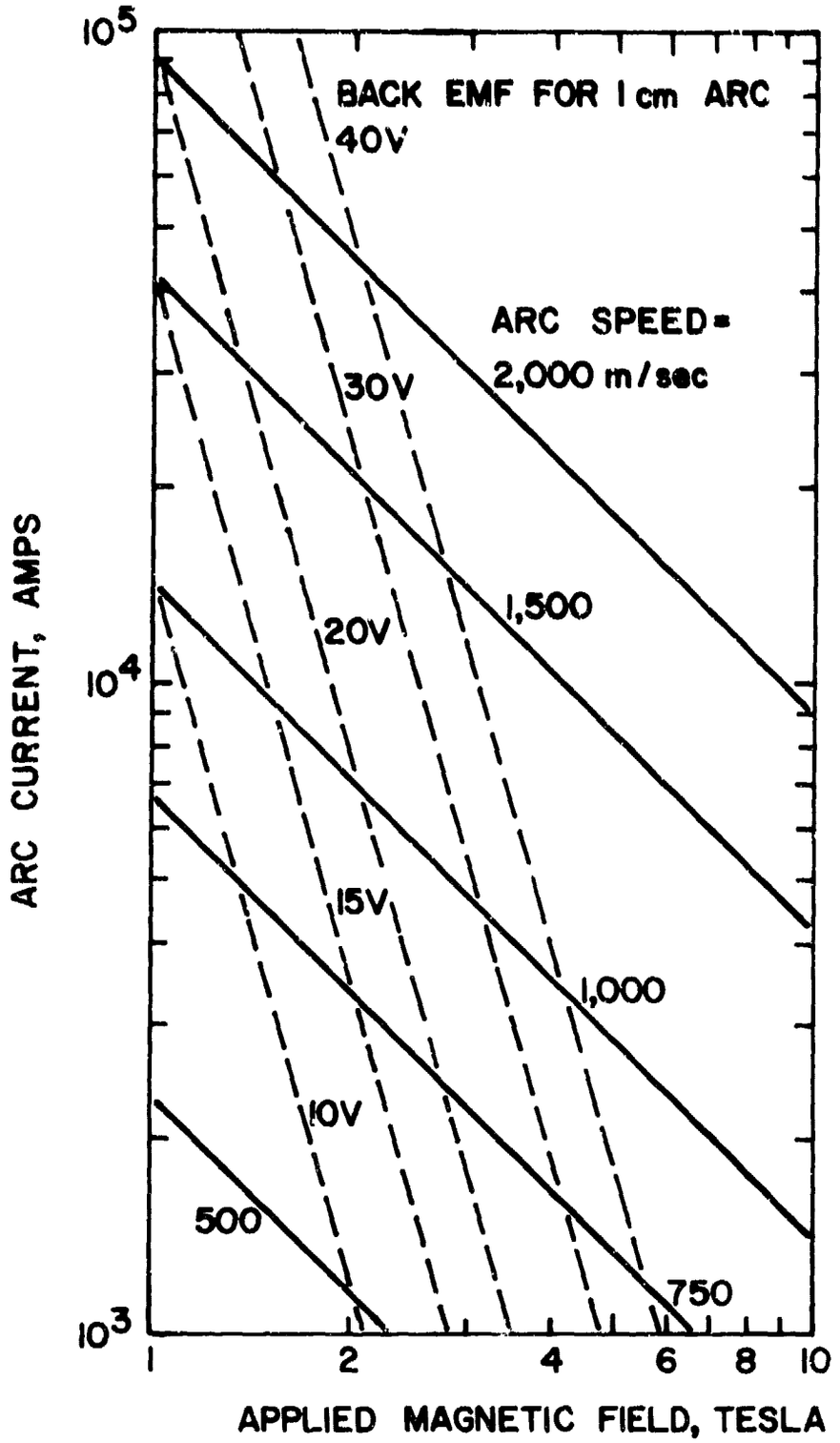

Figure 17. Arc speed and back emf as a function of arc current and applied magnetic field. Speed data are based on arcs in air (see Appendix I) and may be expected to be a lower limit for arcs in vacuum.

FA 1477

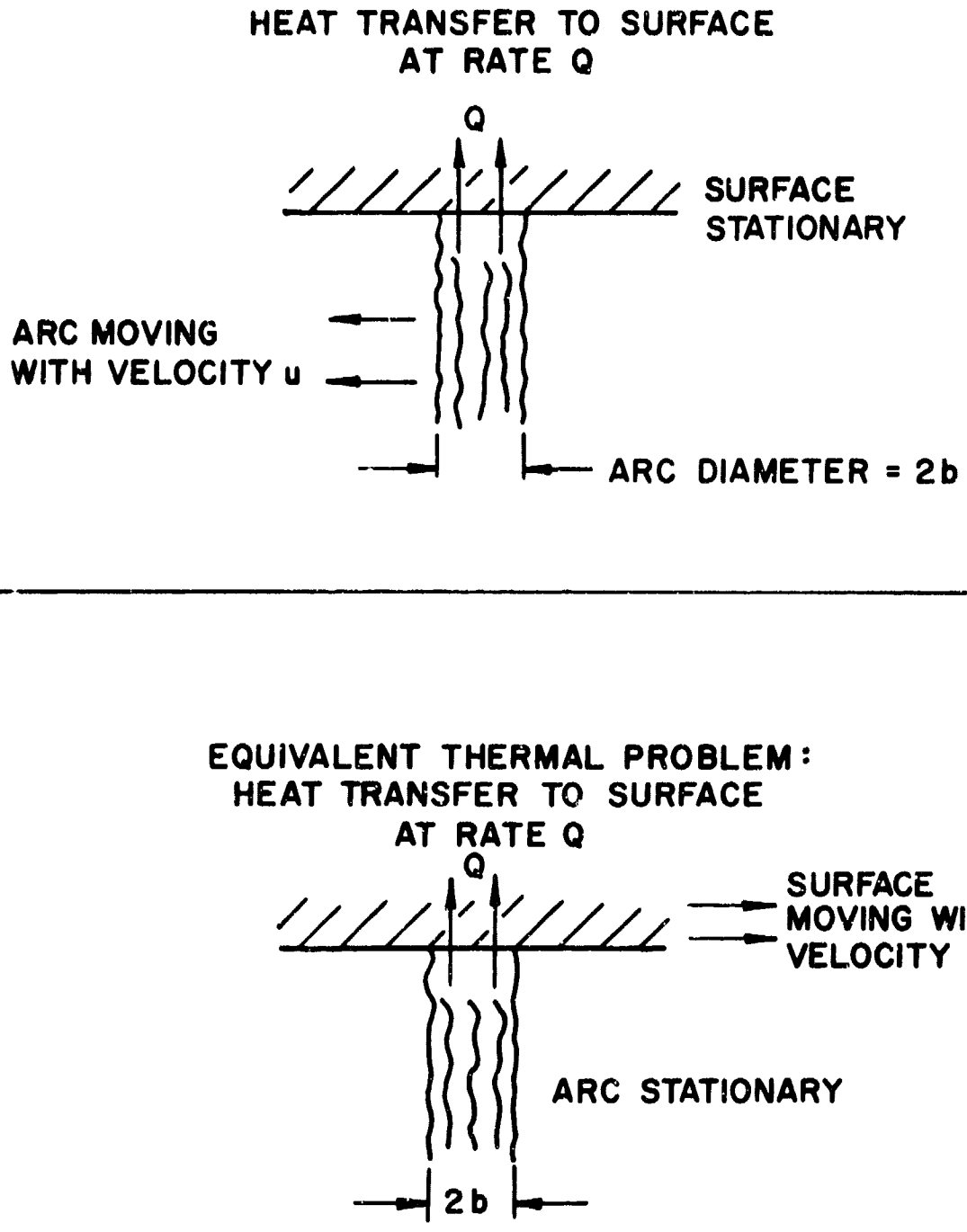

Figure 18. The problem of solving the temperature rise of a surface being heated over an area of length 2b by a source moving with speed u is most easily solved in a coordinate system fixed relative to the heat source.

where:

Y = $U(X+1)$

Z = $U(X-1)$

X = $\frac{x}{b}$ = dimensionless distance

U = $\frac{ub}{2K}$ = dimensionless velocity

K = Thermal diffusivity of surface material

b = half width of arc

x = co-ordinate along surface measured from arc center

Θ = $\frac{kT}{Qb}$ = dimensionless temperature rise

k = thermal conductivity of surface material

Q = heat input to surface from arc per unit area per unit time

T = temperature rise along surface

$K_{0,1}$ = modified Bessel function of the second kind of order 0, 1.

The above relationship is plotted in Figure 19 which shows the dimensionless temperature rise versus distance along the plate for various values of dimensionless velocity. To interpret this graph, the arc may be imagined to be located on the horizontal axis between the co-ordinates -1 and +1. It is transferring heat into the slab which is moving to the right with dimensionless velocity U. Far to the left there is no temperature rise for any of the velocities shown; since, for the cases plotted, the slab is moving to the right fast enough for very little heat to diffuse towards the left. There is no heat input to the slab for $(x/b) < -1$, since the arc boundaries are at $x = \pm b$. The faster the slab moves, the lower the overall temperature rise, with the maximum temperature always occurring at $X = +1$. In a reference frame in which the surface is stationary, $X = +1$ represents the trailing edge of the arc at point of contact with the surface.

For contacts with a moving arc, the maximum arcing temperature occurs at the trailing edge of the arc. The dimensionless maximum temperature is shown plotted in Figure 20 as a function of the dimensionless speed. This clearly indicates the decreases in contact temperature possible by increasing arc speed for any given contact material (fixed k, κ), fixed arc size (b) and fixed heating rate (Q).

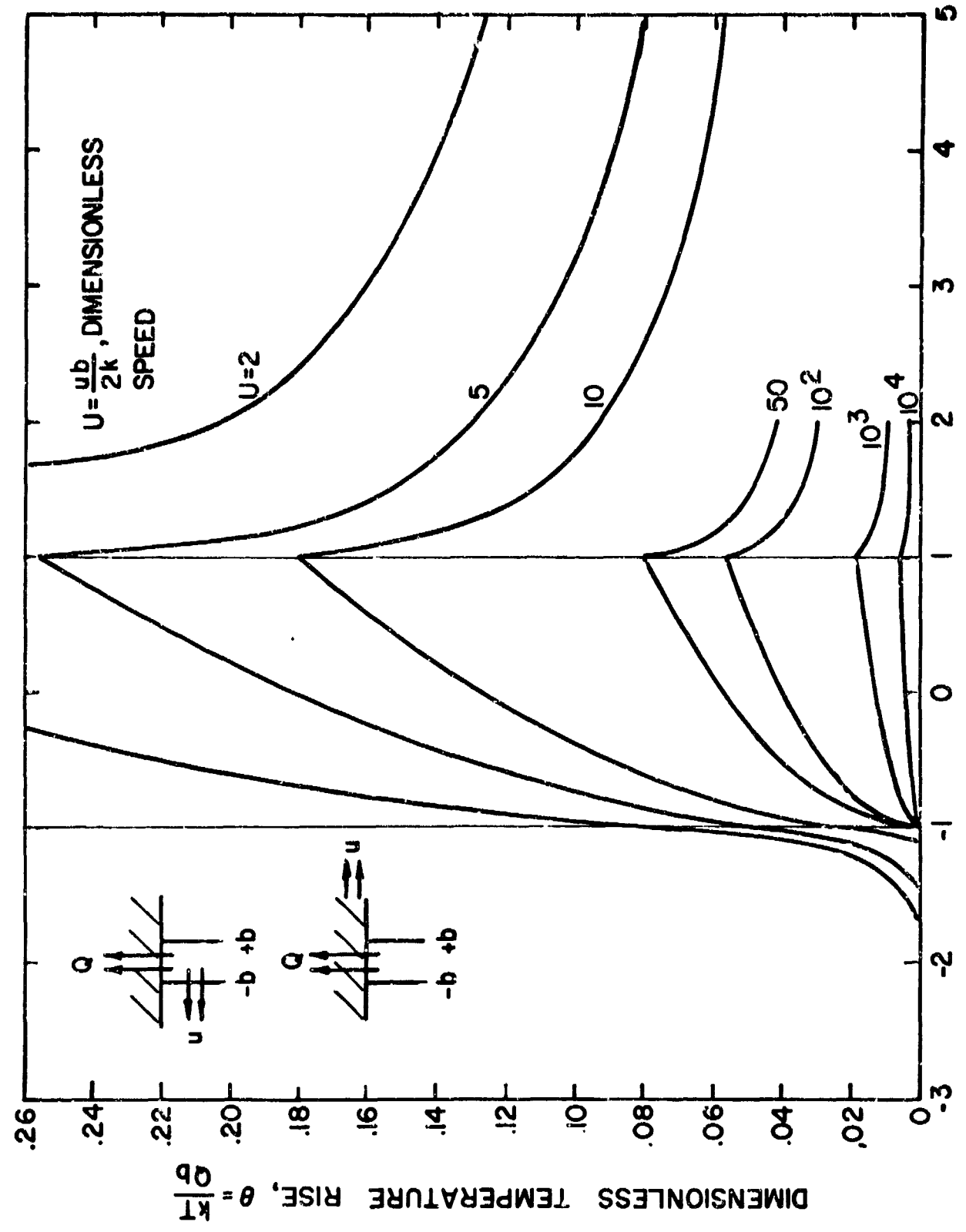

Figure 19. Dimensionless temperature rise vs. dimensionless distance along a surface for an arc moving with dimensionless velocity U. The plot is made in the reference frame of the moving arc and the surface appears to be moving to the right with speed U. Heat input to the surface occurs between $-1 < (x/b) < +1$.

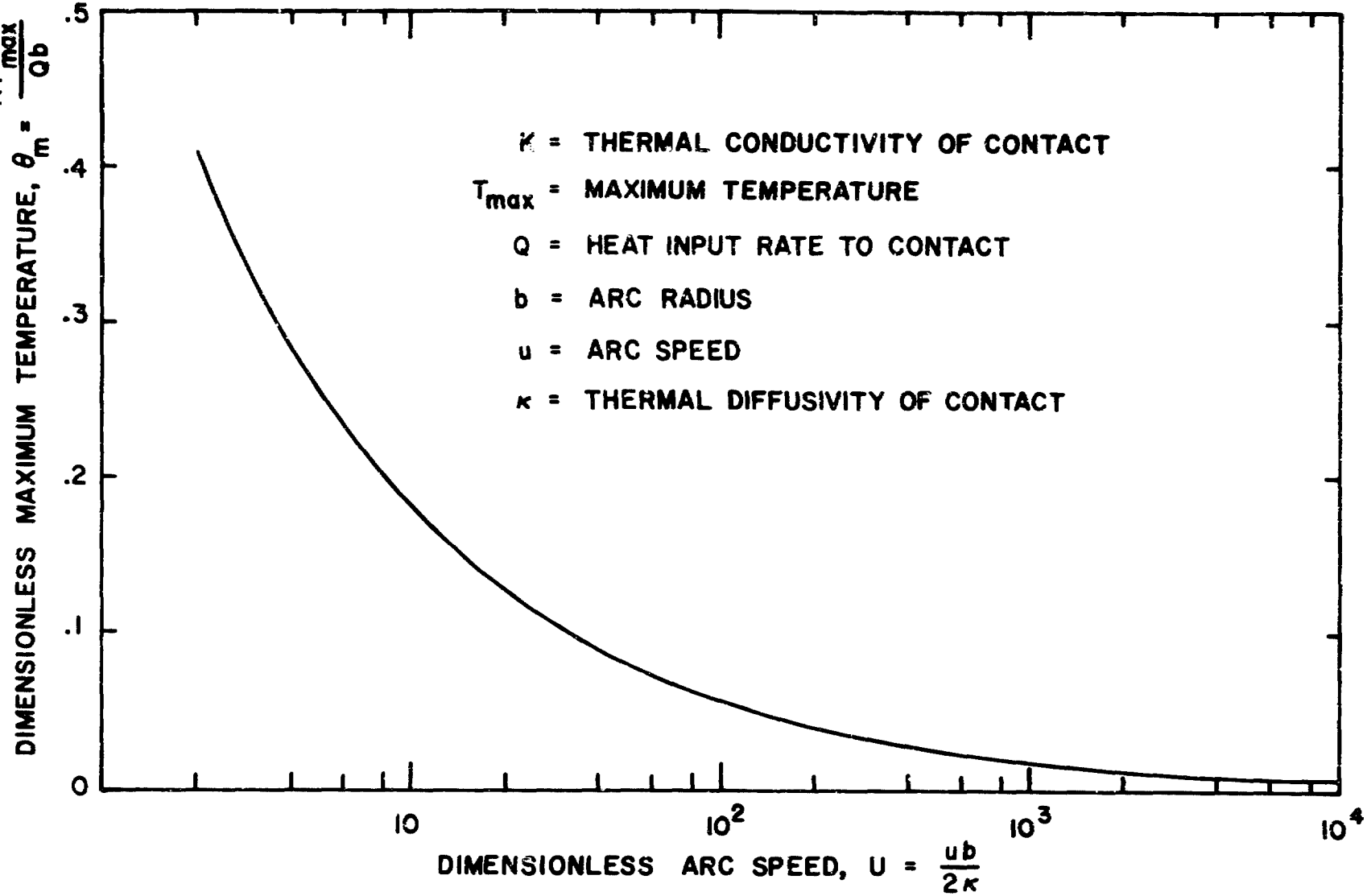

Figure 20. Dimensionless maximum temperature rise as a function of dimensionless arc speed: typically, for copper contacts and magnetically induced arc speeds of 500 m/sec, the contact temperature rise would be a factor of nine lower than for a randomly moving arc at a speed of 10 m/sec.

Based on this plot, calculations indicate that an arc moving with speed 500 m/sec over a copper contact will result in a maximum temperature rise which is a factor of nine lower than the temperature rise due to a motion at 10 m/sec.

As pointed out in an earlier section, 500 m/sec is the expected lower limit for arc speed in the applied field from an energy storage coil. The use of this field in the switch configuration may, therefore, be expected to substantially increase contact life.

d. Switch Dissipation, Constraints on Actuation and the Use of Multiple Switches

The current in the energy storage coil as a function of time during a single pulse is illustrated in Figure 21. At the required rate of five pulses per second, the total time per pulse, t_p, is 0.2 seconds which is divided among: (1) the interval required for charging, t_c; (2) the interval required to electrically disconnect the energy storage coil from its power supply, t_a; (3) the time required to discharge the coil, t_d; and (4) the time from the end of discharge to the beginning of the next charge, t_i. During t_c the switch is closed and dissipates energy at a rate determined by the resistance of its leads and its contact resistance. During t_a the switch contacts open, an arc is drawn and energy is dissipated in the arc and switch leads though the latter is insignificant. During t_d and t_i the switch is essentially non-dissipative.

If an upper limit is fixed for allowable switch losses, the maximum allowable arcing time consistent with this constraint may be shown to be:

$$t_a = \frac{[E_e - (I_o^2 R_s t_c)/3]}{V_a I_o}$$

where:

E_e = allowable switch loss

I_o = peak current

R_s = switch resistance when closed

t_c = charge time

V_a = voltage drop across arc

t_a = maximum allowable arcing time consistent with E_e

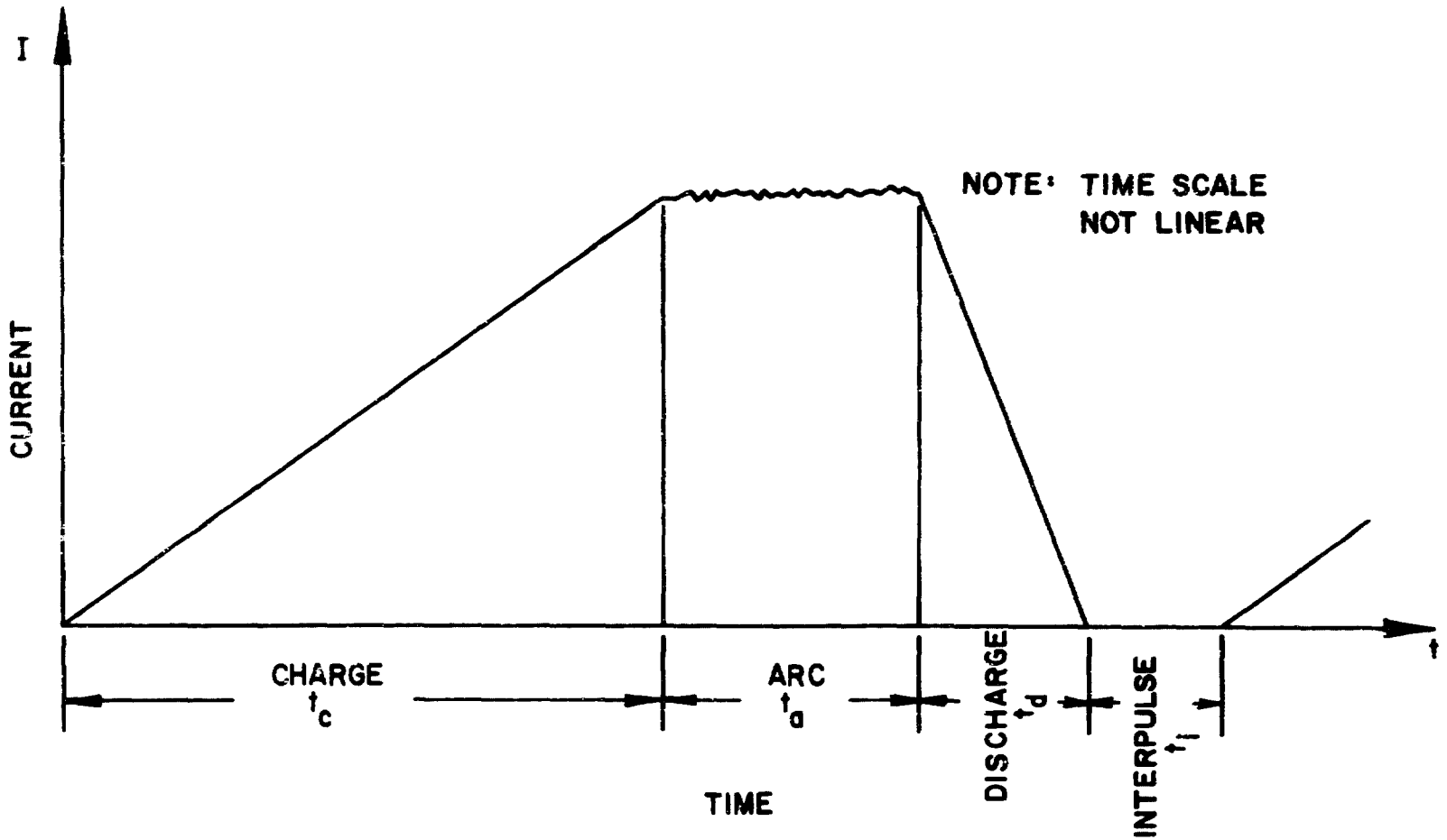

Figure 21. Sketch of a single current pulse on an expanded time scale. During charge time t_c, the switch must be closed and have minimum resistance; the switch opens and an arc forms during the interval t_a at the end of which the arc is extinguished and the energy storage coil discharges.

The above is plotted in Figure 22 as a function of switch resistance for an allowable switch loss of 5,000j, a charge time of 0.1⁹ sec and several arcing voltages. Arc voltages in the 100–200 volt range correspond to currents of the order of 20,000a (see Figures 5 & 6) while arc voltages in the 20–40 volt range correspond to currents of the order of 6,000a or less (see Figure 5). The band between the 100 and 200 volt curves in Figure 22 correspond, therefore, to a switch system in which the entire 20,000a is carried in a single vacuum switch while the band between the 20 and 40 volt curves corresponds to a switch system in which the 20,000a is divided among vacuum switches in parallel. If 0.1 milliohms is assumed as a reasonable design goal for a total switch resistance when closed, Figure 22 indicates that a single switch carrying 20,000a must open and its arc must be extinguished in less than 1.5 millisec in order to keep the switch loss per cycle below 5,000j. Since the contact gap must be of the order of 1 cm or greater to withstand the 100 KV imposed after arc break, the 1.5 millisec requirement for contact travel places a severe requirement on the switch actuation mechanism. On the other hand, the figure indicates that switches in parallel may be allowed 3.5 to 6.5 milliseconds for contact travel which places a more realistic demand on the actuation mechanism.

The contact travel requirement for both the single switch and the parallel switches is essentially the same since they must both withstand 100 KV after arc break. Furthermore, the contact mass for the single switch may be assumed to be the same as the total contact mass of the parallel switches if the current density in each system is the same. The average power required to open the contacts may be estimated by:

$$P_{ave} = 2m \frac{d^2}{t^3}$$

where:

m = contact mass

d = contact travel

t = travel time

If travel times of 1 and 5 milliseconds are assumed for the single and multiple switches, respectively (see Figure 22) and if equal mass and equal contact travel are assumed as indicated above, then the average power required for the single switch is 125 times that required for the multiple switches.

The requirement for faster operation also requires the actuation linkage for the single switch to be heavier since the forces transmitted are larger. To a first approximation the weight of the linkage may be shown to be inversely proportional to the square of the actuation time, hence, for the operating times chosen above, the linkage for the single switch would be 25 times heavier than that for the multiple switches.

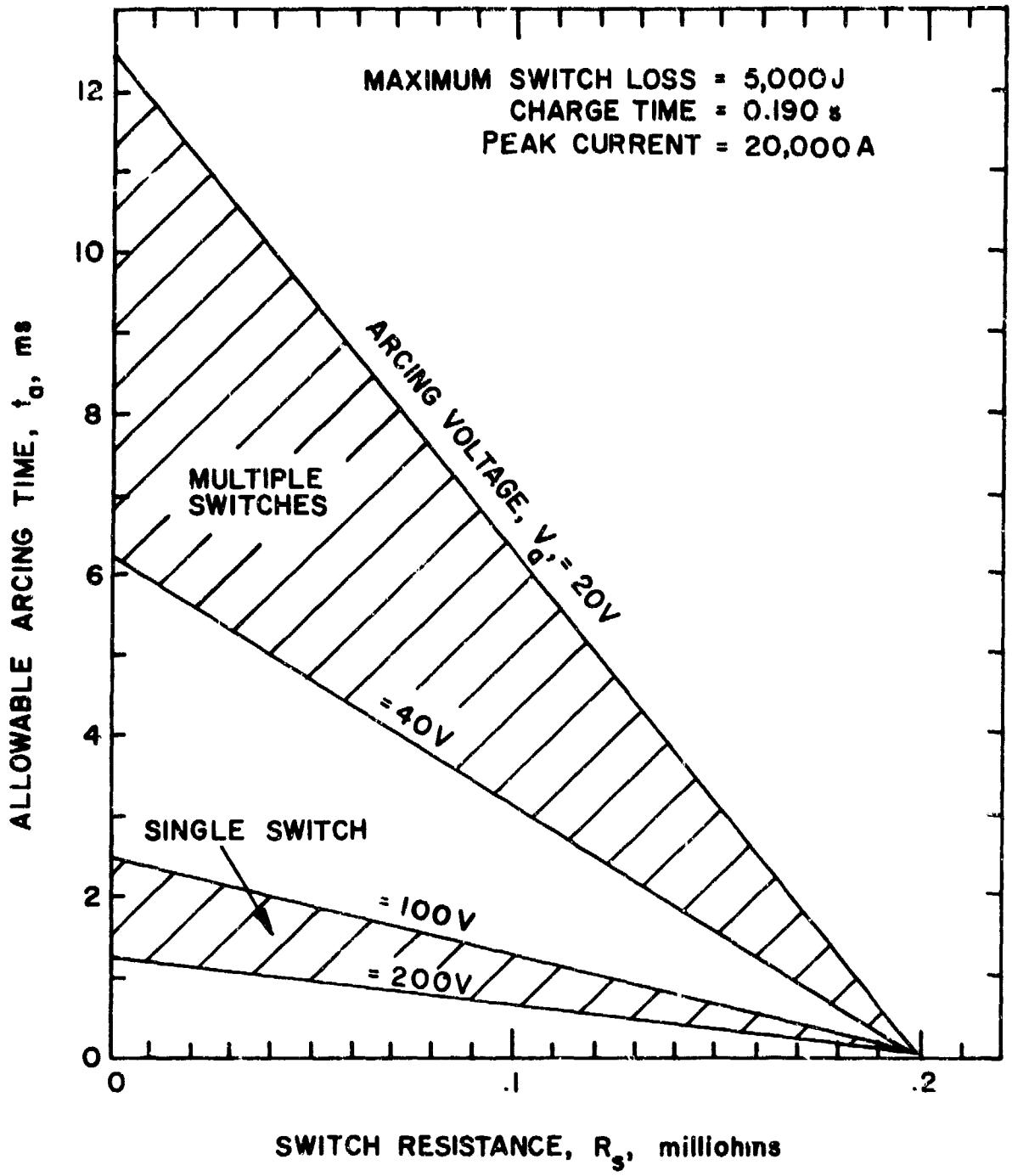

Figure 22. Maximum allowable arcing time consistent with a fixed total switch loss as a function of closed switch resistance and arc voltage drop.

This approximation neglects effects such as the difference in length of the linkage for the two systems. Such effects may alter the result by as much as a factor of two, but the basic conclusion is unchanged: the linkage for the single switch may be expected to be as much as an order of magnitude heavier than that required for all the multiple switches because of the difference in required operating time.

The above discussion indicates that multiple switches in parallel place less stringent demands on the mechanical actuation mechanism. The total weight of the multiple switches may be expected to be slightly more (contact weight essentially the same, but more connectors and greater total surface area for vacuum shells, vapor condensing shields, etc.). This is compensated for by a lighter actuating linkage and reduced power requirement. A summary of these results is given below:

allowable operating time: $\frac{\text{single switch}}{\text{multiple switches}} \sim 0.2$

average power required for actuation: $\frac{\text{single switch}}{\text{multiple switches}} \sim 100$

weight of actuating linkage: $\frac{\text{single switch}}{\text{multiple switches}} \sim 10$

weight of switch components: $\frac{\text{single switch}}{\text{multiple switches}} \sim 1$

In addition to the above, it must be noted that a single switch will require a 20,000a arc to be extinguished as opposed to the lower arc currents in the multiple switch arrangement. In the latter, however, problems of extinguishing parallel arcing switches must be solved.

The conclusion to be drawn is that a multiple switch arrangement offers a better chance of achieving a low-weight, low-loss system provided the problems associated with simultaneously extinguishing parallel arcing systems may be solved.

e. Switching Alternates

The following will outline several alternates for performing the switching function in an inductive energy storage system. For arcing elements the presence of a switch support subsystem (arc quench circuit) is implicitly assumed. The choice among the alternates which are listed below must be determined by data generated in an experimental development program, however, several advantages and disadvantages may be listed beforehand:

1) linearly actuated switch with single contact pair
2) linearly actuated switch with multiple contact pairs in parallel
3) two-terminal rotary switch in parallel with linearly actuated arc interrupter
4) three-terminal rotary switch with arc chute.

Item 1 represents an advanced vacuum interrupter which would carry the full charge current from zero to its peak value then open, arc, break, reclose, etc. A prototype design for a test unit of this type will be discussed in Section III, and will utilize cryogenic cooling and an applied magnetic field. It is unlikely that this configuration can fulfill the 5000 J constraint on switch loss per cycle because of the high voltage drop associated with the 20,000 A single arc as indicated in the previous section. Furthermore, operation at rates substantially in excess of the 5 pulses per second required by this program is unlikely. The advantage to this alternate lies in the fact that it appears to be a feasible step forward in standard vacuum interrupter design if applied field and cryogenic effects are utilized.

Alternate number 2) also involves a linearly actuated device, but would utilize multiple pairs of contacts in parallel. Estimates indicate that this would be lighter and require less actuation power than alternate 1), however, the major disadvantage lies in the necessity to develop techniques to reliably extinguish multiple parallel arcs simultaneously without restrike.

The third alternate would utilize two switches in parallel. The first would be a rotary device designed to be a compact, low-loss unit intended primarily for the charging portion of the cycle. Near the end of the charge, a relatively high resistance parallel switch would close and allow the rotary switch to open. When the rotary device was opened sufficiently far to withstand the system discharge voltage, the parallel linearly actuated switch would open, arc and extinguish the arc. The rotary switch could be compact provided a high current density brush system were available. (Note: Test results on a filamentary brush system operated at current densities of about 3000 $A/in.^2$ will be given in Section IV.) The linearly actuated switch could be more compact than those in alternates 1) or 2) because it carries current for a much smaller fraction of the cycle. An increase in repetition rate beyond 5 pps by factors of two or three may be possible because the linear switch would be less massive than in alternates 1) or 2).

Alternate number 4) is a three-terminal rotary switch which operates in a fashion electrically similar to that described for alternate 3). Both the highly conducting charge "switch" and arc interrupter are rotary in nature and a device of this type will be discussed in Section IV. Its major advantage lies in its potential for increasing repetition rate by orders of magnitude because the rotary action negates the acceleration problems inherent in a linearly actuated device. The major problem areas involve: 1) development of a high current density brush system, 2) generation of data on arc and magnetic field interractions and 3) generation of data on effects of arcing on brush life.

SECTION III.

LINEARLY ACTUATED SWITCH

The previous section discussed the advantages of incorporating: (1) a vacuum environment, (2) cryogenic cooling and (3) a transverse magnetic field relative to an arc between contacts, in a switch designed to fulfill the stringent requirements of this program. This section will describe a linearly actuated switch designed to carry 20,000 A peak current and withstand 100,000 volts when open. A discussion is then given of a prototype which has been constructed with the design flexibility necessary to investigate cryogenic and magnetic field effects on switch operation. Consideration is then given to the test circuit necessary to operate the switch to the design limits of 20,000 A and 100 KV.

1. SWITCH DESIGN WITH APPLIED FIELD & CRYOGENIC COOLING

In Section II. of this report, the basic characteristics of a standard vacuum interrupter were described (Figure 8). The following will discuss an advanced vacuum interrupter which was designed to make use of cryogenic cooling and an applied magnetic field. A drawing of this linearly actuated switch is shown in Figure 23. The following is a descriptive list of some of the components of the switch with numbers corresponding to those shown in the drawing.

1. Stationary high voltage terminal (OFHC copper)
2. Removeable contacts on stationary and moveable terminals
3. Coolant shroud for stationary terminal
4. Moveable low voltage (grounded) terminal
5. Bearing
6. Bellows Position when contacts open
7. Bellows Position when contacts closed
8. Coolant chamber surrounding moveable contact
9. Non-conducting outer housing of interrupter
10. LN_2 fill and vent tubes for cooled vapor deposition and radiation shield.
11. LN_2 cooled vapor deposition and radiation shield
12. LHe cooled shield with molecular sieve coating to perform cryo-pumping of vacuum space.

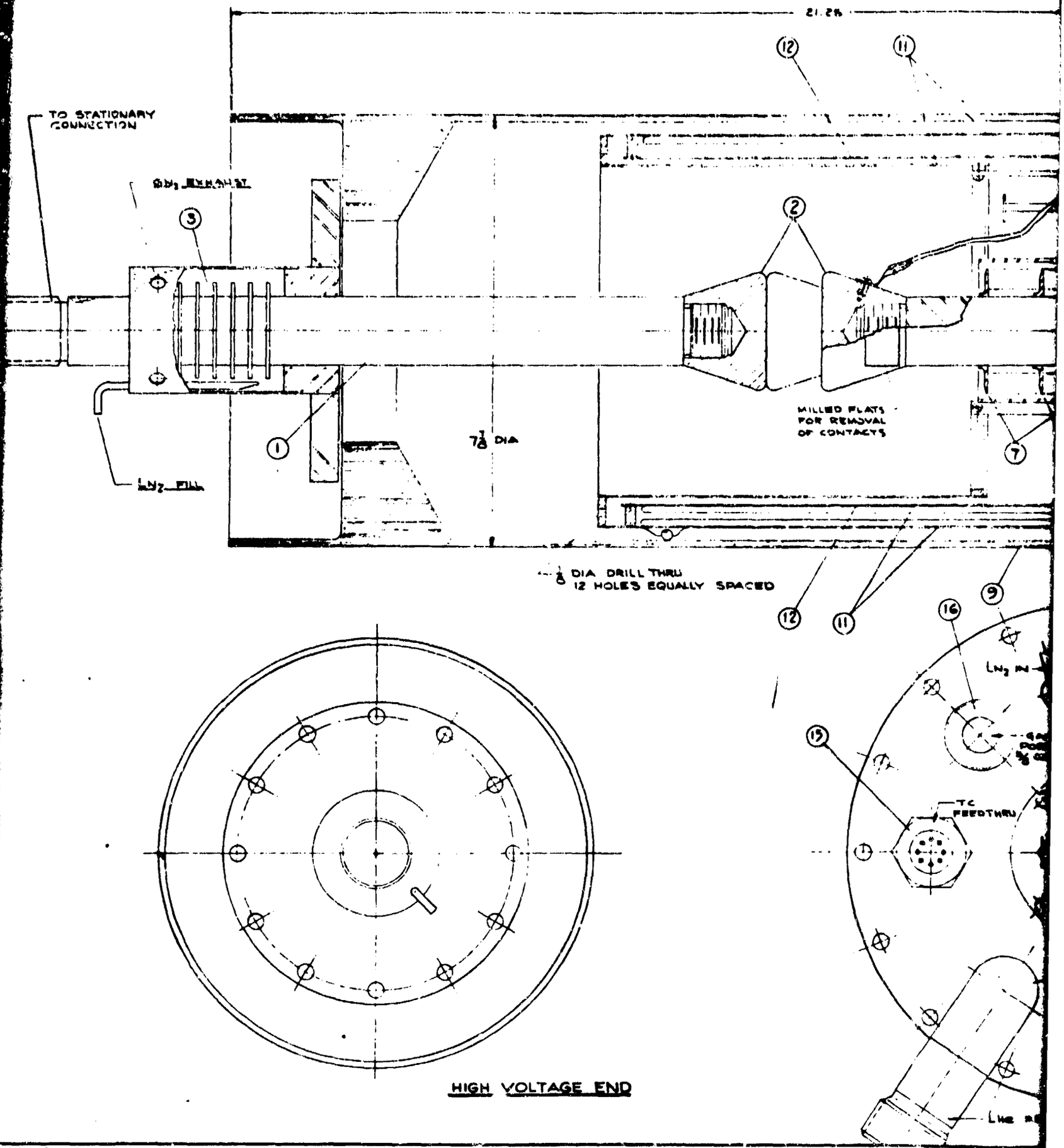
TO STATIONARY CONNECTION
GN_2 EXHAUST
LN_2 FILL
7/8 DIA
MILLED FLATS FOR REMOVAL OF CONTACTS
1/8 DIA DRILL THRU 12 HOLES EQUALLY SPACED
LN_2 IN
TC FEEDTHRU
HIGH VOLTAGE END

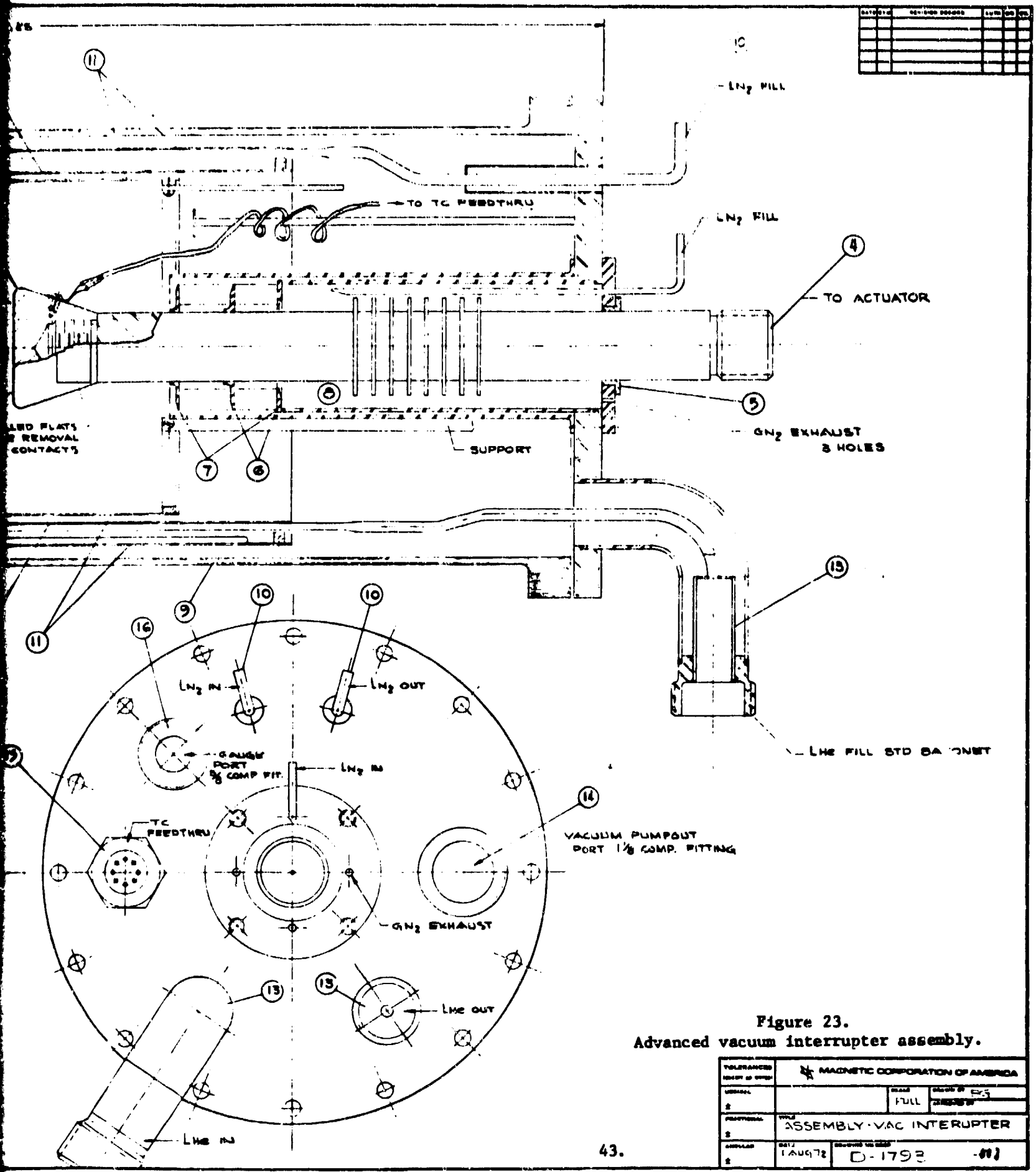

Figure 23.
Advanced vacuum interrupter assembly.

MAGNETIC CORPORATION OF AMERICA	
SCALE FULL	DRAWN BY BS
TITLE ASSEMBLY-VAC INTERUPTER	
DATE 14AUG72	DRAWING NO. D-1792 -001

13. LHe fill and vent ports for cooled shield

14. Vacuum pump-out port

15. Thermocouple multipin feedthrough

16. Port for vacuum gauge.

The switch features heat exchangers on the stationary and moveable leads. These are suitable for use with liquid nitrogen and allow the cross-sectional area of the contact arms to be relatively small. In addition, cryogenic cooling is used on the vapor condensation shields. These consist of three nested cylinders, with the inner and outer cylinders cooled by liquid nitrogen and the middle cylinder cooled by liquid helium. The purpose of the liquid nitrogen cooled shields is to intercept radiation and shield the liquid helium temperature cylinder.

In carrying out the design, the overall diameter was made as small as possible, consistent with tolerances required for assembly and the design "withstand" voltage. This will allow the switch to be mounted in the bore of a specially constructed field coil which could produce a controlled magnetic field in the contact region. The contacts shown are OFHC copper butt electrodes and would be used in initial testing to establish a base line for switch performance without the applied field, cooled shields, or cooled contacts.

The contacts in the switch are removeable so that different contact materials or different contact shapes could be tested. A contact configuration which would utilize the magnetic field to move the arc is illustrated in Figure 24. When the contacts part, the arc is drawn in the conical annulus between the contacts. The arc current interacts with the magnetic field and the resultant Lorentz force drives the arc around the periphery of the contacts. This arc motion enhances switch performance by preventing excessive electrode heating locally, increasing the arc resistance by impeding charge motion across the field lines and creating a "back emf" which appears as an increased arc voltage drop.

Photographs of the partially assembled linearly actuated switch are shown in Figures 25 and 26. Figure 25 shows the movable contact mounted on the actuating rod which projects through the bottom of the fixed flange. The vacuum seal between the moveable rod and the fixed portion of the switch is provided by a welded bellows which is compressed in the photograph and appears as a collar around the shaft on top of the cylinder welded to the fixed flange. The three relatively tall rods on top of the flange are phenolic stand-offs which will support the vapor condensation shields within the switch. The two short cylinders which can be seen on top of the flange are fittings which position two of the tubes which will carry cryogens to the shields.

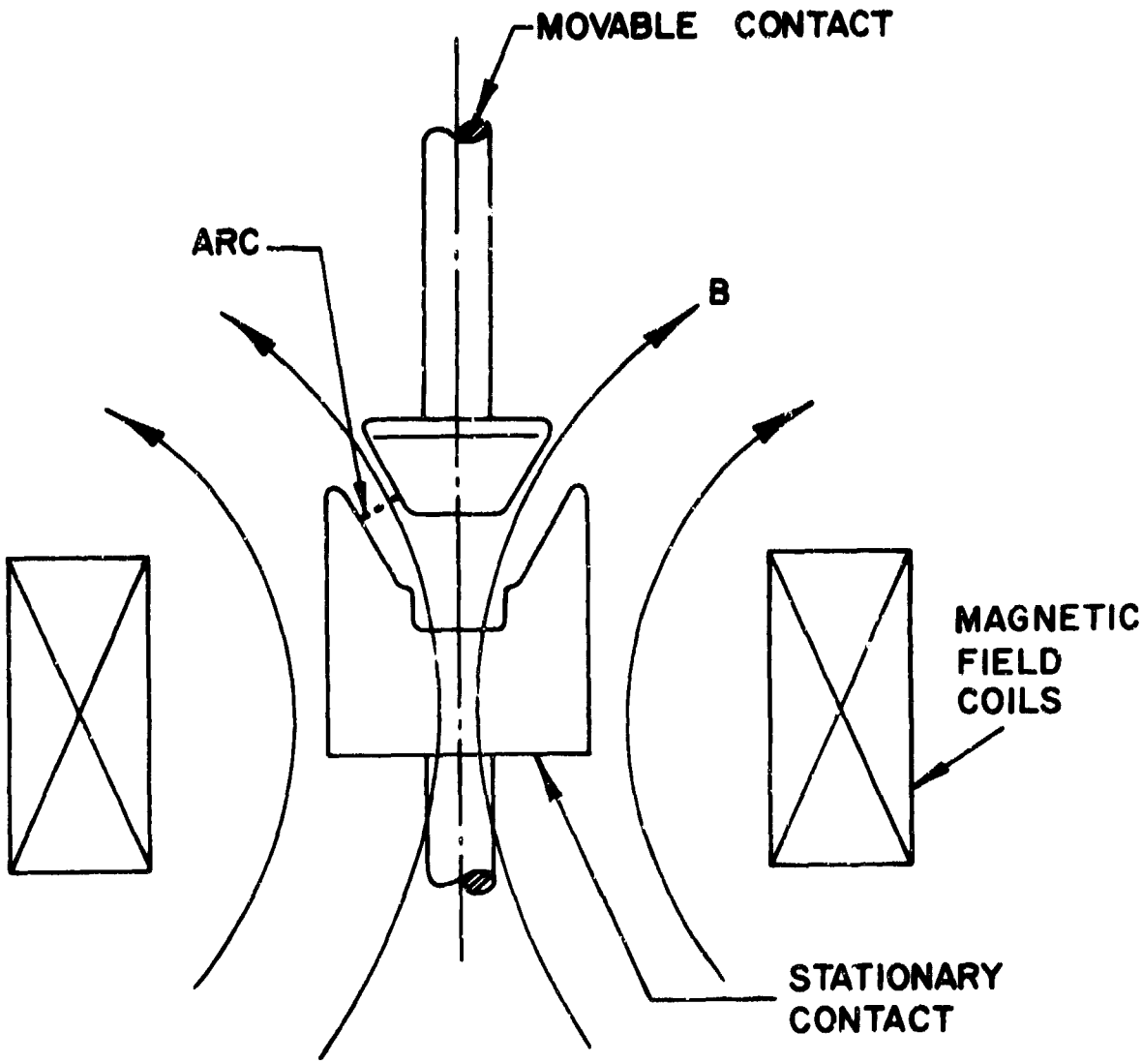

Figure 24. Possible contact configuration for production of magnetic field component perpendicular to arc column.

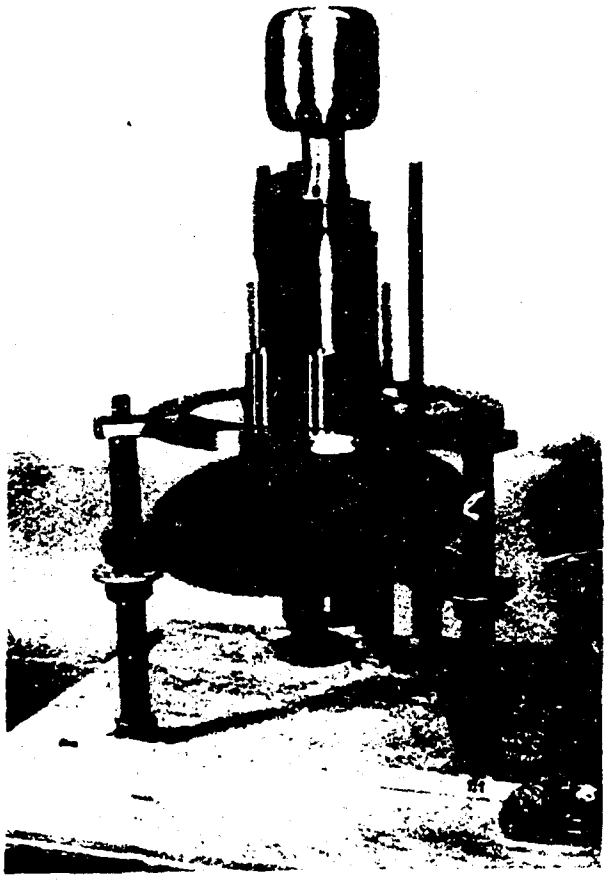

Figure 25. Partially assembled, vertically mounted, linearly actuated switch. The photograph shows the movable electrode and contact mounted relative to the fixed base plate.

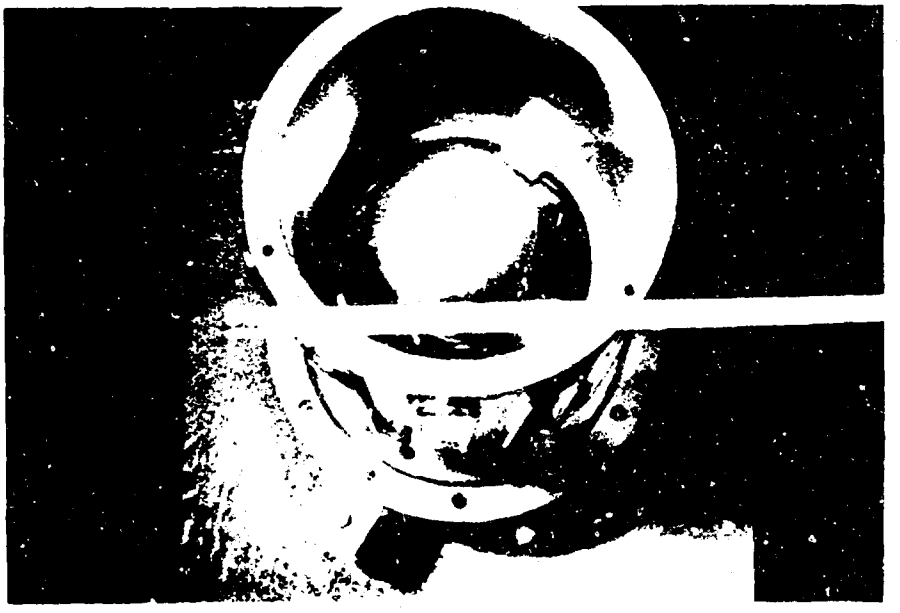

Figure 26. Top view of the switch showing the relative position of the vapor condensation shields and the movable contacts. The vapor condensation shields are provided with tubes through which cryogens may be pumped to reduce their temperature.

Figure 26 is a view looking down on the moveable contact when the vapor condensation shields are in place. The coolant tubes are visible on the outside of the shields. The tubes shown will carry liquid nitrogen or cold nitrogen gas and will cool the shield shown which consists of two concentric cylinders with an annular ring on top. A liquid helium cooled shield (not visible) is located in the annular space between the two concentric nitrogen cooled cylinders. The purpose of the helium cooled shield is to cryovacuum-pump the switch.

A photograph of the switch at a later stage in the assembly process is shown in Figure 27. Surrounding the contacts and cryogenically cooled shields is the vacuum envelope. This shell, made from an epoxy impregnated glass composite material, serves two basic functions. First, it insulates the fixed upper contact (anode) from the moveable lower contact (cathode). Second, it serves as the vacuum container for the device. Just below the vacuum envelope, the helium fill and vent ports, as well as the vacuum pump out port, are visible. The liquid nitrogen fill and vent tubes (not visible in this photograph) are located on the other side of the device. Below the helium fill and vent ports, the switch actuation mechanism is visible. This mechanism was designed for use in the single pulse mode and consists of four springs and a pneumatic cylinder. Just below the cryogen ports, two of the four control springs are visible. When the switch contacts are closed, the springs are compressed. Pneumatic separation of the switch contacts is aided by the spring forces. The motion of the moveable contact may thus be controlled by changing the air pressure in the actuating mechanism and/or by changing the tension on the control springs.

To achieve five pulses per second (multiple pulse mode), the actuator could be changed to a hydraulic system. This will not be considered here, but is considered feasible since a hydraulic actuation mechanism was designed, constructed, and operated at a rate of five pulses per second with a standard vacuum interrupter at MCA. Details concerning the design of that actuator were reported in AFAPL-TR-72-38-Vol I, Dec. 1972. For the actuator for this system the design would be similar since the moveable contact mass and stroke are comparable.

In an integrated system, the switch could be mounted in the base of the energy storage coil such that the magnetic field produced by the coil was utilized in switching. In such a system the switch and coil would be in series, consequently the magnetic field experienced by the switch would be dependent on the current through it. At present the effects of the magnetic field on the switching process are not well understood, consequently in an experimental system it would be desirable to have independent control over the applied field and the switch current. This requires a switch test circuit (to be described later) which is independent of the field coil circuit.

In order to provide a magnetic field of substantial strength (≥ 2 Wb/m^2) in a bore large enough to contain the switch described above, the decision was made to construct a liquid nitrogen cooled coil which would be driven by a constant voltage power supply. Table V presents a summary of the characteristics of this coil.

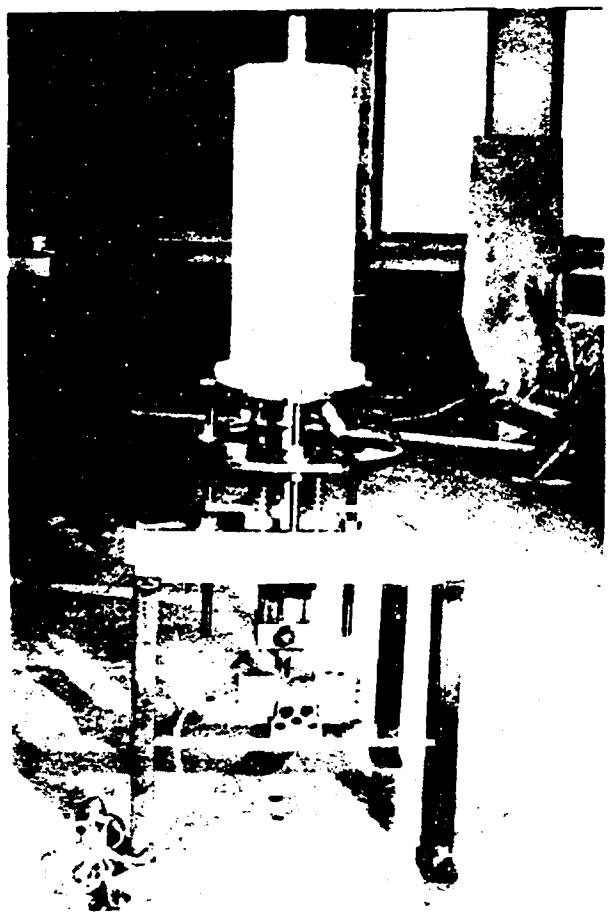

Figure 27. Linearly actuated switch mounted on base with insulating vacuum envelope in position. Also visible are the cryogen fill and vent ports, two of the four adjustable linear motion control springs, and the actuation mechanism.

Table V.

Field Coil Characteristics

Inner Winding Diameter	22.8 cm (9.0 in.)
Outer Winding Diameter	41.9 cm (16.5 in.)
Winding Depth	33.0 cm (13.0 in.)
Conductor	8 strands of AWG #8 heavy formvar insulated copper
Connection	parallel
Number of Turns	250
Inductance (measured)	9.8 mH
Room Temperature Resistance (measured)	61 mΩ
Operating Temperature	77°K
Initial Operating Resistance (calculated)	8.72 mΩ

The total wire length in the coil is 6500 ft. and the coil weight is estimated at 350 lbs.

The field coil is suitable for mounting with axis vertical in a non-conducting, liquid nitrogen container as shown in Figure 28. The prototype linearly actuated switch would be mounted in the warm bore of the coil with high voltage end extending from the top and the moveable, low voltage end projecting from the bottom where it would be connected to the actuator.

Several field coil transients have been calculated and are given in Figures 29 and 30. Figure 29 is a plot of the central magnetic field and coil temperature as a function of time for a constant applied voltage of 10 volts. Figure 30 is a plot of the central magnetic field and coil temperature as a function of time for a constant applied voltage of 30 volts. Power supply internal impedance was neglected for these calculations.

In a typical transient, a battery bank would be connected to the field coil at t = 0. The rate of field rise is then primarily dependent on voltage and coil inductance. The field rises to a peak value, then begins to decay because of the increase in coil resistance with time which results because of joule heating. Figure 30 illustrates that with a power supply voltage of 30 volts, the peak field of 2.1 Wb/m^2 is attained after 4 seconds and that, after 100 seconds, the coil temperature rises 100 K with an attendent field decay to 0.65 Wb/m^2. It is clear that higher applied voltages lead to higher peak fields, faster temperature rises, and shorter working times in the vicinity of the peak field.

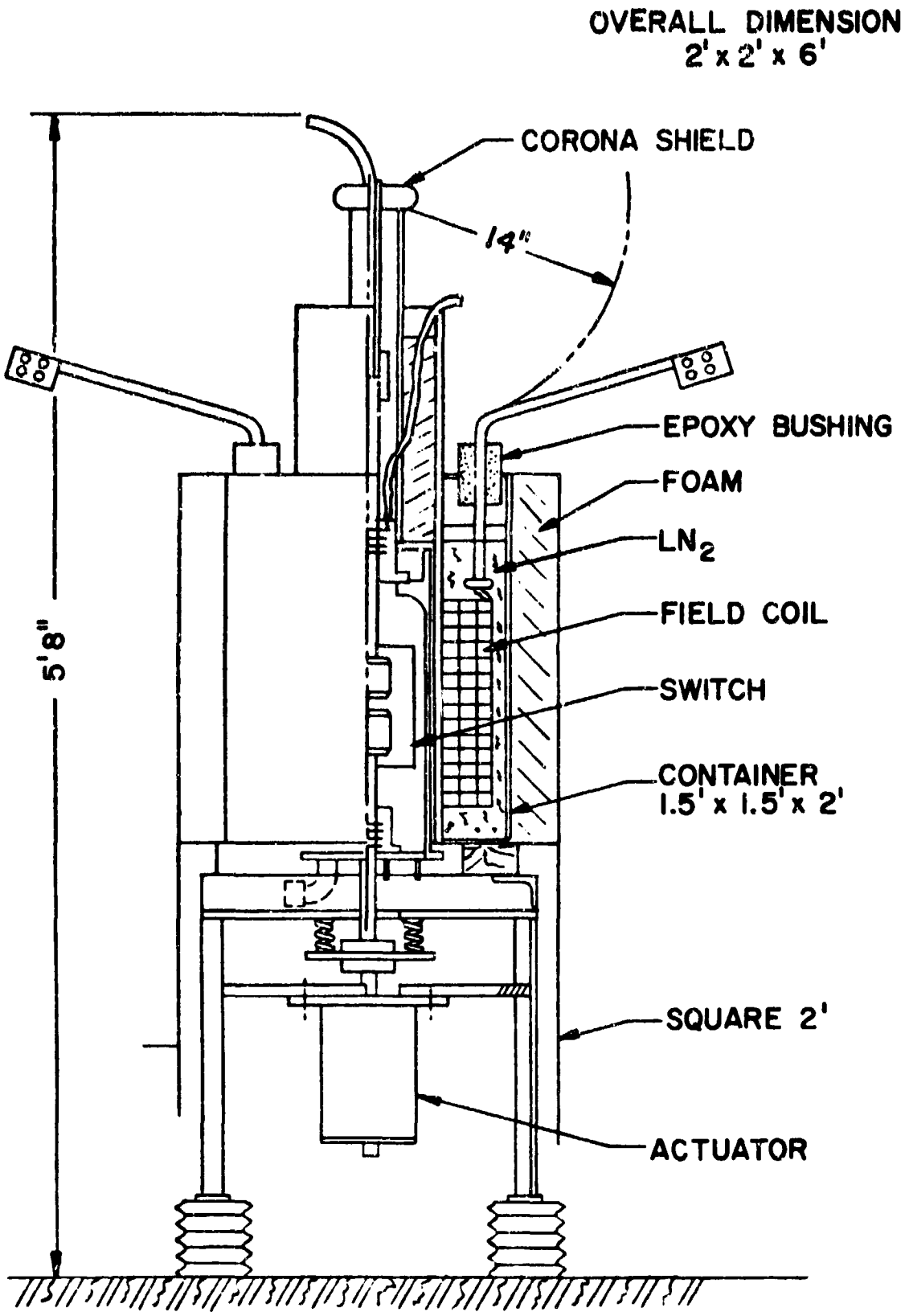

Figure 28. Prototype linear switch mounted in bore of field coil and dewar.

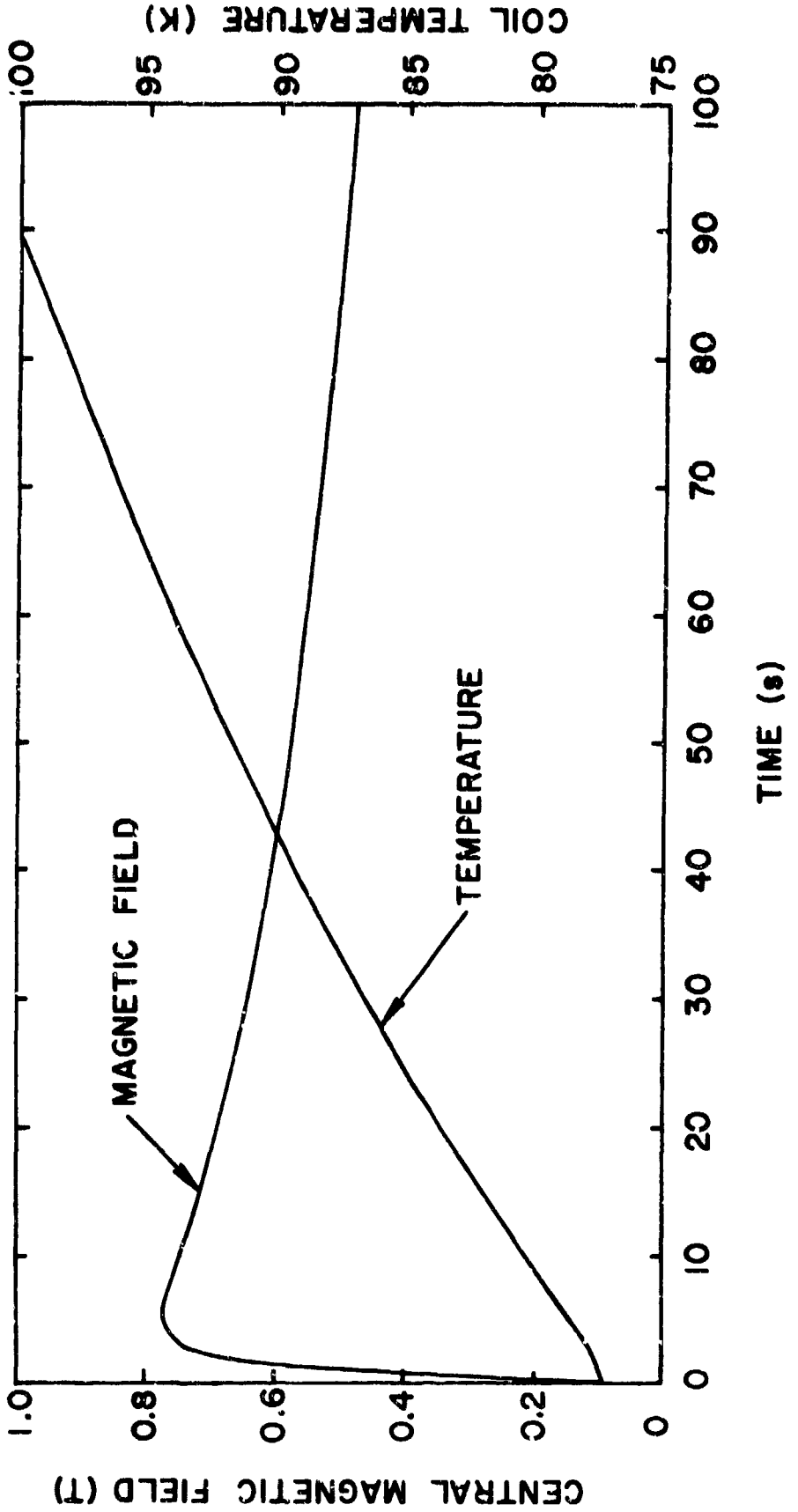

Figure 29. Field coil transient for a constant applied voltage of 10 volts.

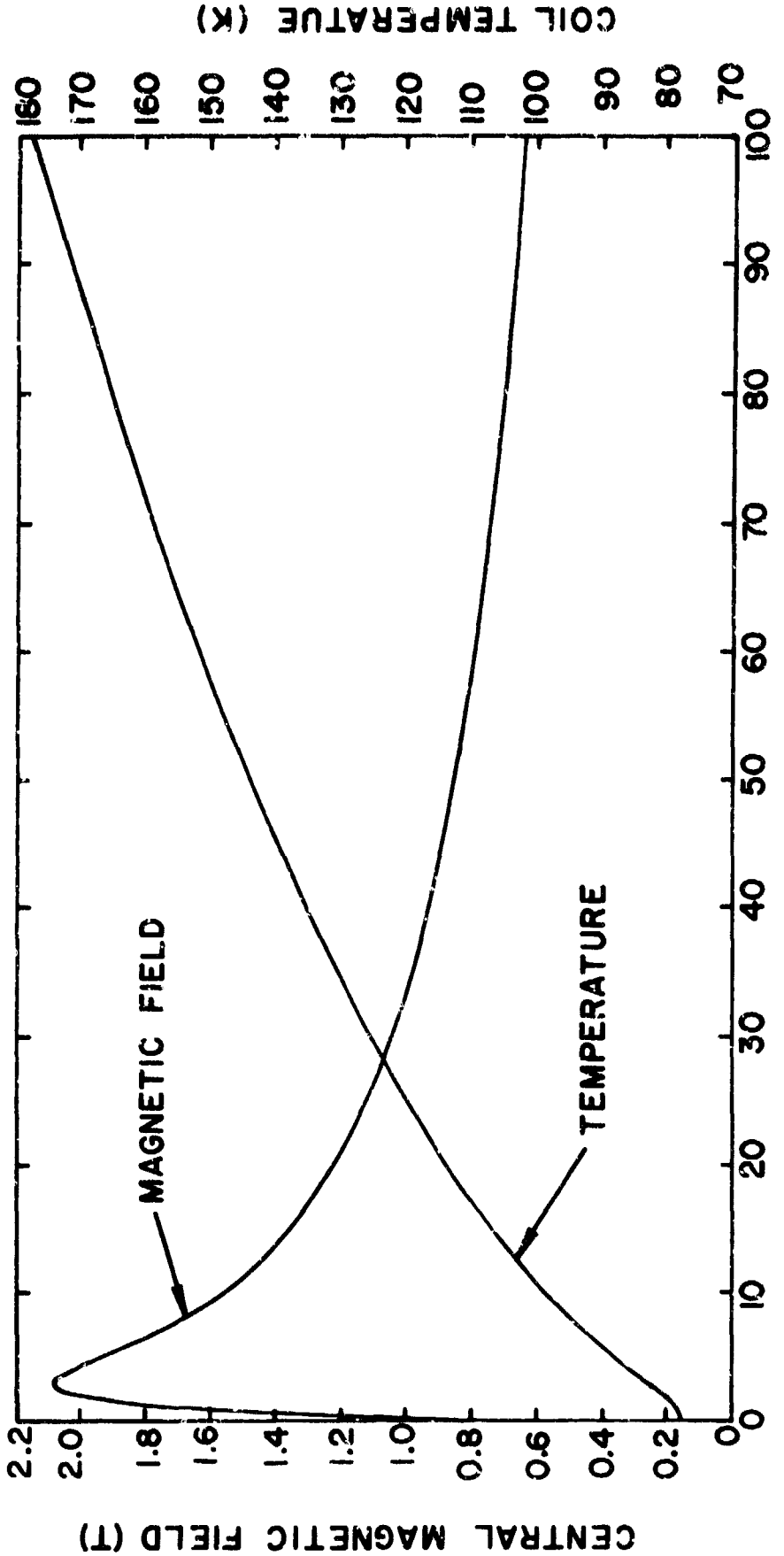

Figure 30. Field coil transient for a constant applied voltage of 30 volts.

Figure 31 is a calibration curve for the field coil and gives the magnitude of the magnetic field at the center of the contact plane of the linear switch electrodes as a function of the coil current. Field uniformity in the vicinity of the electrodes is given in Figures 32 and 33. Figure 32 is a plot of the magnetic field along the axis of the coil as a function of distance from the plane of contact of the linear switch electrodes. The field has been normalized to the value of the field at the plane of contact so that this one plot may be used at any current level. Figure 33 is a plot of the axial component of the magnetic field as a function of the distance perpendicular to the coil axis. These measurements were taken in the contact plane of the switch electrodes. Again, the field has been normalized to the value of the field at the center so that this one plot may be used at any current level.

The liquid nitrogen requirement for the field coil has been calculated and is shown in Figure 34 as a function of coil total "on time" for various values of central field. The graph indicates, for example, that operation at 2 Wb/m^2 for one minute will require about 50 liters. The results do not take into account the heat transfer characteristics of the winding and bath. These effects limit the maximum field which can be generated in the steady state. At levels above this value (2.5 Wb/m^2) the required heat transfer to the bath is higher than that which can be supported continuously, consequently total "on time" must be limited to prevent an unsafe increase in winding temperature. In operation, the coil voltage drop would be monitored continuously since this is an indicator of average coil resistance and, in turn, average temperature.

2. TEST CIRCUIT

To provide a realistic test of the switch, an energy storage component is required in the switch circuit. Without the inductive component (load coil), a power supply such as a battery bank cannot provide sufficient voltage to sustain the arc after the switch opens. Consequently, the arc would extinguish and a "successful," but unrealistic break of the circuit would occur.

Figure 35 is an illustration of a switch test circuit in which the switch would be placed in series with a battery bank and load coil. A back-up circuit breaker would also be used in the line but is not shown. The diagram of the switch shows the stationary and moveable contacts which pass through the conducting end flanges of the switch. The flanges are held in position by the non-conducting shell. The sketch also shows the nitrogen cooled and helium vapor condensation shields which are fed by tubes which pass through the lower flange. During operation, following each arc break, the stationary contact and upper flange will experience a high voltage V_2 determined primarily by the current level before break and the magnitude of the resistor across the load coil. Following arc break the voltage on the low side of the switch, V_1, will attain a value determined primarily by the line inductance.

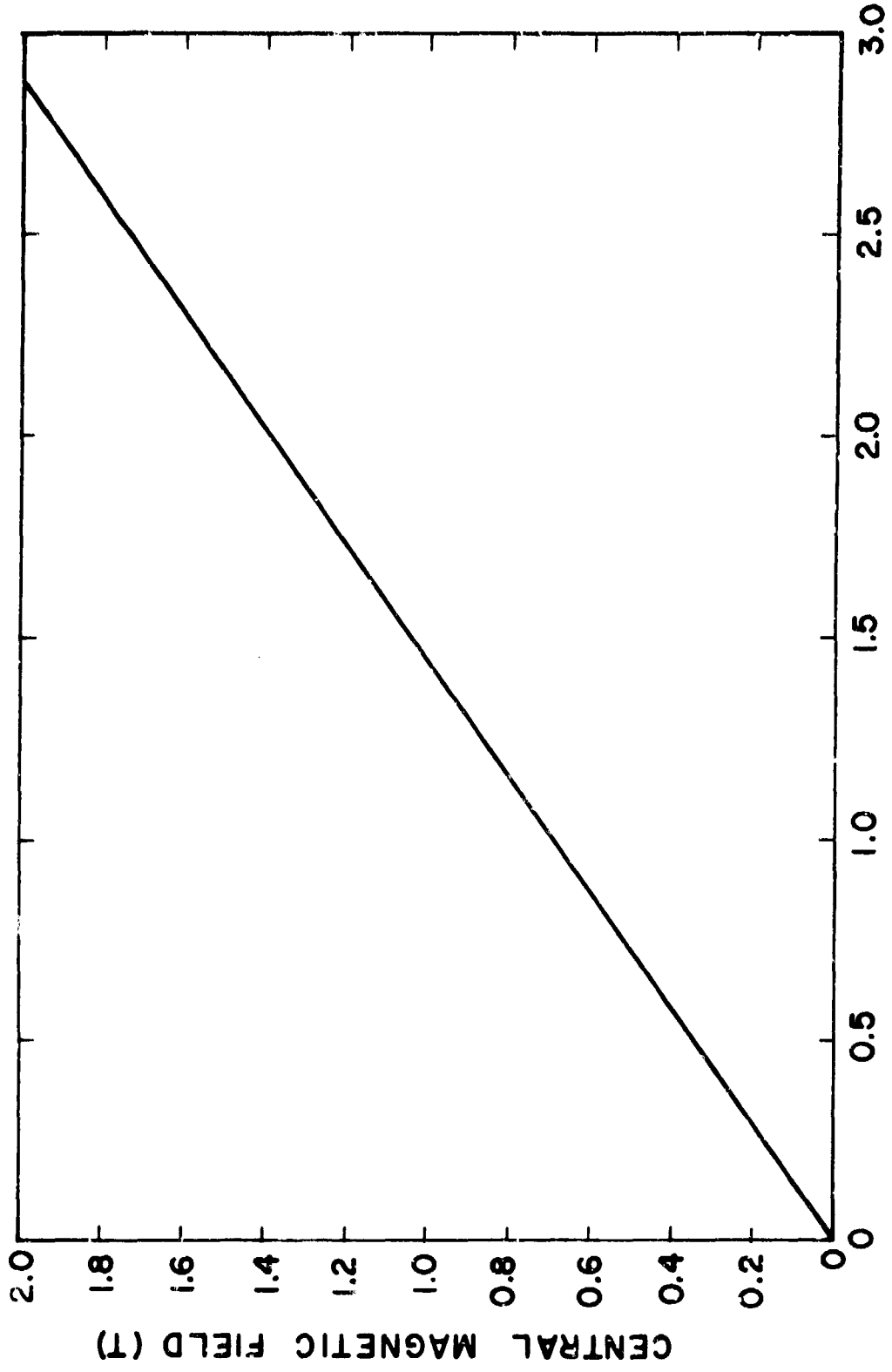

Figure 31. Magnetic field at the linearly accuated switch contacts as a function of the current in the field coil.

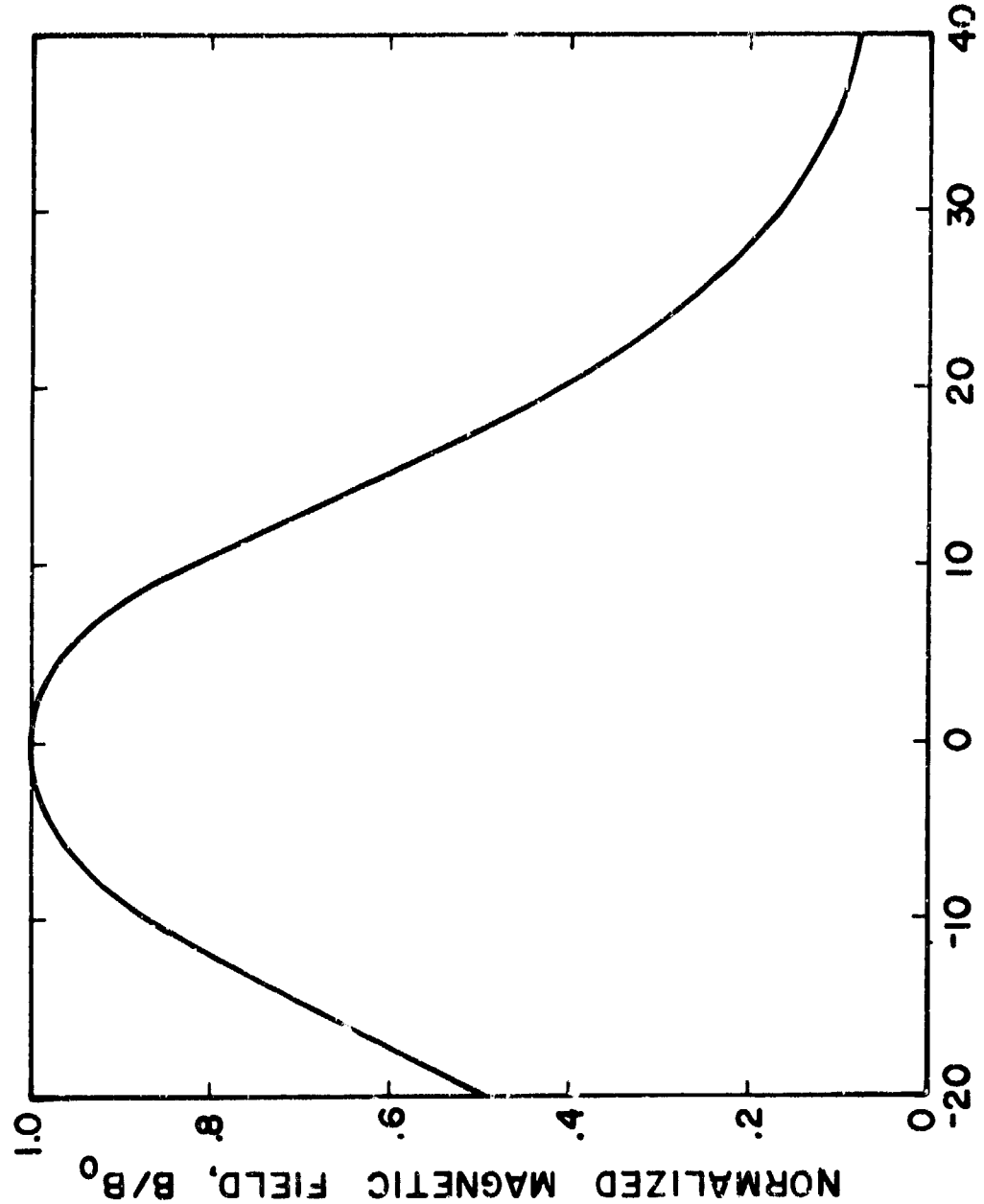

Figure 32. Normalized measured magnetic field on the axis of the field coil as a function of the distance along the axis from the expected switch electrode contact plane.

FA ITE 0

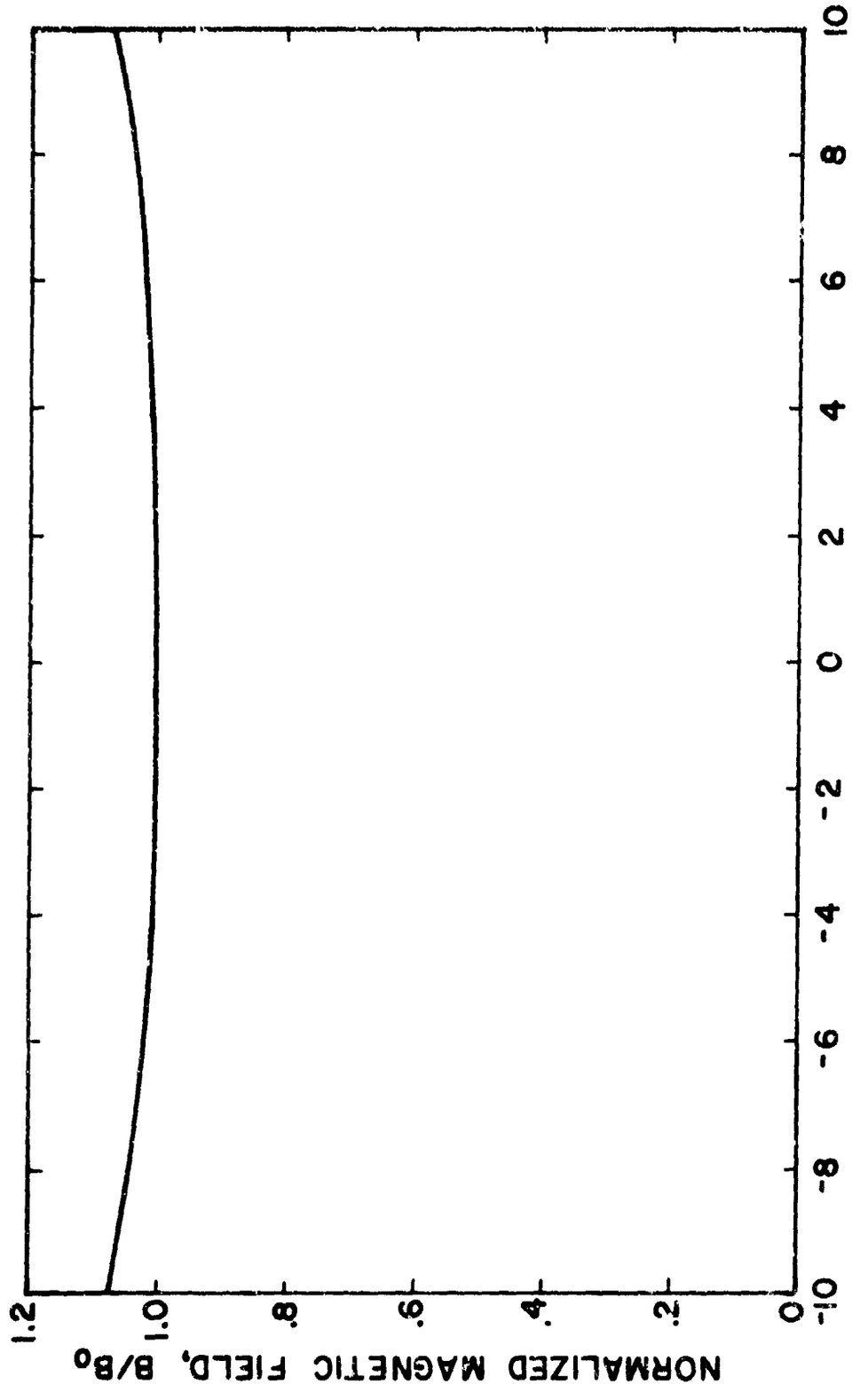

Figure 33. Normalized measured magnetic field of the field coil as a function of the distance from the axis. Measurements were taken in the expected contact plane of the switch electrodes.

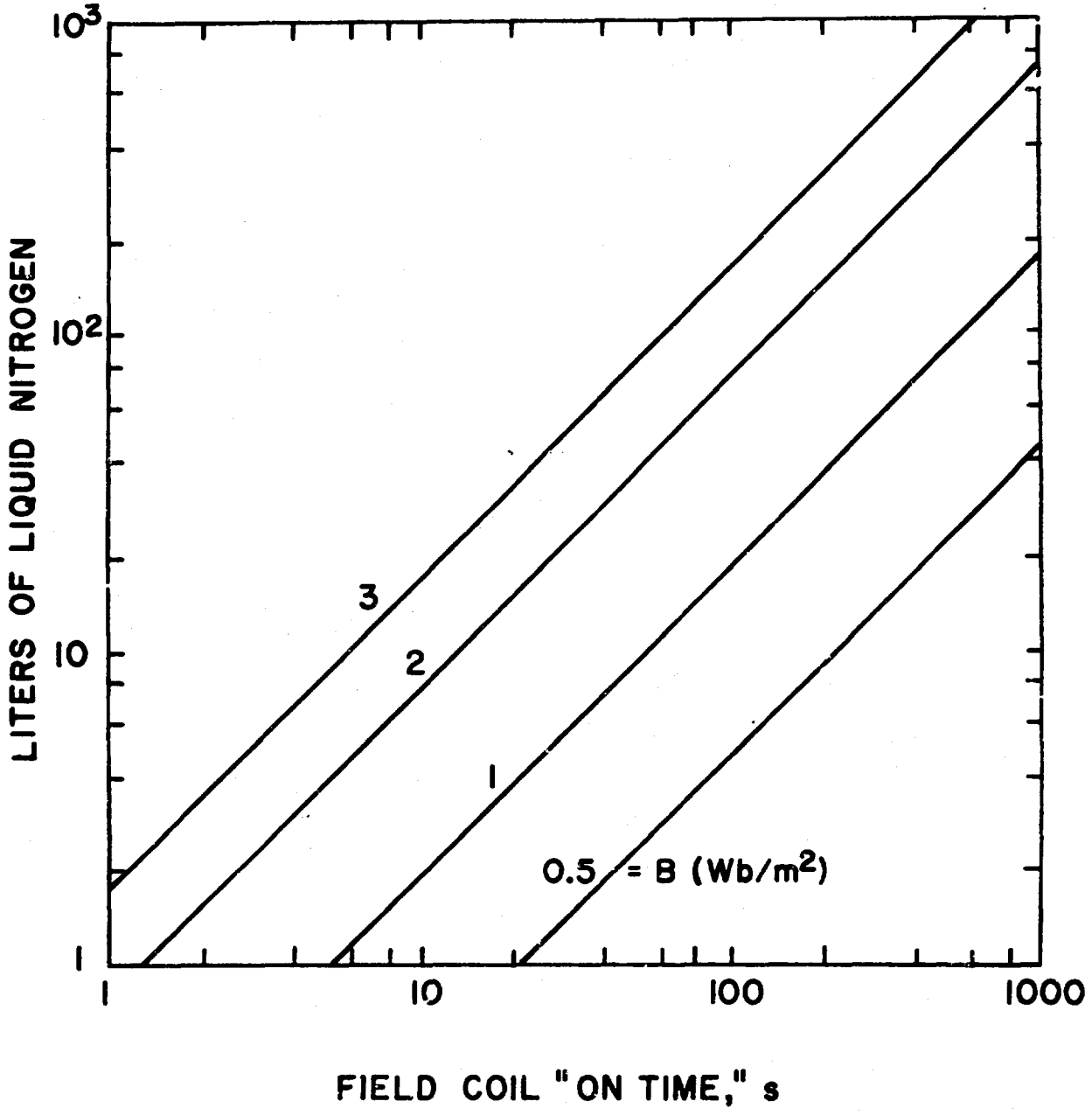

Figure 34. Liters of liquid nitrogen consumed by field coil as a function of field level and total "on time."

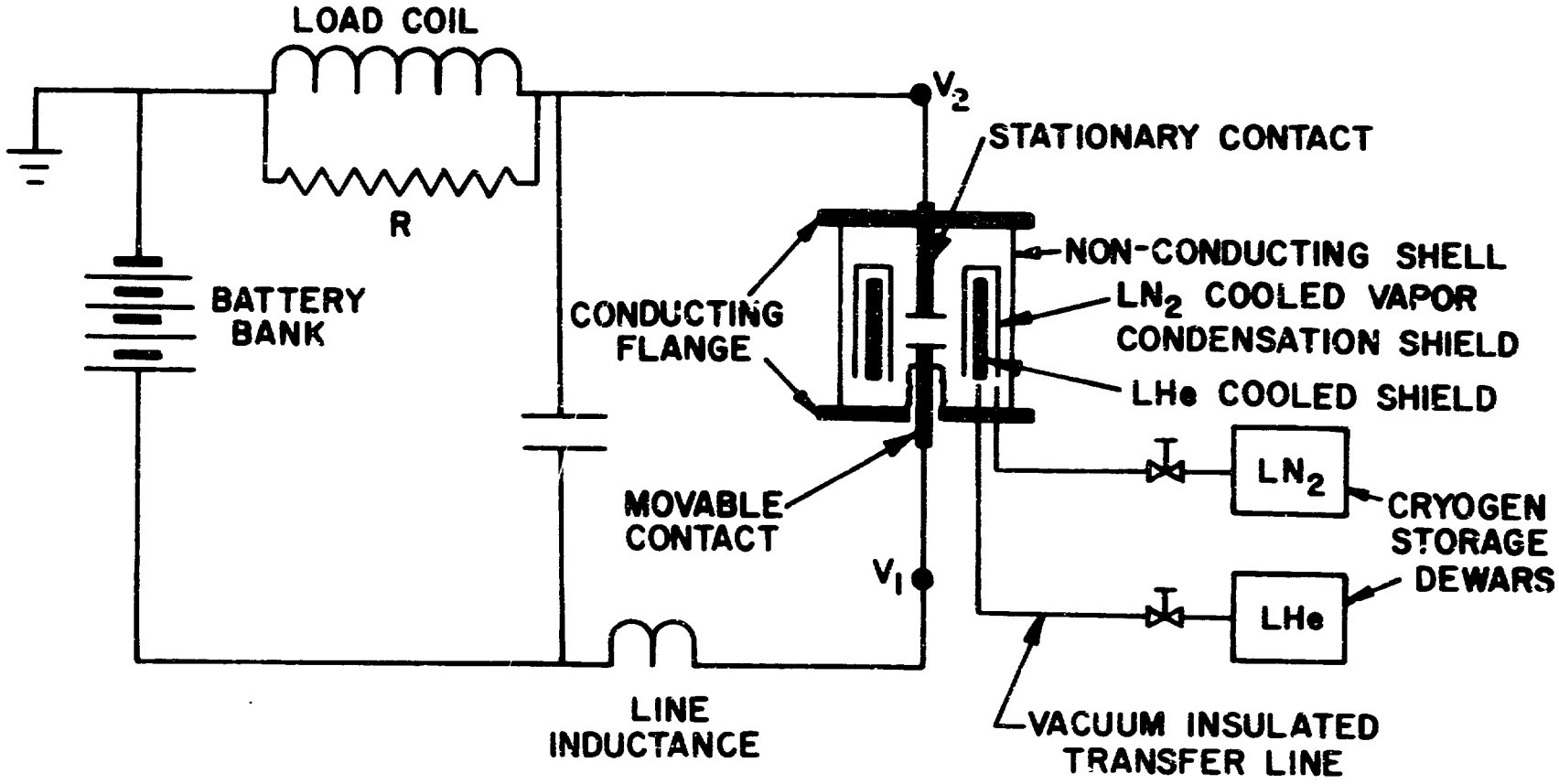

Figure 35. Schematic of switch circuit illustrating use of cryogen storage dewars which must be allowed to "float" electrically.

This voltage may be of the order of several hundred volts and cannot be neglected from the safety standpoint. The liquid nitrogen storage dewar can be isolated from this voltage if necessary, by grounding it and using non-conducting tube to feed the nitrogen shield. The liquid helium storage dewar cannot be easily isolated, however, since the transfer line must be vacuum insulated and from a practical standpoint, must be metal. The result is that it will be necessary to let the helium dewar and transfer line float to the potential V_1. Since the latter cannot be avoided for the helium vessel, the nitrogen container would also be allowed to float. This approach would not pose any problems during testing since at that time all personnel would be suitably placed and protected by a grounded screen surrounding the test facility. Figure 35 does not show the liquid nitrogen cooled field coil which will be placed around the switch and excited by a separate circuit.

A sketch of the load coil which was constructed for use in the switch test circuit is given in Figure 36. It consists of 39 turns of twenty parallel conductors. Each conductor is aluminum with a rectangular cross-section, 0.14 x 0.5 in. The estimated weight of the coil is 525 pounds. This coil will be placed in series with the switch and serve as an energy storage component to provide sufficient voltage to sustain the arc. The coil is made up of sixteen individual pancakes, all of which are connected in parallel. Thus, the total number of coil turns (39) is equal to the number of turns per pancake. Table VI is a summary of the characteristics of the load coil and a photograph is given in Figure 37.

Table VI.

Load Coil Characteristics

Inner Winding Diameter	55.2 cm (21.75 in.)
Outer Winding Diameter	99.8 cm (39.25 in.)
Winding Depth	29.2 cm (11.5 in.)
Conductor	0.356 cm x 1.27 cm (0.14 in. x 0.5 in.) bare Aluminum bar
Winding Configuration	16 pancakes
Connection	parallel
Number of Turns	39
Inductance	0.902 mH
Room Temperature Resistance	3.80 mΩ
Steady Operating Current	2 kA
Short Term Operating Current	20 kA

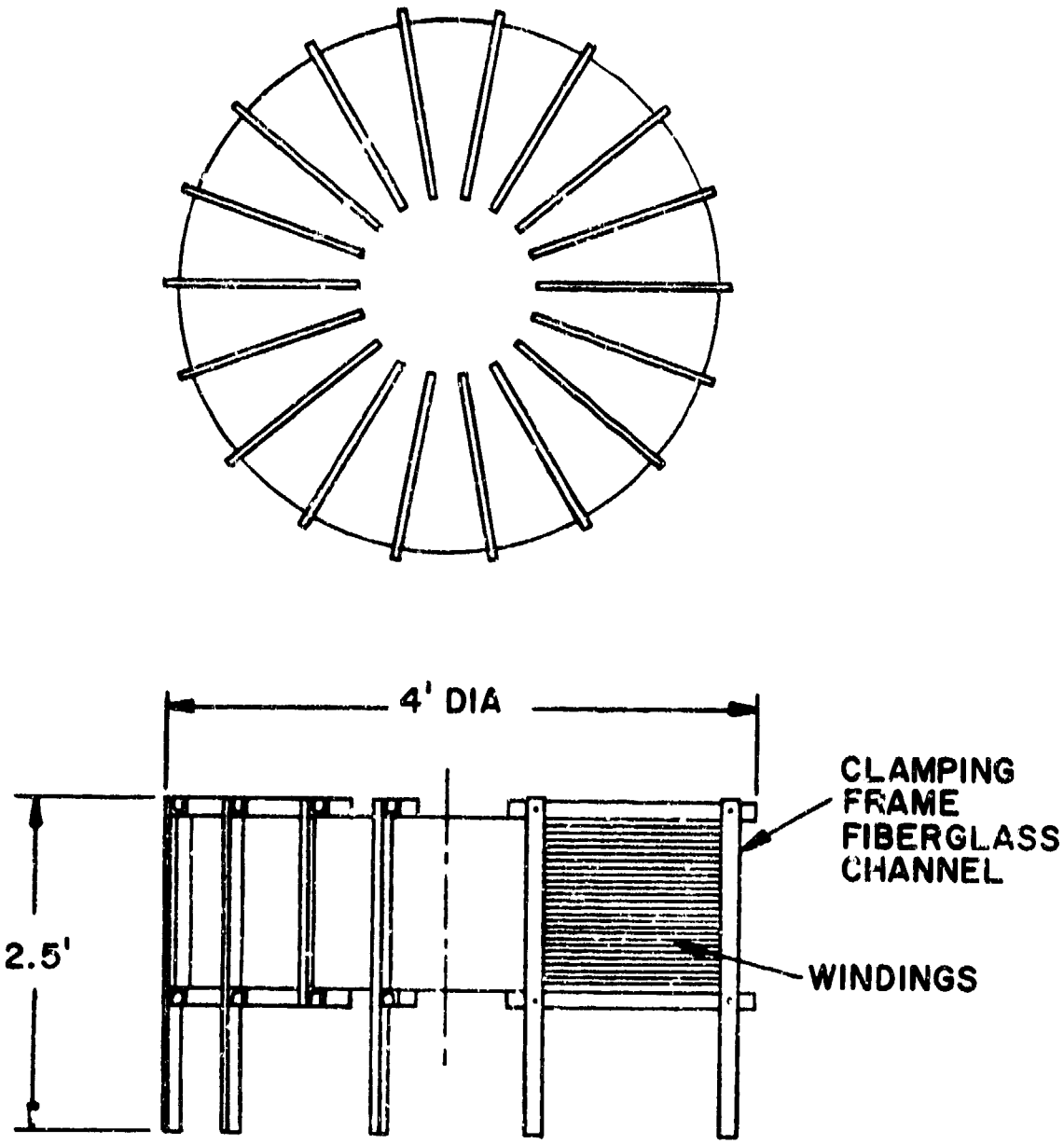

Figure 36. Sketch of inductive component for switch test circuit.

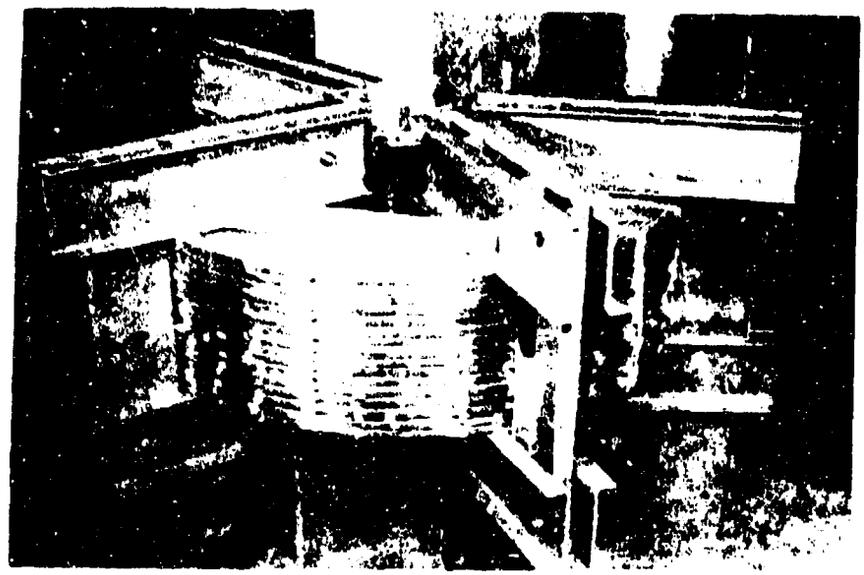

Figure 37. Energy storage coil, showing the sixteen winding pancakes and the coil supporting structure. The calculated inductance and resistance of the coil are 0.966 mH and 4.68 mΩ respectively.

Two large circuit breakers are presently available. Either one would be suitable for use as the back-up circuit breaker in the circuit up to the full test current. Each breaker weights 450 lbs., is of the two-pole type, has a thirty minute closed rating of 7000 A and an interrupt capacity rated at 50,000 A. The opening mechanism may be triggered manually, remote mechanically or remote electrically.

An analysis was performed to determine the circuit parameters required to yield a test configuration capable of providing 20 kA and 100 kV, 40 μsec after interruption. The latter constraint is of particular interest. Results are shown in normalized form in Figure 38. The circuit, which is initially charged to a current I_{10} from an external supply (not shown), was analyzed to determine the values required for the resistor and capacitor such that the circuit characteristics would be compatible with the previously discussed load coil (L = 0.902 mH) and the program requirements of producing 100 kV of voltage 40 μs after the interruption of 20 kA. In the figure, the voltage and time are normalized such that, for unity damping factor (d = 1), the magnitude of the maximum normalized voltage, as well as the normalized time at which the maximum voltage occurs, are both equal to one. For values of the damping factor greater than one, the circuit is overdamped, and the voltage decays without oscillation. For values of the damping factor less than one, the circuit is underdamped, and the voltage oscillates before decaying to zero. For d = 1, the circuit is critically damped. Figure 38 thus shows the discharge characteristics of the test circuit for various combinations of circuit parameters.

Based on these results, a test plan was outlined by choosing the current and voltage levels desired at each stage during testing. Once the load inductance, maximum current, and maximum voltage are chosen, then choosing a value for the damping factor (i.e., choosing the shape of the voltage pulse during discharge) is sufficient to specify the values of R and C required for the circuit, as well as specifying the time at which the maximum voltage occurs. If the resistance of the external charging circuit is known, the required power supply voltage may be determined such that the specified current is obtained within a given charge time. Table VII shows an outline of a test plan for a full scale switch and the required circuit values, calculated on the basis of a load inductance of 0.902 mH, an external resistance of 7.0 mΩ, and a charge time of 190 msec.

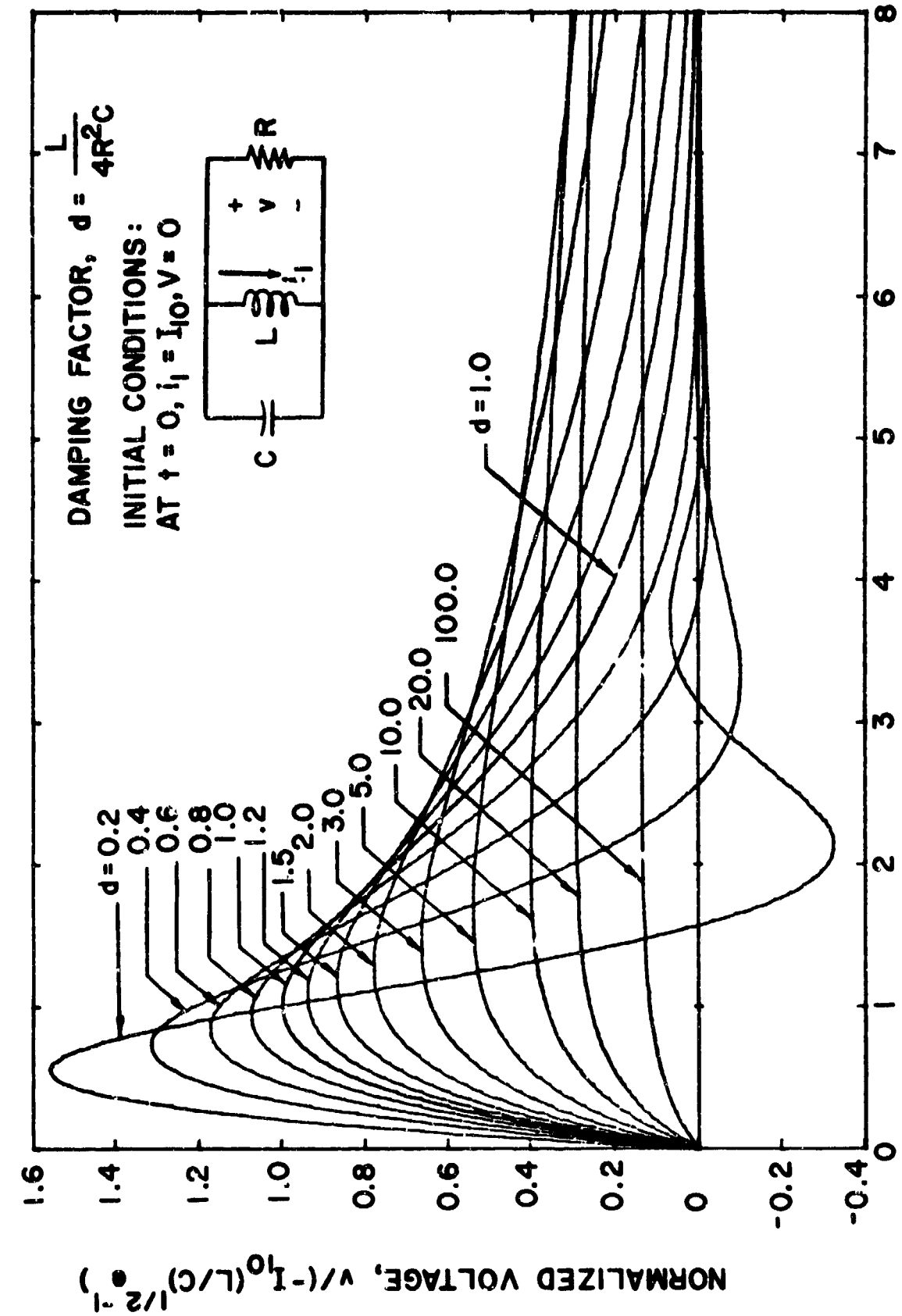

Figure 38. Parallel LRC circuit characteristics for various values of the damping factor.

Table VII .

Outline of Test Plan
Specifying Circuit Characteristics Required
to Achieve Full Scale Switch Parameters

I_{max} (KA)	V_{max} (kV)	d	C (μF)	R (Ω)	t_m (μs)	V_{ps} (V)	V_o (V)
0.8	4	2.5	2.5	5.99	40	7.3	1.7
4.0	4	2.5	62.7	1.20	200	36.4	8.4
4.0	20	2.5	2.5	5.99	40	36.3	8.3
20.0	4	2.5	1566.0	0.24	1000	184.0	42.7
20.0	4	87.5	62.7	0.20	75	184.0	42.8
20.0	20	2.5	62.7	1.20	200	182.0	41.8
20.0	100	2.5	2.5	5.99	40	182.0	41.6

The column headed t_m represents the time at which the maximum voltage occurs. The last column in Table VII represents the voltage across the circuit at the end of the charge cycle. A comparison of these voltages with the maximum discharge voltages shows that the charging voltage is negligible, and the discharge characteristics appear as shown in Figure 38.

The test procedure outlined in Table VII was chosen so that the switch would not initially be tested with high currents and high voltages simultaneously. The list is not all inclusive since no attempt was made to indicate repeated voltage levels. The purpose of the list is to show the range of variables necessary to begin testing at low voltages and currents and work up to the high levels corresponding to program goals. As shown, the maximum current is increased first, while voltage is held low initially, and then brought up to a level corresponding to the current. The fourth and fifth rows of the table demonstrate the effects on the circuit components of changing the shape of the discharge voltage. The availability of circuit components would ultimately determine the actual test procedure and discharge characteristics; however, Table VII does provide a basis from which to work.

Consideration was also given to the use of a switch support subsystem or arc quench circuit which would utilize two parallel LC circuits across the switch to provide a quench current pulse shape with a low rate of change of current when the quench current was close in magnitude to the switch current. The circuit under consideration is shown in Figure 39.

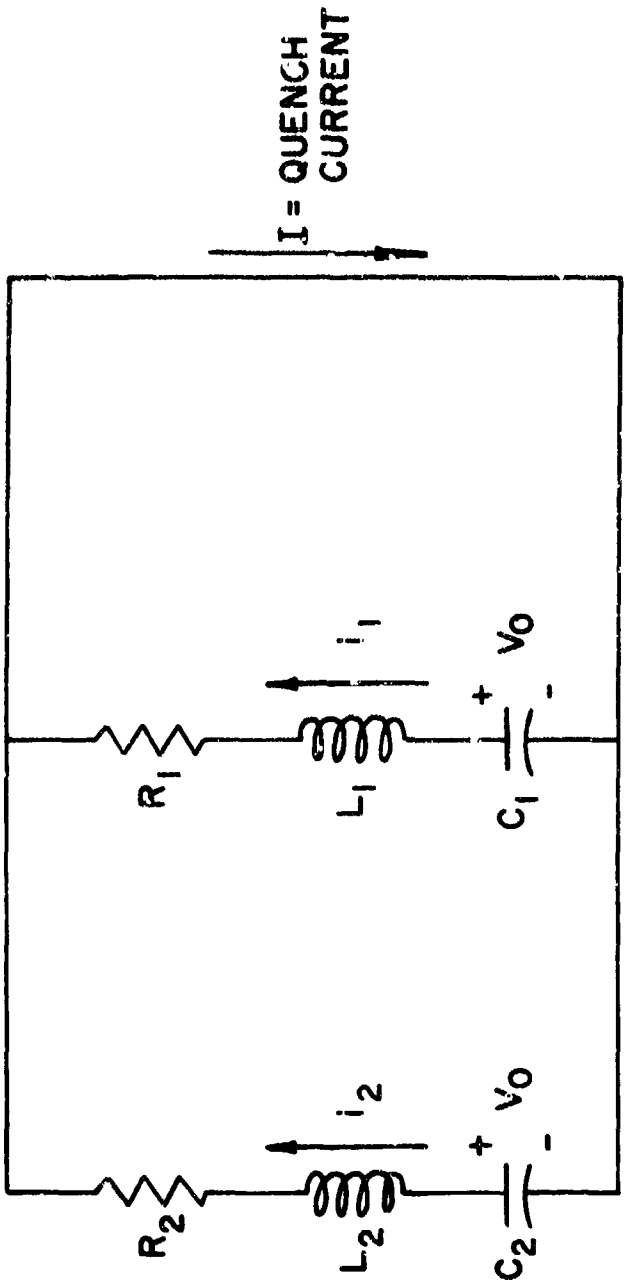

Figure 39. Circuit diagram for quench current analysis. The two parallel capacitor branches are discharged simultaneously into the arcing switch, driving the current in the switch to zero with the quench current, I.

For purposes of analysis, it was assumed that the switch impedance was low enough, so that coupling between the two parallel arc quench branches could be neglected. The total quench current, I, is thus just the sum of the currents from the two individual branches. In addition, the circuit damping was neglected ($R_1 = R_2 = 0$). The total current may then be obtained and normalized as follows:

$$i = \sin T + a \sin bT$$

where:

$$i = \frac{I}{V_o}\sqrt{L_1/C_1} = \text{normalized current}$$

$$a = \left[\frac{L_1C_2}{L_2C_1}\right]^{1/2}$$

$$b = \left[\frac{L_1C_1}{L_2C_2}\right]^{1/2}$$

$$T = \frac{t}{\sqrt{L_1C_1}}$$

Figures 40 and 41a through 41c indicate the general nature of the arc quench currents which may be obtained. The slopes are included for comparison. Figure 40 shows the trivial case consisting of the characteristic with only one branch ($C_2 = 0$). A variety of alternatives are available with both branches, as shown in Figures 41a through 41c. Figure 41b is, of the four cases, the configuration of choice for arc quenching, because of the relatively slow and linear current decay after the first peak, during which the arc would be extinguished.

This section has described an advanced vacuum interrupter designed to satisfy the program goals on interrupt current and withstand voltage. The switch incorporates features suited to a test program for evaluation of the effects of cryogenic cooling, cryovacuum pumping, shaped contacts and applied magnetic field on switch operation. The ranges of test circuit parameters necessary to provide the full scale test currents and voltages were discussed. A promising concept for the arc quench circuit was presented and the flexibility of control over the quench pulse shape was indicated with computed transients.

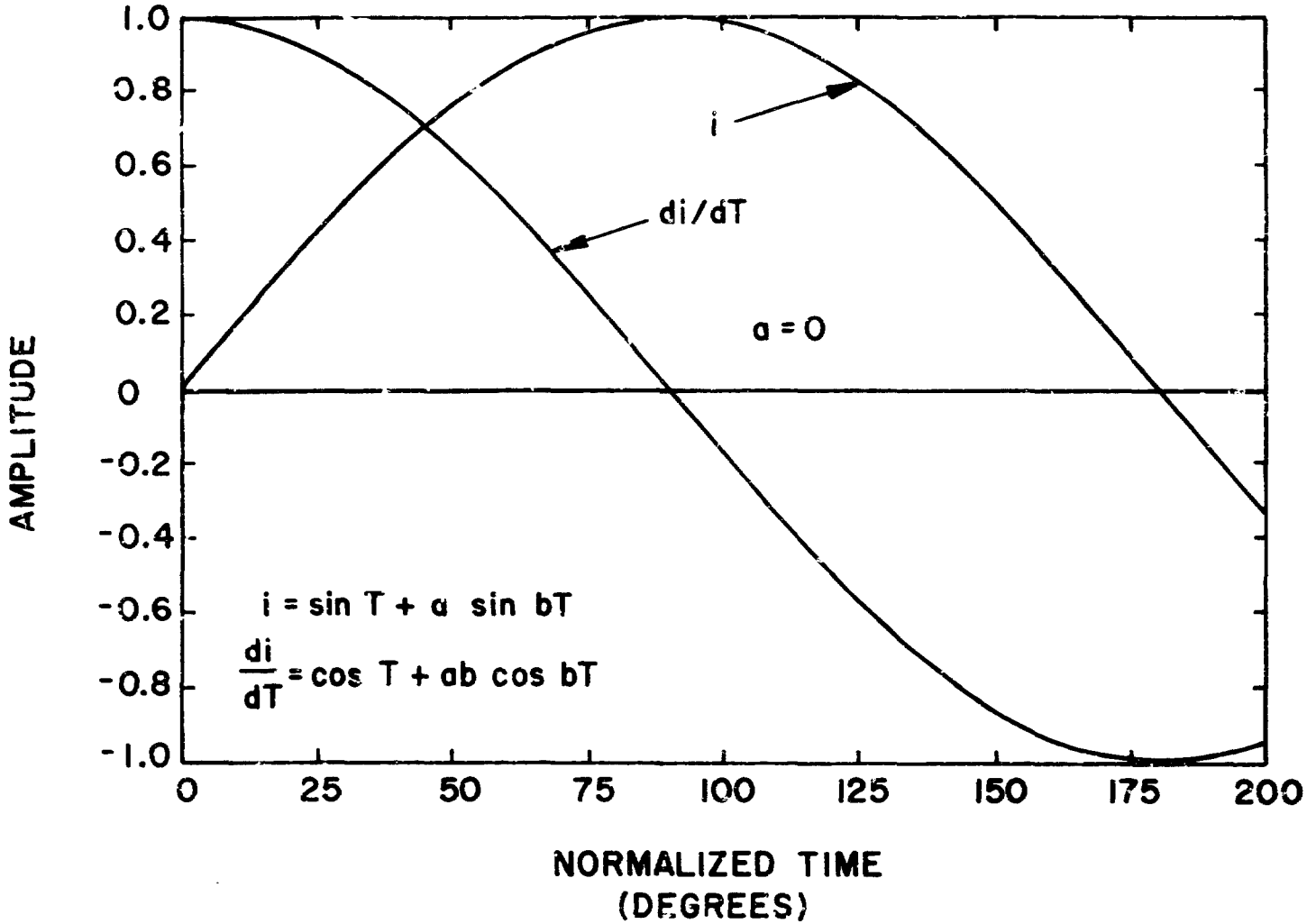

Figure 40. Normalized quench current and its derivative as a function of normalized time for the trivial case: a = 0.

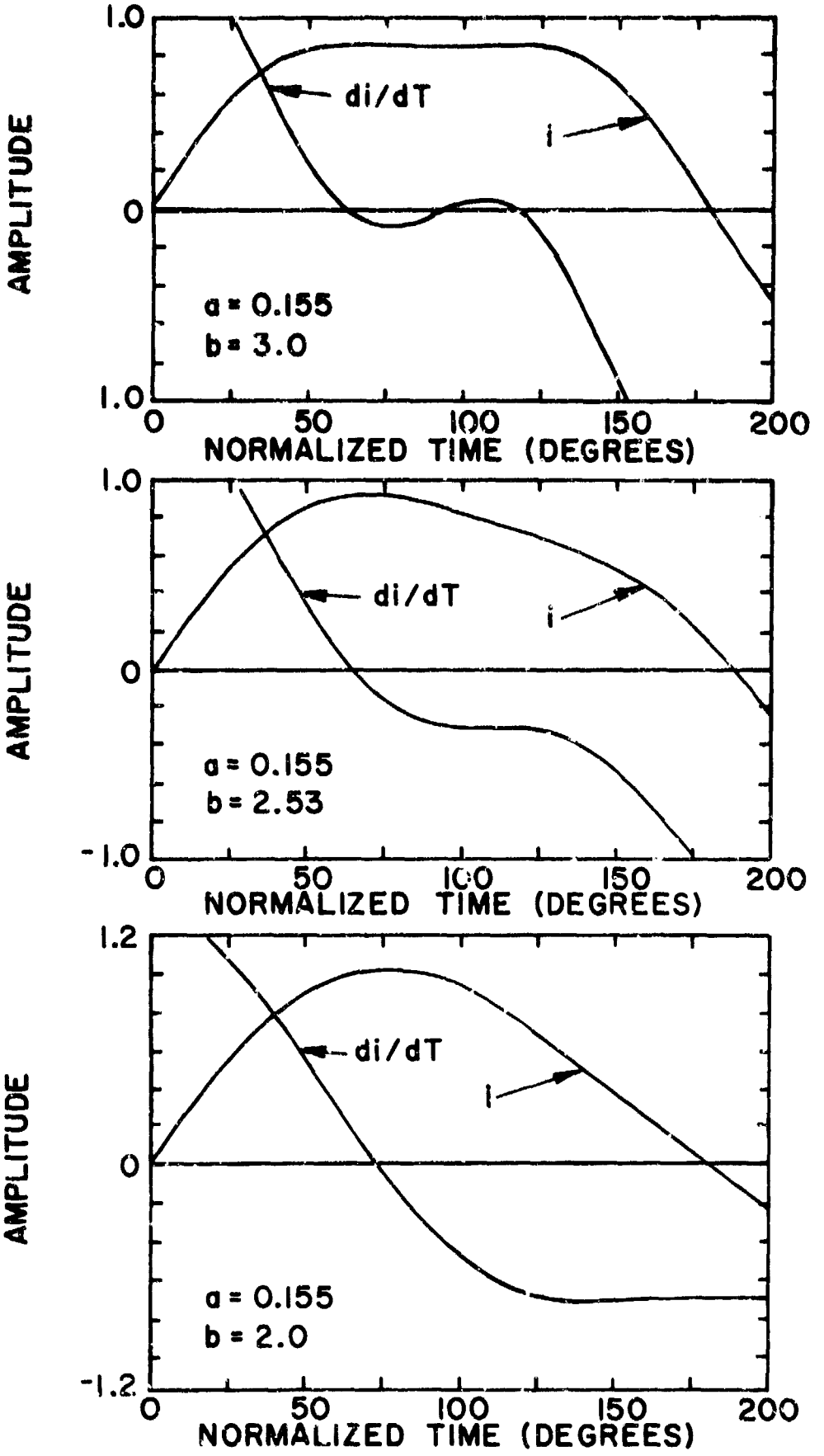

Figure 41. Quench currents and their derivatives for various values of a and b.

SECTION IV.

ROTARY SWITCH

The requirement in this program for a repetition rate of five pulses per second translates into a very stringent design constraint for a linearly actuated device. The switch actuating mechanism must move the non-stationary contact mass through a distance of approximately 0.75 in. in a few milliseconds. At the end of the closing stroke, the mass must be decelerated to a low impact velocity to minimize contact bounce or chatter. Operation at the repetition rate required approaches the limit of present technology. It is, therefore, natural to consider a rotary device since the mass acceleration problem is automatically negated. In a rotary device the breakdown voltage problem will be of major importance, however, the potential for utilization at much higher repetition rates makes consideration worthwhile.

In this section, a rotary switch configuration will be presented. The dominant factor in determining its overall size is the size of the brushes necessary to transfer current from the stationary to the rotating components. A new concept for a brush configuration will then be presented. The brushes consist of a large number of metallic filaments in contact with a rotating drum. Preliminary tests indicate that current densities of 3000 $A/in.^2$ may be achieved in the brushes as opposed to current densities an order of magnitude lower in more standard configurations.

1. SWITCH DESIGN & DEPENDENCE ON BRUSH CURRENT DENSITY

In an earlier Air Force program (F33615-71-C-1454) a rotary switch concept was conceived for possible use in future inductive energy storage systems. It utilizes a magnetic field which, in an integrated system, could be provided by the energy storage coil itself. For convenience, Figures 42, 43, and 44 which follow, will be repeated here (from: AFAPL-TR-72-38-VOL.I).

The basic principle of operation is illustrated in Figure 42. The switch utilizes an externally applied magnetic field together with a segmented rotor and brush system. Position 1 in the figure shows the switch in its closed mode of operation. Current passes from the rotor through the brush to the fixed contact assembly. To "open" the switch, the shaft is rotated until its insulating segment covers the brush. At this time, an arc is drawn at point "a" in the gap between contacts. The current in the arc interacts with the externally applied field $\overline{B}$ and the resultant $\overline{I} \times \overline{B}$ force drives the arc around the periphery of the rotor. The gap widens thus increasing the arc length and, in turn, its resistance. If the arc does not extinguish before traversing the entire periphery, one end anchors at point "b" as shown in position 3 and the arc continues to lengthen.

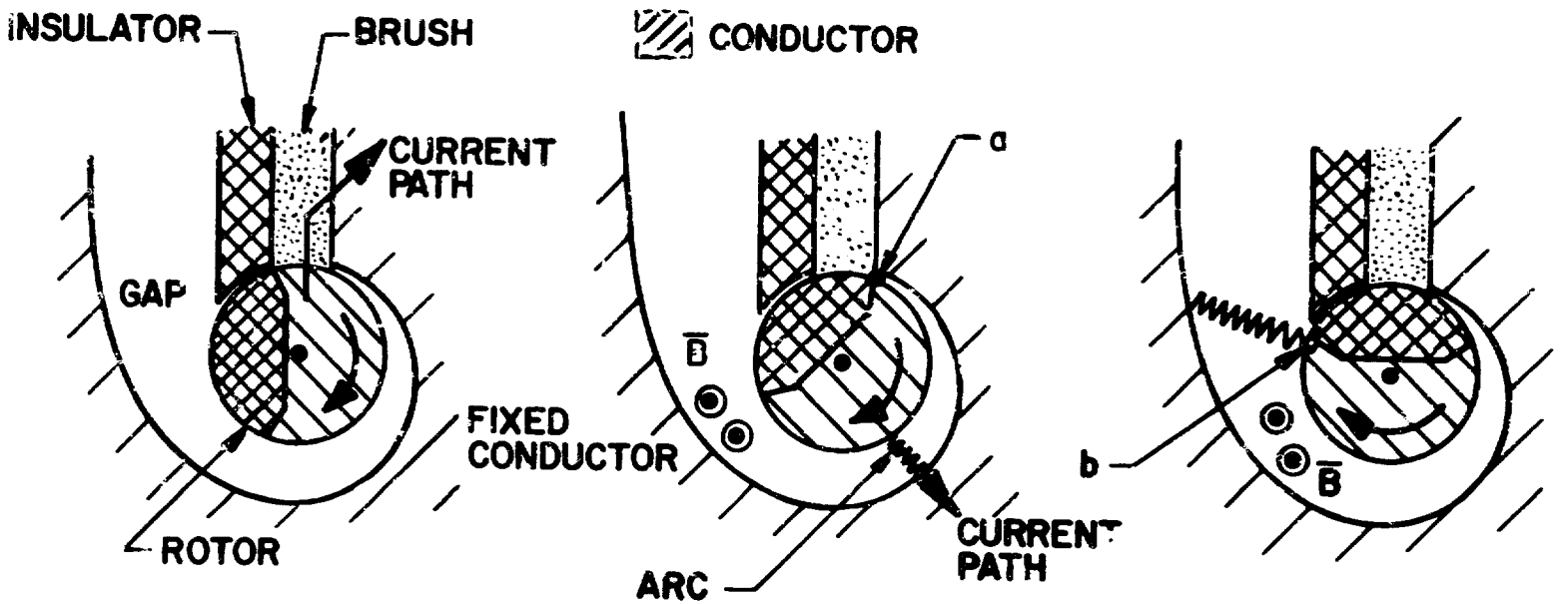

(1)

Current passes from the conducting rotor through the brush to the fixed conductor.

(2)

The shaft rotates, the current to the brush is interrupted, and an arc strikes at point "a". The current in the arc interacts with the applied field B and the resultant Lorentz force drives the arc around the gap. The gap continually widens and lengthens the arc.

(3)

If the arc does not extinguish as it travels completely around the rotor, one end anchors at point "b", and the arc continues to lengthen under the influence of I x B.

Figure 42. Operational sequence of rotary switch with magnetically driven arc

A preliminary design configuration based on the above is shown in Figure 43. The device consists of a rotating electrically conducting shaft which has an insulated segment along its entire length. Current enters the conducting portion of the shaft via a slip-ring assembly, then passes through one of two brush sets depending on shaft orientation. As shown, the switch is in its "open" or no current flow position. Two brush sets are utilized and are rotationally out of phase relative to the shaft. To close the switch and initiate current flow, the shaft is rotated clockwise (when viewed as shown in the sectional drawings) until the conducting portion of the shaft is adjacent to the high conductivity brush. This is the switch configuration during most of the switch "on time." To terminate the current flow, the shaft continues to rotate clockwise. In doing so, the insulated section of the shaft cuts off current flow into the high conductivity brush section before cutting off the low conductivity brush; thus, the current transfers into the latter section. This is done to control the location at which the subsequent arc will form.

As the shaft continues to rotate, the insulated section terminates current flow through the low conductivity brush and an arc is formed at the narrowest part of the gap between contacts at a point adjacent to the low conductivity brush. To insure that the arc forms at this section of the shaft, the shaft is machined with a curved, raised shoulder in this region. The arc then interacts with an externally applied field with direction shown and the resulting Lorentz force drives the arc around the periphery of the shaft. The gap widens as the arc progresses and, depending on details of the circuit, the arc may be extinguished. The cycle is repeated by continued rotation.

A possible variation of the above design is shown in Figure 44 which is a similar device with multiple low conductivity brush sections. Two low conductivity brush sections are shown, separated by a slip-ring type, high conductivity section, the purpose of which is to return the current to the rotor. These two sections are electrically connected such that they are in series, hence, two separate arcs must form and both interact with the applied field. A statistical advantage is gained in such a system since, in essence, only one of the two arcs must extinguish in order for the current to terminate. This concept may be extended to more than two sections. The limit on number of sections would be governed by the length of the applied field region and the breakdown strength of the gap in the high conductivity region.

The actual size of a rotary switch will be largely dependent on the attainable current density in the brushes. The required cross-sectional dimensions for a brush system carrying 20,000 A are given in Figure 45 as a function of current density. Conventional brushes are capable of long term operation at current densities up to 150A/in.^{2} as indicated in the figure. For short periods, conventional metal filled graphite brushes may be run up to the 300-500 A/in.^{2} range. Note that, even at this level, the brush cross-sections required would be very large.

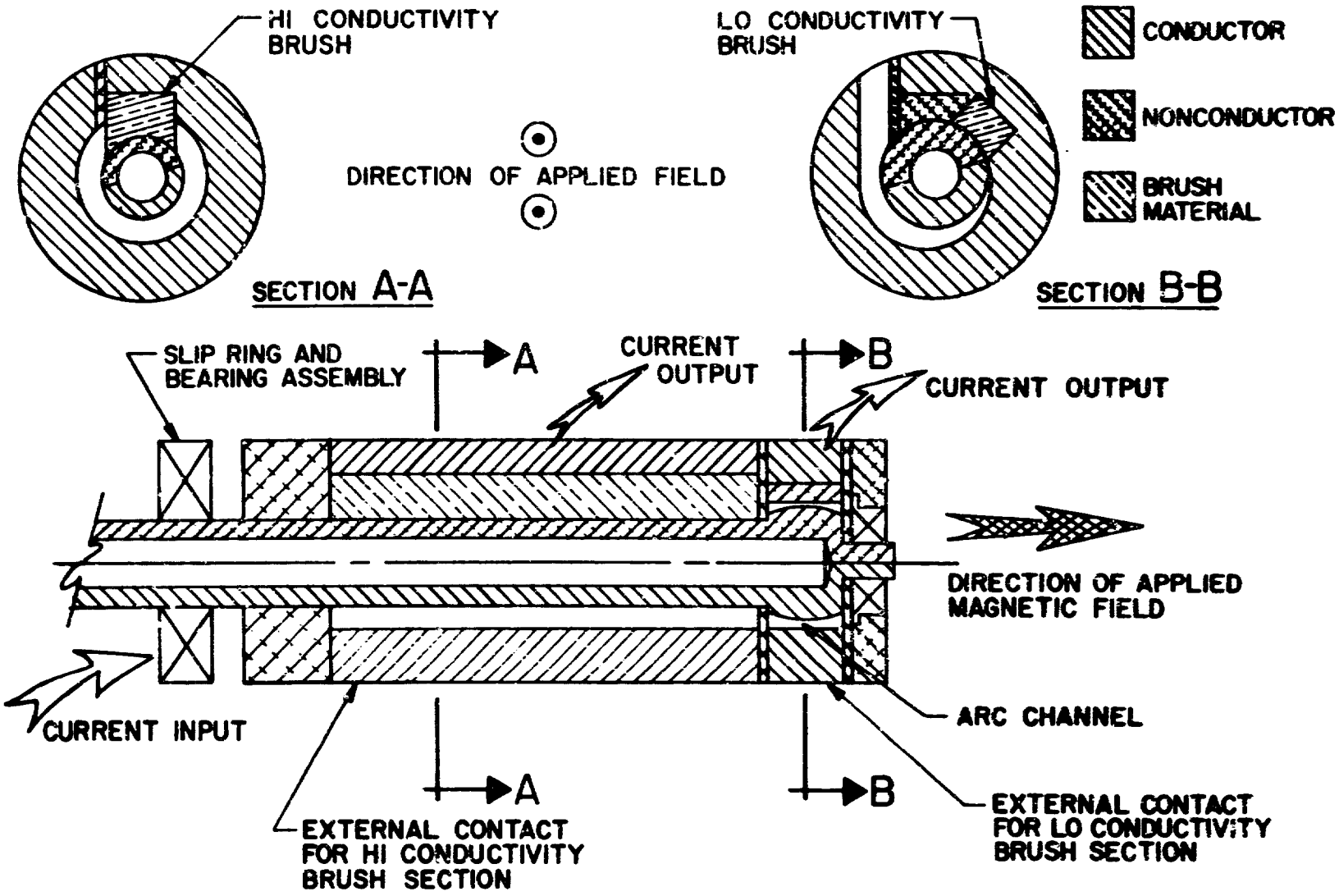

Figure 43. High current rotary switch with single arc channel.

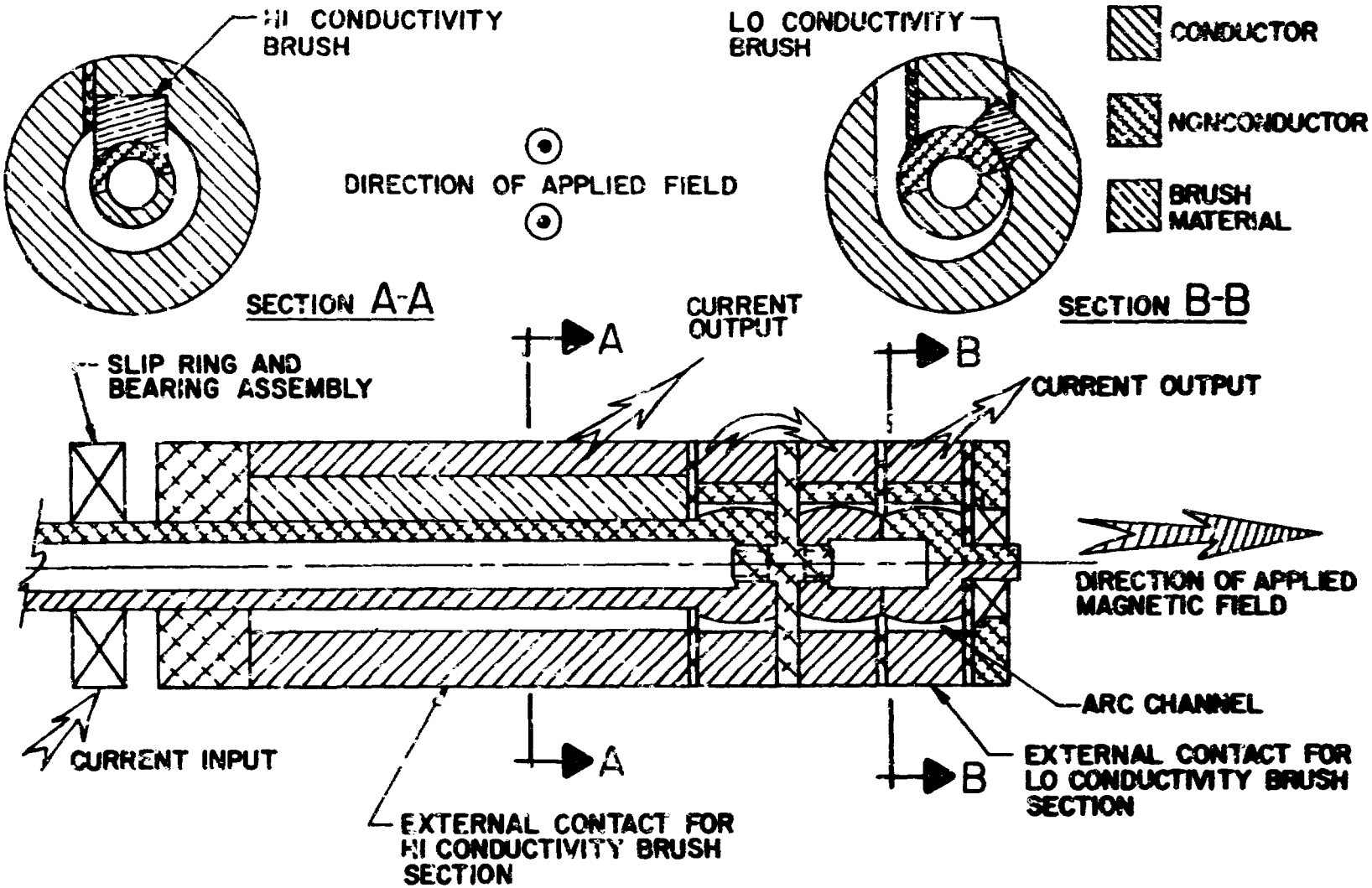

Figure 44. High current rotary switch with multiple arc channels.

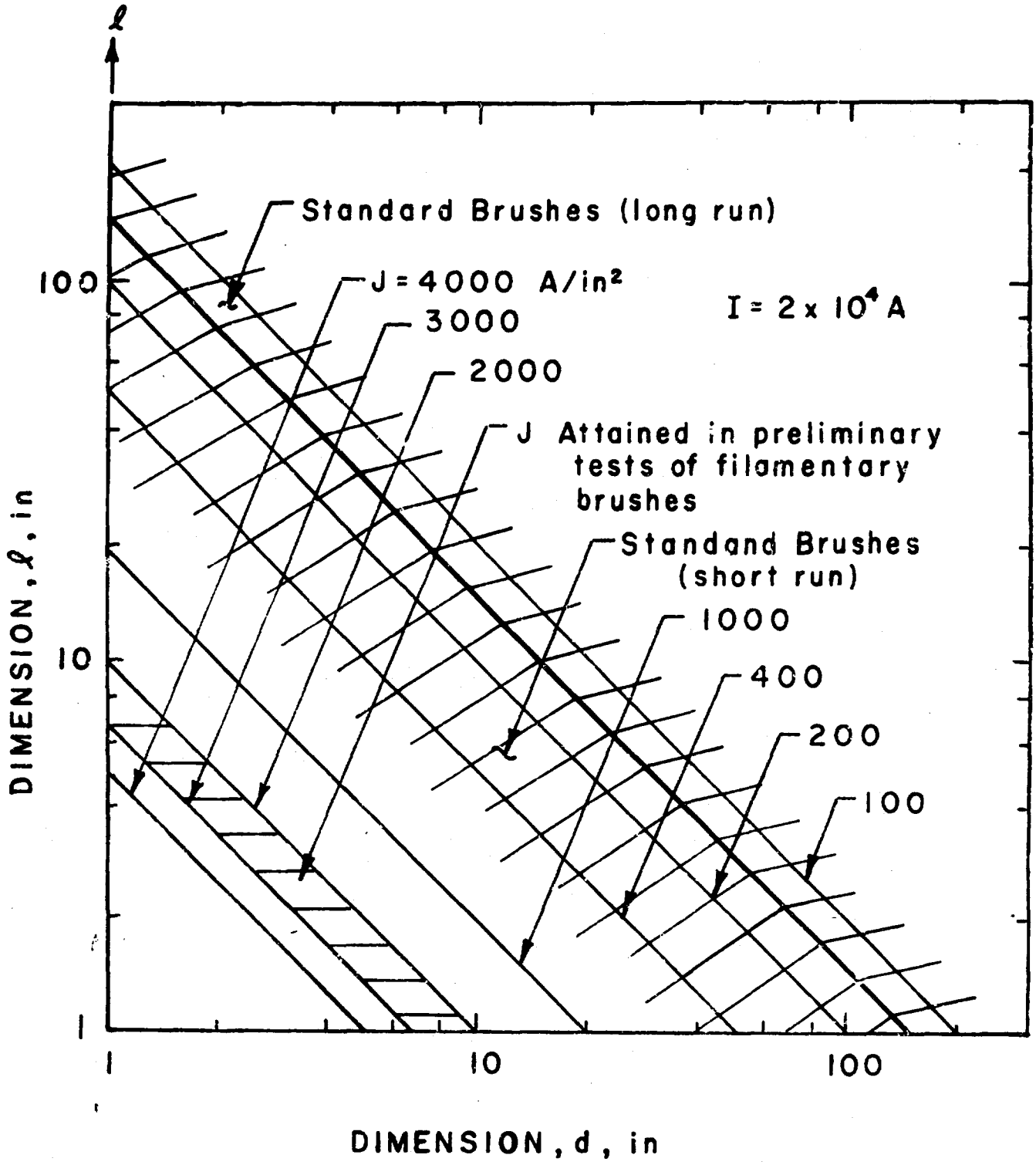

Figure 45. Cross-sectional dimensions of brushes carrying 20,000 A as a function of current density.

In this program, several brushes were constructed and consisted of metallic fibers running on a solid metal surface. Current densities attained in the tests were in the 2,000-3,000 A/in^2 range. This area is also shaded on Figure 45 and indicates the decreased size which is possible with brushes of this type. Results will be detailed later in this section, however, it is obvious that brushes of this type have the potential for decreasing weight and size in a large number of applications.

The ability of filamentary brushes to withstand arcing requires investigation. For the purposes of this section, however, a switch design will be presented in which arcing is allowed in the brush region. In the event that future work indicates that this is not allowable, then other configurations may be considered (e.g., using a rotary unit with filamentary brushes as the main charging switch as discussed at the end of Section II)

2. PROTOTYPE ROTARY SWITCH - SCALING TO 100 pps

The operation of the rotary switch design to be presented will be illustrated first with the sketch in Figure 46. The concept is similar to that discussed relative to Figure 43 except that the rotor is tapered downstream of the low conductivity brush section, and has a helical raised shoulder. With this design, the arc may travel around the rotor several times in the arc channel and be forced to an ever increasing length.

The additional arc time is actually necessary because the speed of the arc may be expected to be large compared with the peripheral speed of rotor, hence, the arc must be sustained until the shaft rotates such that the voltage breakdown strength at the point of arc initiation is large enough to withstand the voltage after arc break.

An assembly drawing of a prototype rotary switch is shown in Figure 47. This design combines the tapered rotor feature illustrated in Figure 46 with the multiple arc channel feature illustrated in Figure 44. The unit has been designed to be mounted with axis vertical and has a diameter small enough for testing with the liquid nitrogen cooled field coil described earlier. Components have been sized for 20,000 A operation on the basis of brushes capable of carrying an rms current density of 3,000 A/in^2. This is consistent with test results summarized above and described in Section IV.2. A variable speed drive motor is shown and is capable of rotating the shaft at switching rates consistent with pulse repetition from 5 to 100 pps. The drive end of the unit also consists of bearings for the shaft and a rotating seal which allows liquid nitrogen to be fed down the center of the shaft for cooling purposes. The electrically active portions of the switch are below the mounting plate and operate in vacuum provided by the vacuum housing and vacuum seals at the upper and lower end of the assembly. Coolant for the nonrotating portions of the switch is provided by liquid nitrogen fed through a tube in the mounting plate. Current input to the switch and into the shaft occurs in Section F which has four filamentary brushes in continuous contact with the shaft (see Section A-A). For the

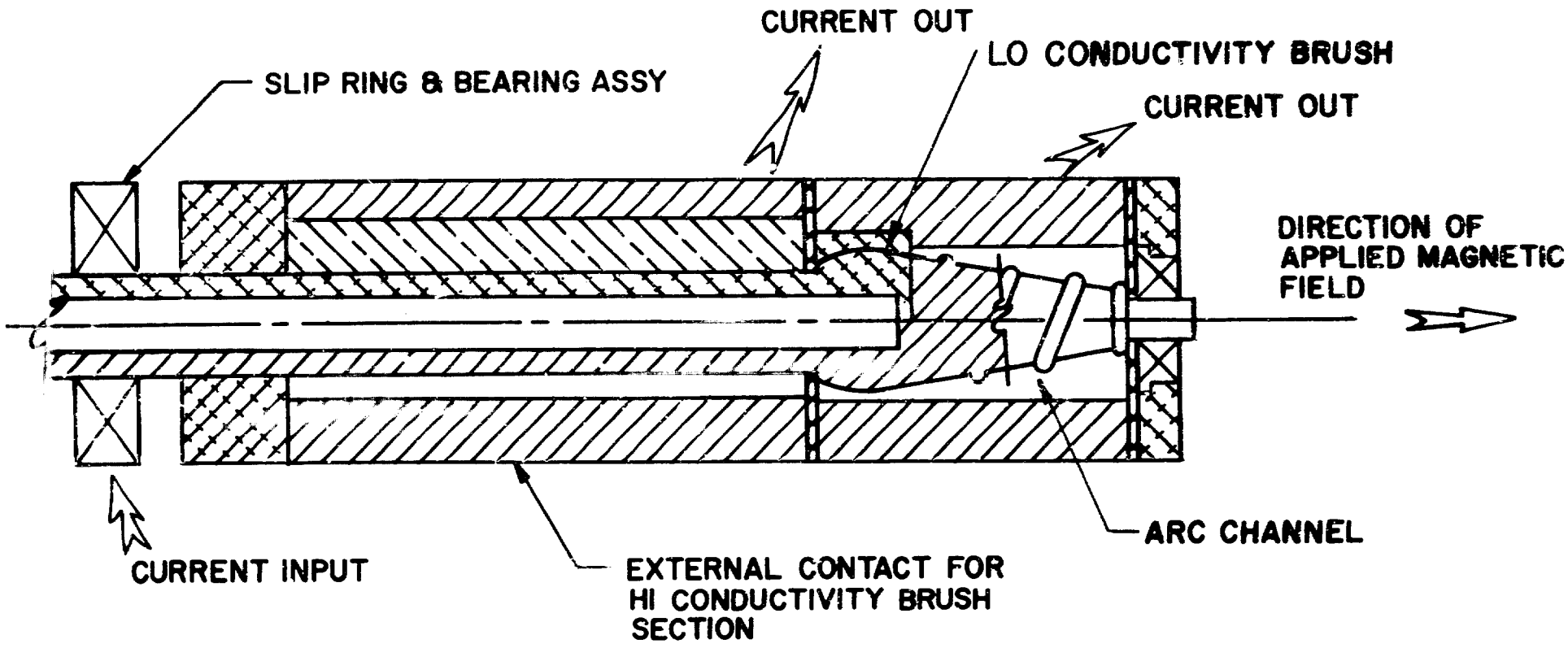

Figure 46. High current rotary switch with single arc channel and tapered rotor.

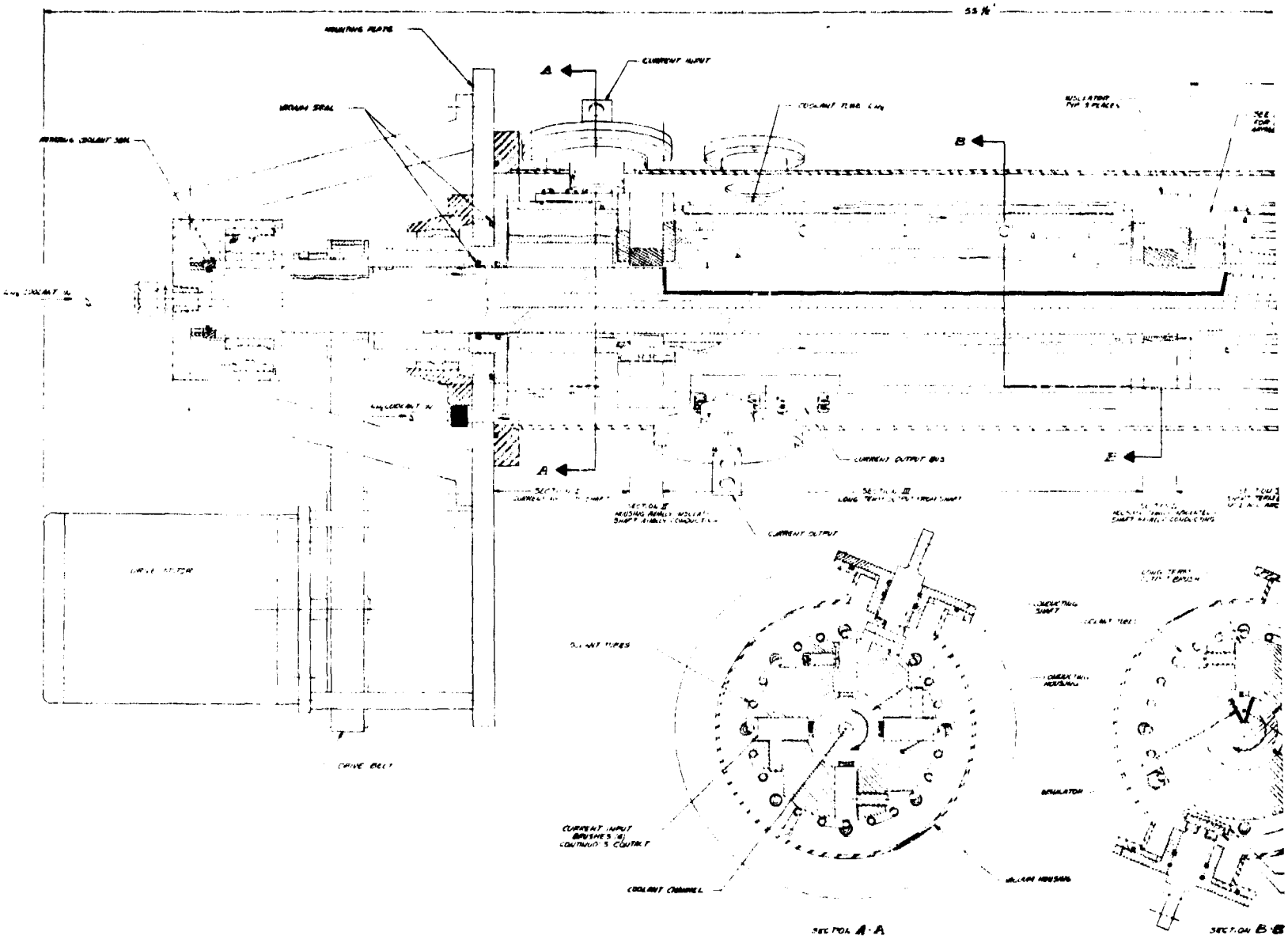
HOUSING PLATE
CURRENT INPUT
VACUUM SEAL
COOLANT TUBE (IN)
ISOLATOR TYP 3 PLACES
A
B
CURRENT OUTPUT BUS
DRIVE MOTOR
DRIVE BELT
CURRENT OUTPUT
COOLANT TUBES
CURRENT INPUT BRUSHES (4) COUNTRUNTS 5 COUNTRUNT
COOLANT CHANNEL
VACUUM HOUSING
ISOLATOR
SECTION A-A
SECTION B-B

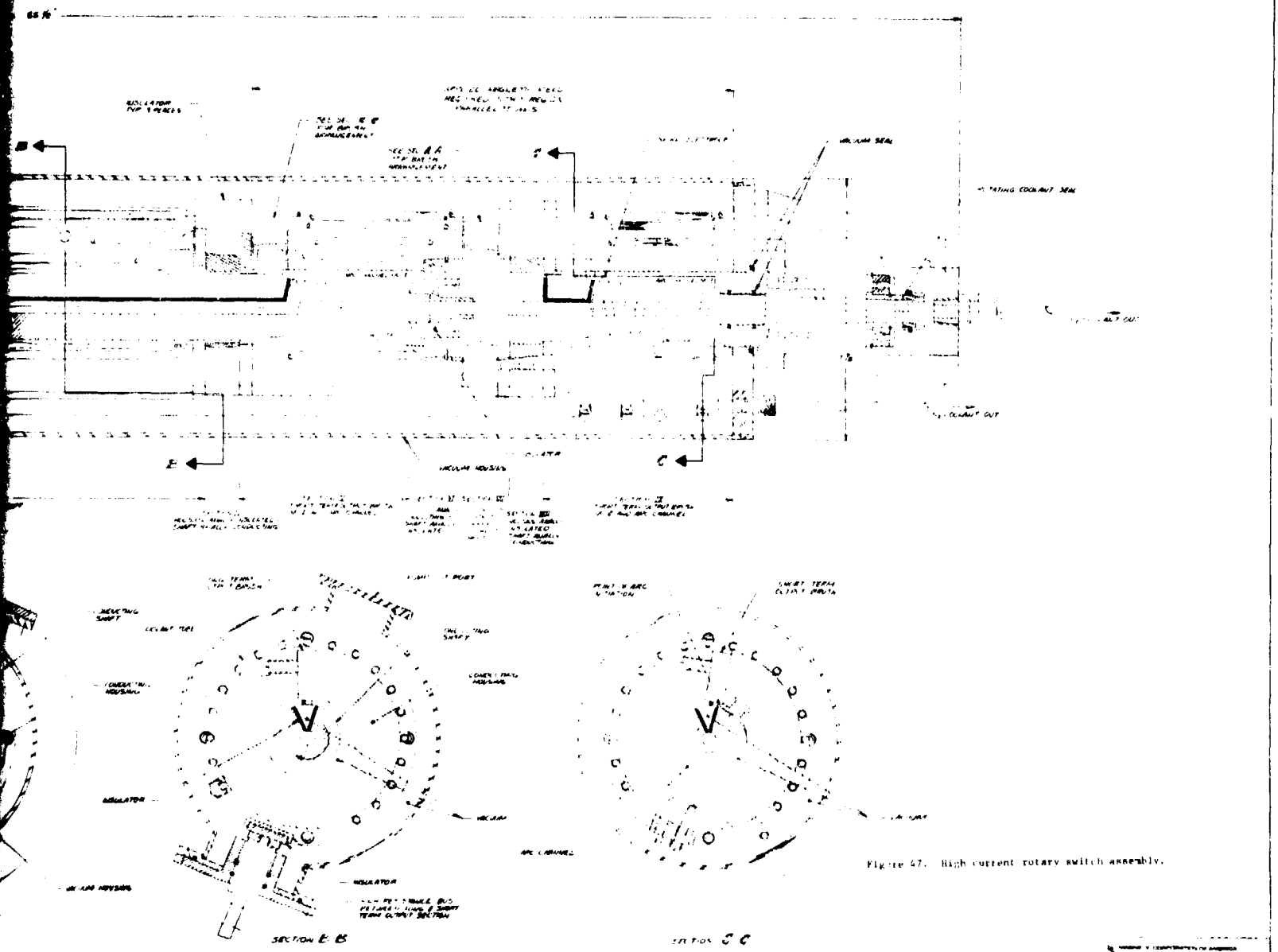

Figure 47. High current rotary switch assembly.

major fraction of the switch on-time, current passes down the shaft, radially outward through the brush in Section III and out through the output buss. Section B-B illustrates the brush in Section III as well as the shaft in this region which has a cut-out to interrupt current flow. As this cut-out interrupts the Section III brush the current is forced to travel down the shaft, radially out to the conducting housing in Section V, down the housing, radially into the shaft through the brush system in Section VII, down the shaft, radially out through the brush in Section IX to the housing and high resistance buss, and, finally, up the buss to the output terminal. As the cut-out on the shaft interrupts the current through the brushes in Sections V and IX (at the instant illustrated in Sections B-B and C-C) an arc forms in the arc channels in these sections and is driven around the periphery of the cones in each section by an externally applied magnetic field parallel to the axis. A distance for arc travel greater than one meter has been provided on each cone. There are two arcs in series and, as they travel around the shaft periphery, each lengthens and also generates a back emf by interaction with the field.

The peripheral distance moved by the arc is determined by the current level, magnitude of the applied field, and arc duration. This relationship is shown in Figure 48 for an applied field of 2 Wb/m^2. An upper limit on allowable arc time is indicated for the case of 5 pps and for 100 pps. At 5 pps this is dictated by the design goal of having a switch on-time of at least 190 msec; at 100 pps the on-time fraction was chosen as 95% (this is equal to an on-time fraction equivalent to that at 5 pps or 0.19/0.2 = 0.95). A lower limit on allowable arc time arises from the need to sustain the arc long enough to allow the shaft to rotate until the leading edge of the shaft cut-out progresses far enough to provide adequate voltage hold-off when the arc is extinguished.

For a rotational speed of 300 rpm (= operation at 5 pps), Figure 49 shows the voltage hold-off distance for the leading and trailing edges of the shaft cut-out as a function of arc duration. The optimum occurs when the brush is midway along the cut-out and corresponds to a hold-off distance of 0.4 cm and an arc duration of 5 msec. In this amount of time, Figure 48 shows that the arc will travel 0.7 m, consequently the 1 m peripheral distance allowed on the "cones" in the design is adequate.

If the same switch design is utilized at a higher repetition rate, several alterations in operation must be considered. First, the peak operating current must be reduced so as to maintain the same rms current density in the system. At 100 pps, for example, the peak operating current would be 1,000 A. Second, the allowable arcing time must be altered to take account of the higher rotational speed. This is illustrated in Figure 50 which is analogous to Figure 49 but was calculated for a repetition rate of 100 pps. Note that the optimum voltage hold-off distance now corresponds to an arc duration of 0.25 msec. The main impact of this result would be felt in the timing of the arc quench circuit for the switch which would have to be fired at a time after arc initiation which was determined by repetition rate. This optimum arc duration is plotted in Figure 51 as a function of repetition rate.

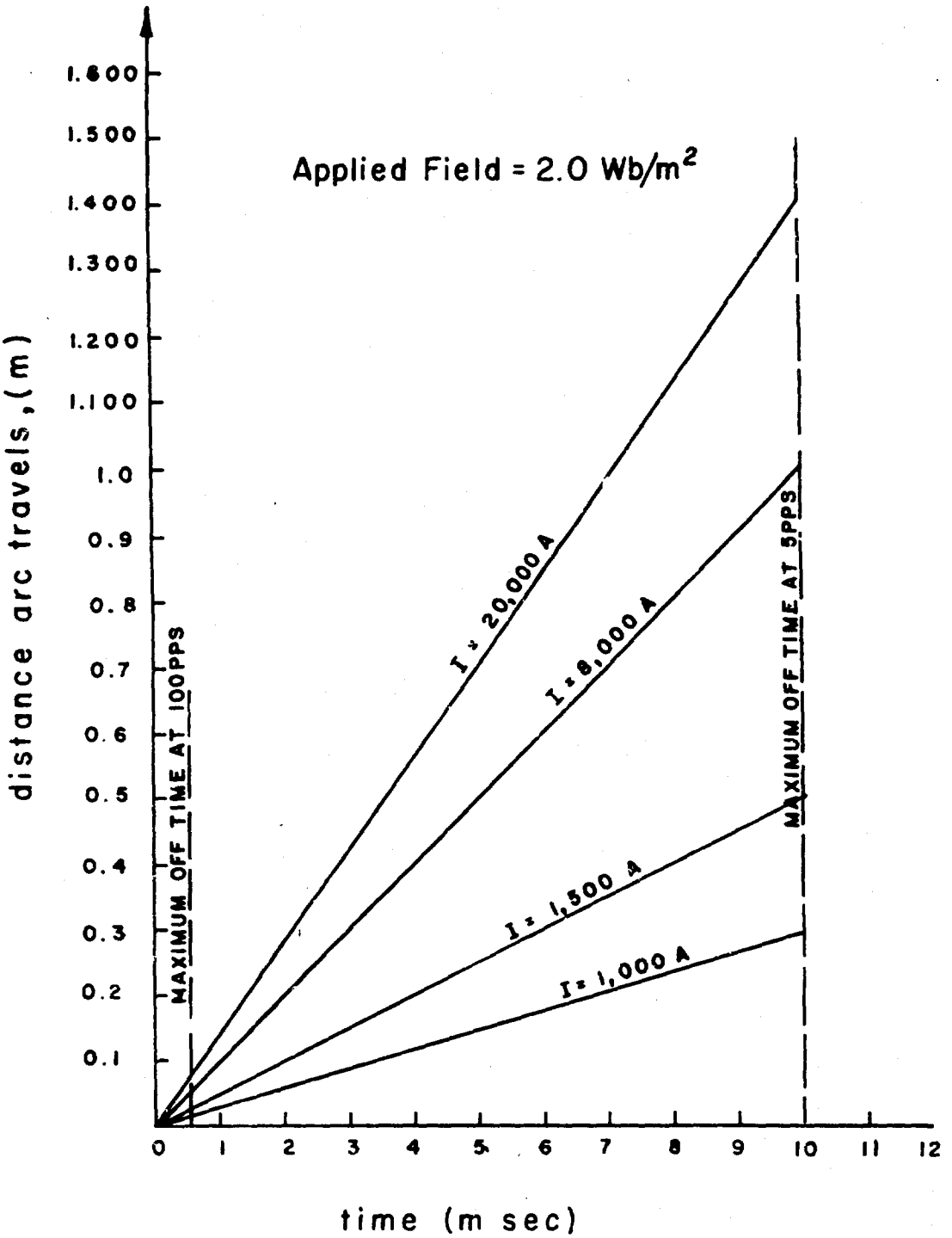

Figure 48. Distance traveled by arc vs. arc duration and current level at an applied field of 2 Wb/m^2.

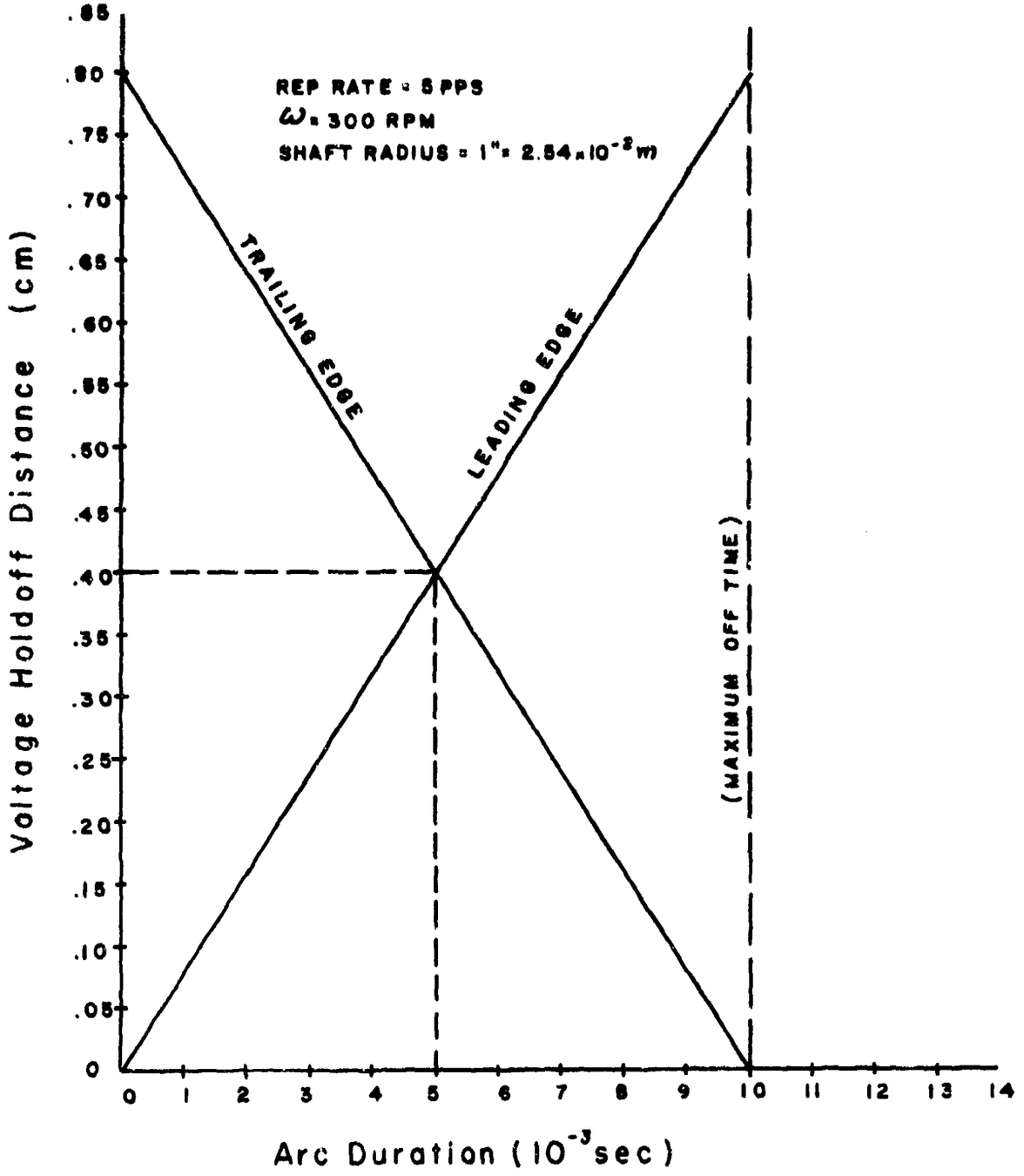

Figure 49. Voltage holdoff distance for leading and trailing edge of shaft cutout vs. arc duration for repetition rate of 5 pps.

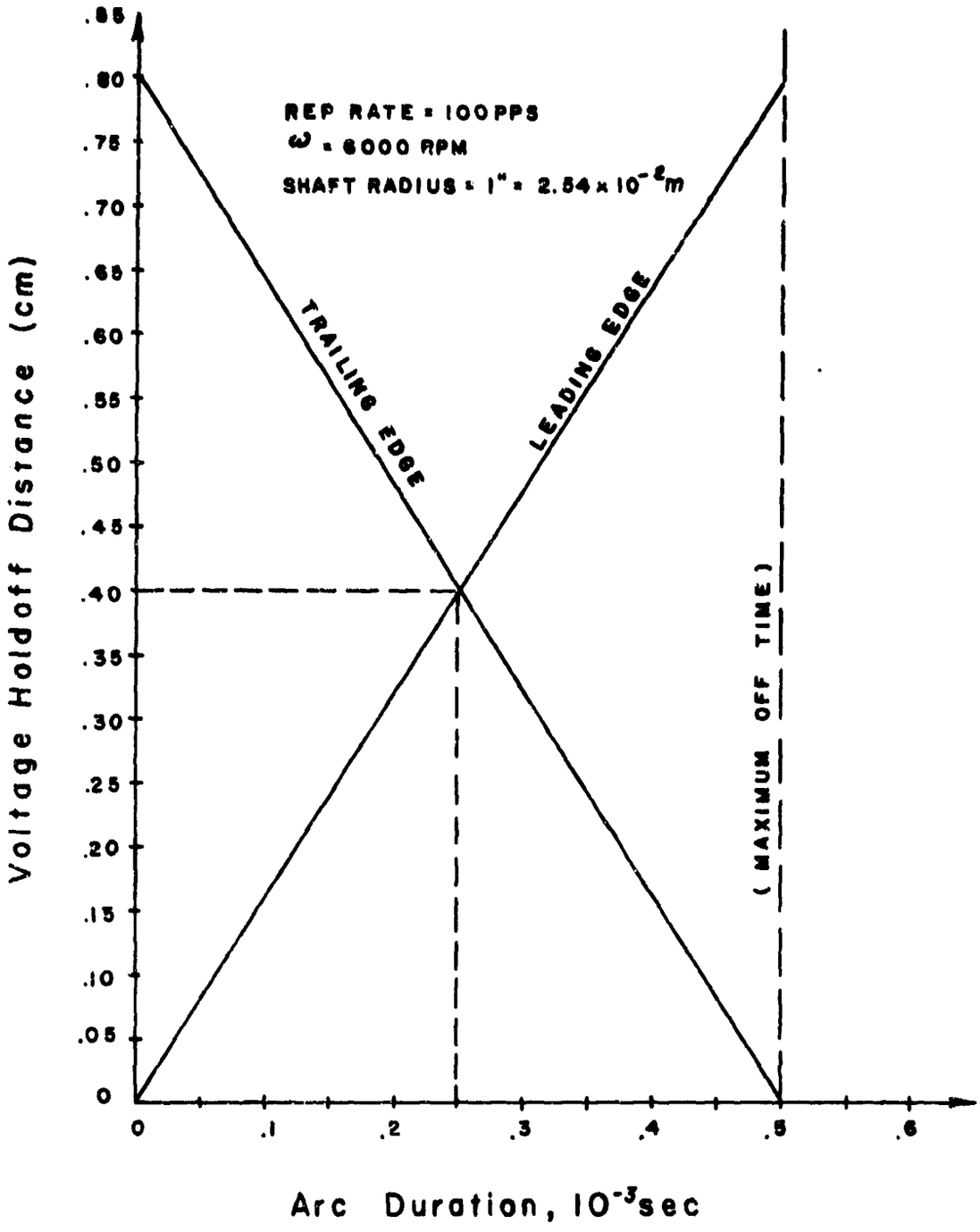

Figure 50. Voltage holdoff distance for leading and trailing edge of shaft cutout vs. arc duration for repetition rate of 100 pps.

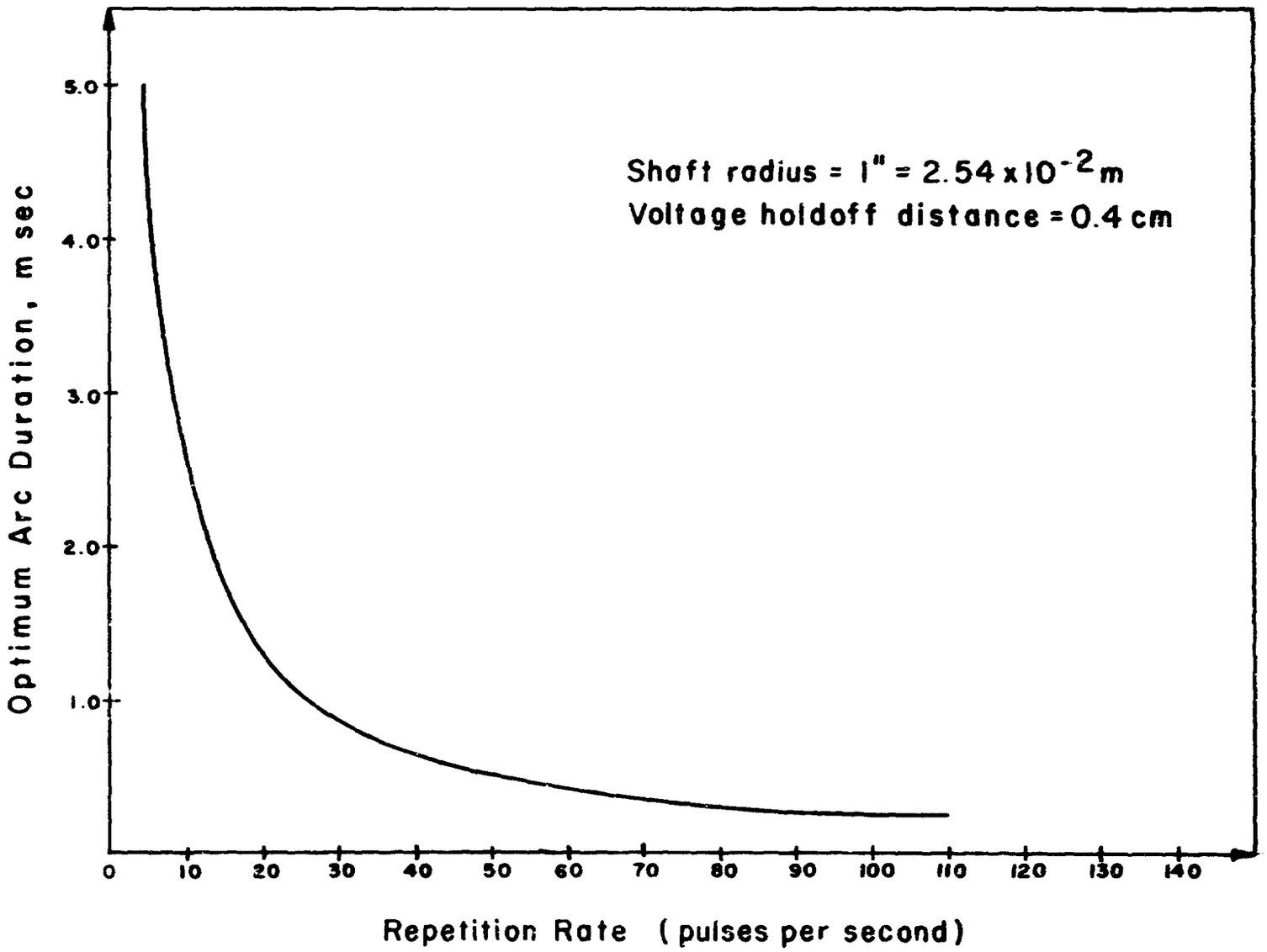

Figure 51. Arc duration vs. repetition rate to correspond to maximum voltage holdoff distance in the design of Figure 47.

All brushes have been sized at an rms current density of 3,000 A/in^2. Since all of the brushes are not "on" all of the time, the required cross-sectional area is different for each set. This is best understood by reference to Figure 52 which is drawn for the case shown in Figure 47. In these diagrams, the rotational position corresponding to a zero angle is that at which the brush in Section III is fully open (i.e., over the shaft cut-out) and about to begin conducting current. The top two diagrams indicate the fully opened and fully closed positions for the brushes in Sections III, V, and IX. As shown, the brush in Section III leads the other two and the choice of angles is such that the Section III brush opens while the other brushes are still closed so as to effect a current transfer into the latter. The solid lines in the top two diagrams indicate the contact area of the brush versus angle. The actual resistance to the circuit is closer to a step function, however, as shown by the dotted line since the constriction resistance varies exponentially with the restriction ratio.

The current through the brush in Section III is illustrated in Figure 52C. It is assumed that a constant voltage source is used with total circuit current governed by an inductance as in an energy storage circuit. For the brushes in Section V, VII and IX, the current for the portion of the cycle $\sim 16^o < wt < \sim 326^o$ is held to a low level even though they are closed and in parallel with the brush in Section III by the use of a high resistance in that leg of the switch circuit. In the design in Figure 47, this would be effected by use of brass, stainless steel, or beryllium copper for the high resistance buss connecting the output of Section IX with the output of Section III. The current in the brushes in Sections V, VII and IX suddenly increases at $wt \approx 326^o$ because the brush in Section III opens at that point. At $wt \approx 342^o$, the brushes in Sections V and IX open but current continues because an arc forms at that instant. Arc duration carries the on-time for Sections V, VII or IX to $wt \sim 346^o$ (assumed for this example). The current through the input brushes (Section I) is shown in Figure 52E and is the sum of the currents shown in Figures 52C and 52D.

Figure 53 illustrates a cross-section of the shaft with superimposed brushes to illustrate the following nomenclature:

r_s = shaft outer radius

r_c = radius of coolant hole in shaft

θ_i = angle subtended by shaft cut-out or insulator

θ_b = angle subtended by brush in Section III

θ_d = angle subtended by brush in Section V and in Section IX

ϕ = angle by which Section III brush leads brushes in Sections V and IX.

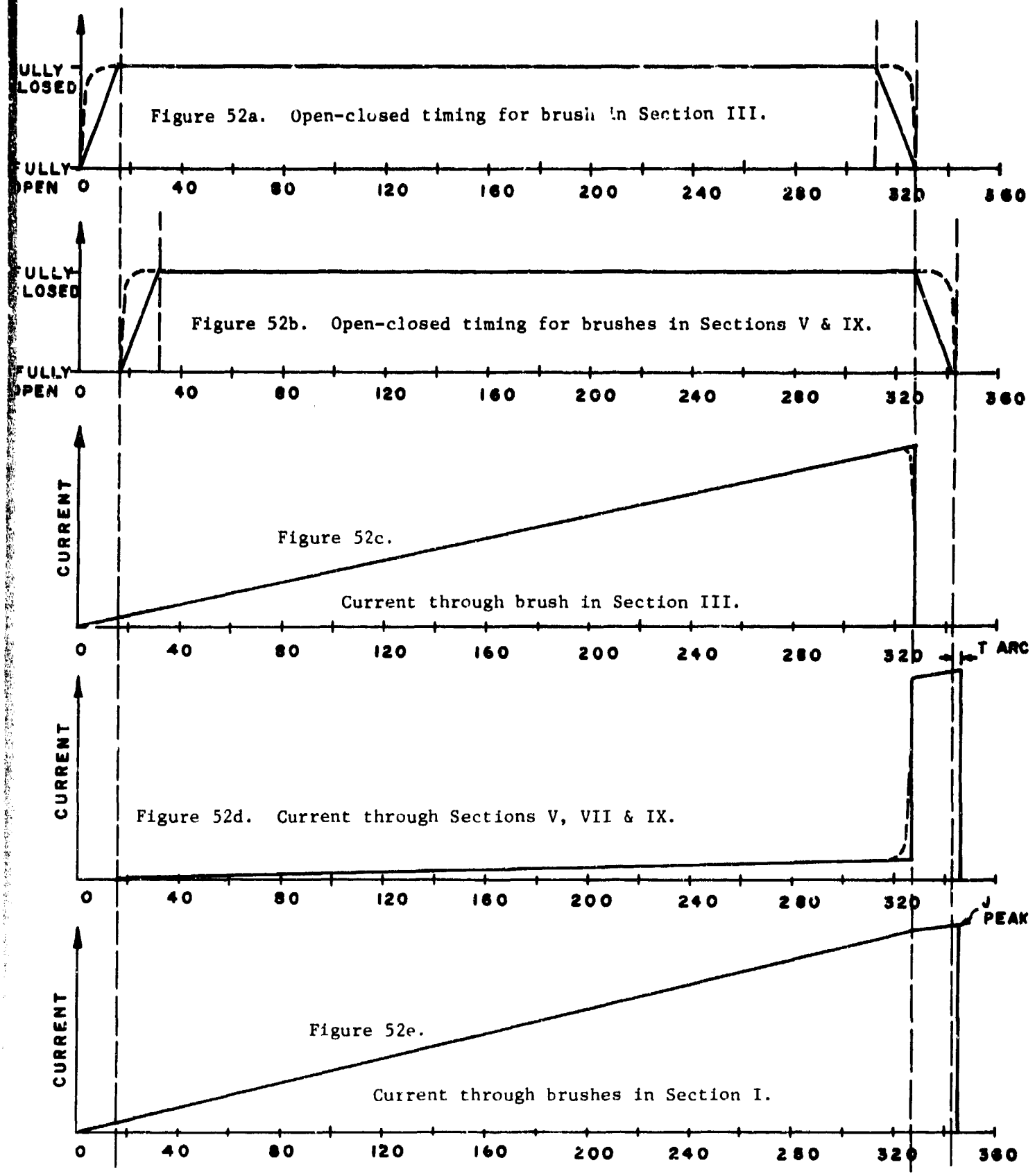

Figure 52. Timing and current diagrams for brushes as a function of rotational position.

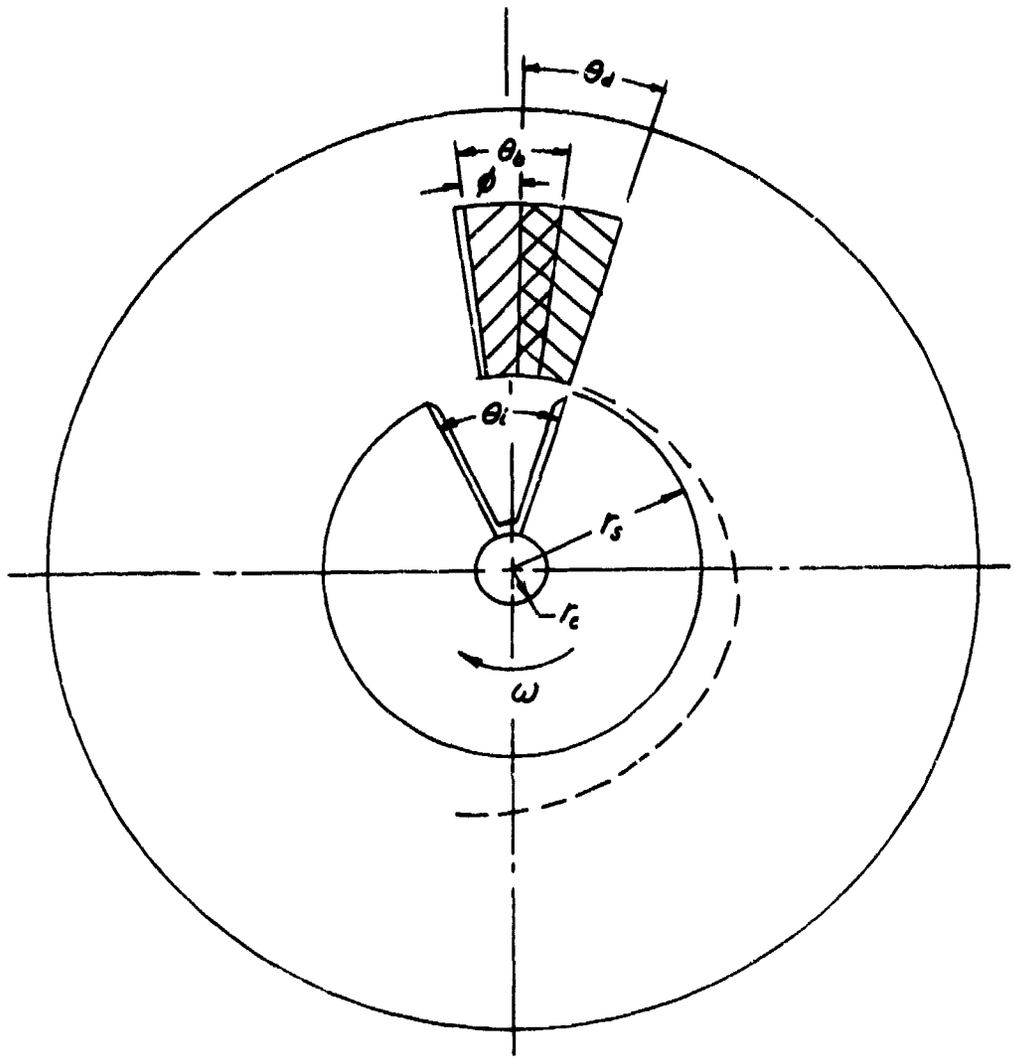

Figure 53. Nomenclature for shaft radii and angles subtended by brushes and shaft cutout (insulator)

If the peak circuit current is defined as I_p, then the rms current through the various brushes for design purposes may be shown to be:

Section I: $$I_{rms} \approx \frac{I_p}{\sqrt{3}}\left(1-\frac{\theta_i-\phi-\theta_d}{2\pi}\right)$$

Section III: $$I_{rms} \approx \frac{I_p}{\sqrt{3}}\left(1-\frac{\theta_i-\theta_b}{2\pi}\right)$$

Sections V, VII & IX: $$I_{rms} \approx I_p\left(\frac{\theta_d+\phi-\theta_b}{2\pi}\right)$$

The above assumes an arc duration of zero time and the circuit conditions associated with the diagrams of Figure 52.

The design in Figure 47 was generated by assuming an allowable brush rms current density of 3,000 A/in^2, a shaft radius of one inch, a material resistivity equal to that of copper at room temperature and an allowable heat transfer rate to nitrogen cooled surfaces of 5 watt/cm^2. Subtended angles for brushes and shaft insulation were then chosen for geometrical and timing consistency and to effect a balance between heat generated and removed. Utilization of a room temperature resistivity is conservative but reasonable for design of a prototype to be tested extensively.

3. FILAMENTARY BRUSH TESTS

The previous section described a design for a rotary switch which utilizes filamentary brushes capable of operating at current densities substantially in excess of the capabilities of standard types of brushes. This section will discuss the filamentary brush concenpt and present test results which illustrate current density and voltage drop characteristics.

When two solid surfaces are placed in contact, the real contact area is substantially less than the apparent contact area. This is shown in Figure 54 which illustrates a magnified view of two solid surfaces in contact. If the plane surfaces were infinitely hard, they would contact at only three points. However, because of elastic and plastic deformation, the number of contact points and their area is determined by the load, surface finish, and stress-strain characteristics of the material. Complete agreement does not exist on the method for calculating the real contact area, but it may be estimated by:(7)

$$A_r = F/\bar{y}$$

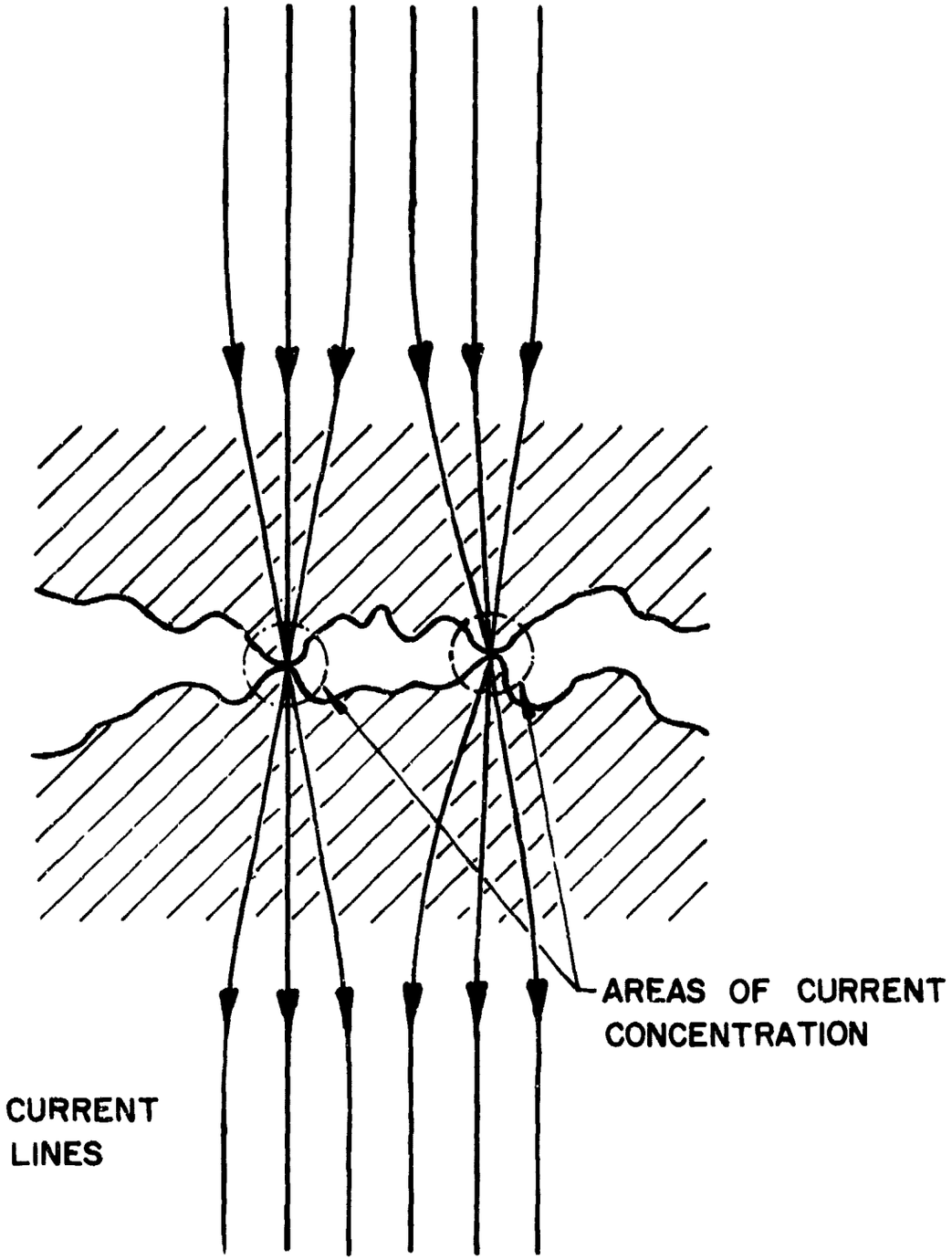

Figure 54. Illustration of the current transfer across solid metal surfaces.

where:

A_r = real area of contact

F = total load on contacts

$\bar{y}$ = average yield pressure of the surface high points

The latter is dependent on the material and surface finish. Holm[8] has shown that $\bar{y}$ may be estimated by about three times the modulus of elasticity for the contact material. On this basis, it is instructive to estimate the ratio of real to apparent contact area for several materials. This is shown in the following table for a fixed contact pressure of 100 psi.

Table VIII.

Estimated Ratio of Real to Apparent Contact Area for Plane Contacts at a Pressure of 100 psi.

Material	Ratio of Real to Apparent Contact Area
copper	6.25×10^{-6}
tungsten	2.0×10^{-6}
gold	8.35×10^{-6}
silver	9.1×10^{-6}
carbon or graphite blocks	1.4×10^{-4}

For the metals, the estimated area ratio falls in the range 10^{-6} to 10^{-5} whereas the carbon or graphite blocks yield a ratio of order 10^{-4}.[1] The point to be made in any case is that the real to apparent area ratio is very small. This limits the current density attainable in the contact because of the constriction of the current at the contact interface (see Figure 54) as it passes through the real contact points. In metallic contacts (eg. as used in the linearly actuated switch) the problem is not as severe since the lower electrical resistivity relative to carbon or graphite leads to less power dissipation at a given current density and the higher thermal conductivity relative to carbon or graphite leads to better heat transfer from the points of localized high dissipation at the interface.

---

[1]It must be noted that the 100 psi. pressure chosen for comparison purposes is relatively high for carbon or graphite and relatively low for metallic contacts (eg:- see Figure 13).

In this section, the primary concern is sliding contacts which will allow current to transfer to and from a rotating mechanism. Graphite and metal filled graphite brushes are the standard means for performing this function, however, they are limited in operational current density. Typically, graphite and copper or silver filled graphite brushes may be expected to operate with current densities and voltage drops as indicated in Table IX.

Table IX.

Typical Current Density & Voltage Drop
for Standard Brushes

Material	Current Density ($A/in.^2$)	Voltage Drop (V)
carbon	35 - 45	1.8 - >2.5
graphite	40 - 60	1.0 - 2.5
metal filled graphite	75 - 150	0.3 - 1.8

For short periods of time operation at levels of 300-500 $A/in.^2$ has been carried out, however, it must be remembered that standard brush characteristics are strongly dependent on the atmosphere in which they operate. In particular, water vapor is essential to maintain the friction, wear and electrical behavior which is usually expected. Because of the requirements of this program the initial development of a high current density brush was undertaken.

Since one of the problems in increasing operational current density is the small ratio of real to apparent contact area which results from a limited number of contact points, a concept was developed to attempt to overcome this difficulty. The approach consisted of utilizing a large number of metallic fibers in contact with a plane surface. Each fiber is a potential contact point and the number of points per unit area would be limited only by the ability to mechanically hold and thermally heat sink the fibers.

A natural candidate for evaluation was available since the superconducting wire manufactured by Magnetic Corporation of America is a composite of continuous Niobium-Titanium filaments distributed in a copper matrix. Cross-sections of two typical conductors are shown in Figures 55 and 56. The conductors are available in a large number of sizes with different numbers of filaments. Removal of the copper and exposure of the NbTi filaments yields a large number density of small diameter parallel fibers which are in intimate contact with copper on one end. The latter is, of course, advantageous from a heat transfer standpoint.

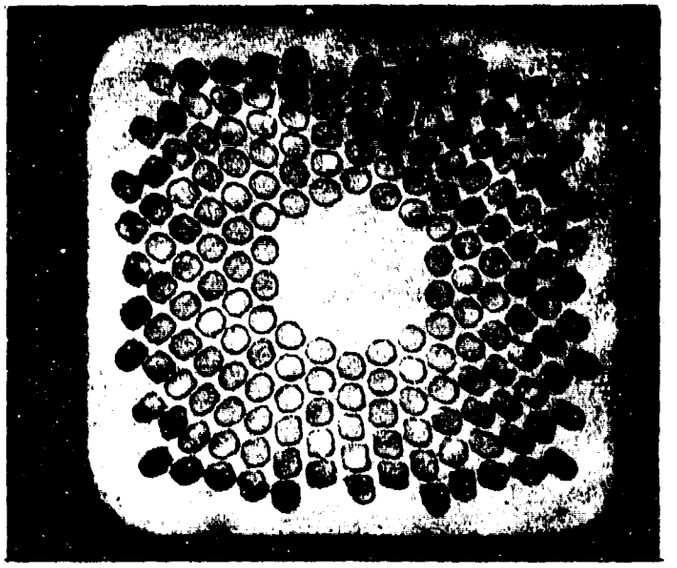

Figure 55. Cross section of NbTi-Copper composite, 1.62 mm square, 180 strands of NbTi, 1 twist/in. The inner strands have not been put in because they do not twist. This conductor is capable of carrying a current of 1050A at 60 kilogauss ($j=4 \times 10^4$ A/cm^2).

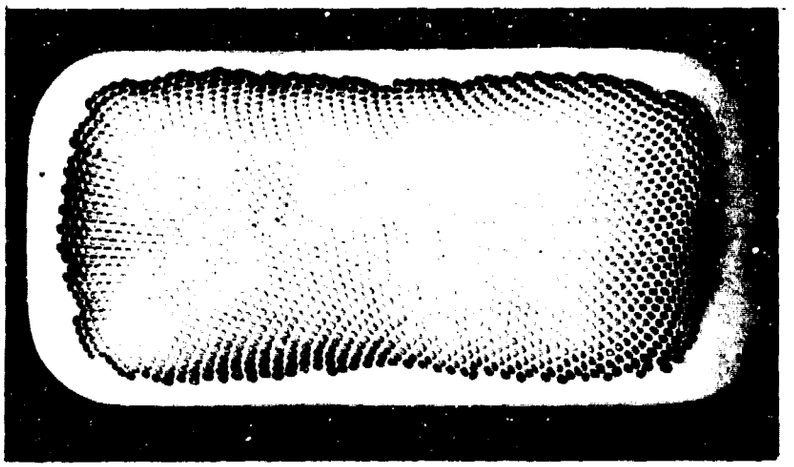

Figure 56. Cross section of 1.67 mm x 3.35 mm NbTi composite containing 2133 strands of NbTi in a copper matrix with 0.5 twists/in. capable of carrying 2200A at 60 kilogauss ($j=5.2 \times 10^4$ A/cm^2).

In order to measure the current-voltage characteristics of the brushes, a rotary test rig was constructed. This is shown in the photograph, Figure 57, and the drawing, Figure 58. The main shaft of the test apparatus is rotated with a belt drive from a 3/4 hp DC motor. Current is fed to the rotating main shaft through a stationary brush assembly. This assembly consists of eight paralleled copper-graphite brushes (SCP Grade 505), each of which has cross-sectional dimensions of 6.35 cm x 2.18 cm (2.5 in. x 0.86 in.). The current flows down the main shaft, then flows through a flexible coupling to a portion of the main shaft which is mounted inside an inverted glass tee. The glass enclosure serves as an environmental control for the equipment. The brush holder, which also serves as a current collector, is mounted vertically in the upper leg of the inverted tee such that the brush contacts a brass wheel which is rigidly attached to the main shaft.

Figure 59 is a photograph of a filamentary NbTi brush (Sample No. 1) mounted in the brush holder. The brush is made up of 2133 NbTi filaments imbedded in a copper matrix. The ratio of copper to niobium titanium is 2:1. The outer diameter of the copper matrix is 0.759 cm (0.299 in.). Each of the filaments has an outer diameter of 0.0095 cm (3.73 mil), and an exposed length of 0.965 cm (0.38 in.). As is shown in the photograph, the filaments tend to spread out at their unattached end. In addition, the majority of the strands at the free end are located in an annular region, the inner and outer diameters of which are 0.514 cm (0.202 in.) and 0.824 cm (0.324 in.), respectively. The outer diameter of the filament bundle at the attached end is 0.671 cm (0.264 in.).

The experimental results obtained with Sample No. 1 are typical and have been very encouraging. The sample carried 162.5 A, which corresponds to a current density of 360 A/cm^2 (2320 $A/in.^2$) in the CuNbTi composite. At this current, the voltage drop across the brush was 0.16 V, and the temperature of the brush at its attached end was 56°C. There was no observed sparking at the interface between the brush and the rotor, although there were indications that brush and/or rotor wear may be severe.

Figures 60, 61, 62, and 63 are plots of the experimental data obtained with Sample No. 1. Figure 60 is a plot of the voltage drop across the brush as a function of the current through the brush for a constant rotational speed of 218 rpm. For comparison with the experimental data, the straight line V/I = 1 mV/A has been included. Figure 61 is a plot of the voltage drop across the brush as a function of the rotational speed for various values of current. As can be seen from this plot, the voltage drop is insensitive to the rotational speed for the low range of speeds covered. Figure 62 is a plot of the maximum thermocouple temperature as a function of the current for a constant rotational speed of 218 rpm. For zero current, the minimum thermocouple temperature is included. The difference between the minimum and maximum temperature at zero current indicates the temperature rise resulting from frictional losses only. Figure 63 is a plot of the maximum thermocouple temperature as a function of the brush power (where brush power is defined as the current times the brush voltage drop) for a constant rotational speed of 218 rpm. As in Figure 62 the temperature rise due to the frictional losses has been included. The data of Figures 62 and 63 were obtained with the thermocouple mounted on the brush holder close to the base of the brush strands. Thus, the temperature of the thermocouple is approximately that of the brush filaments at their attached end. The data contained in Figures 60 through 63 all correspond to steady state operation.

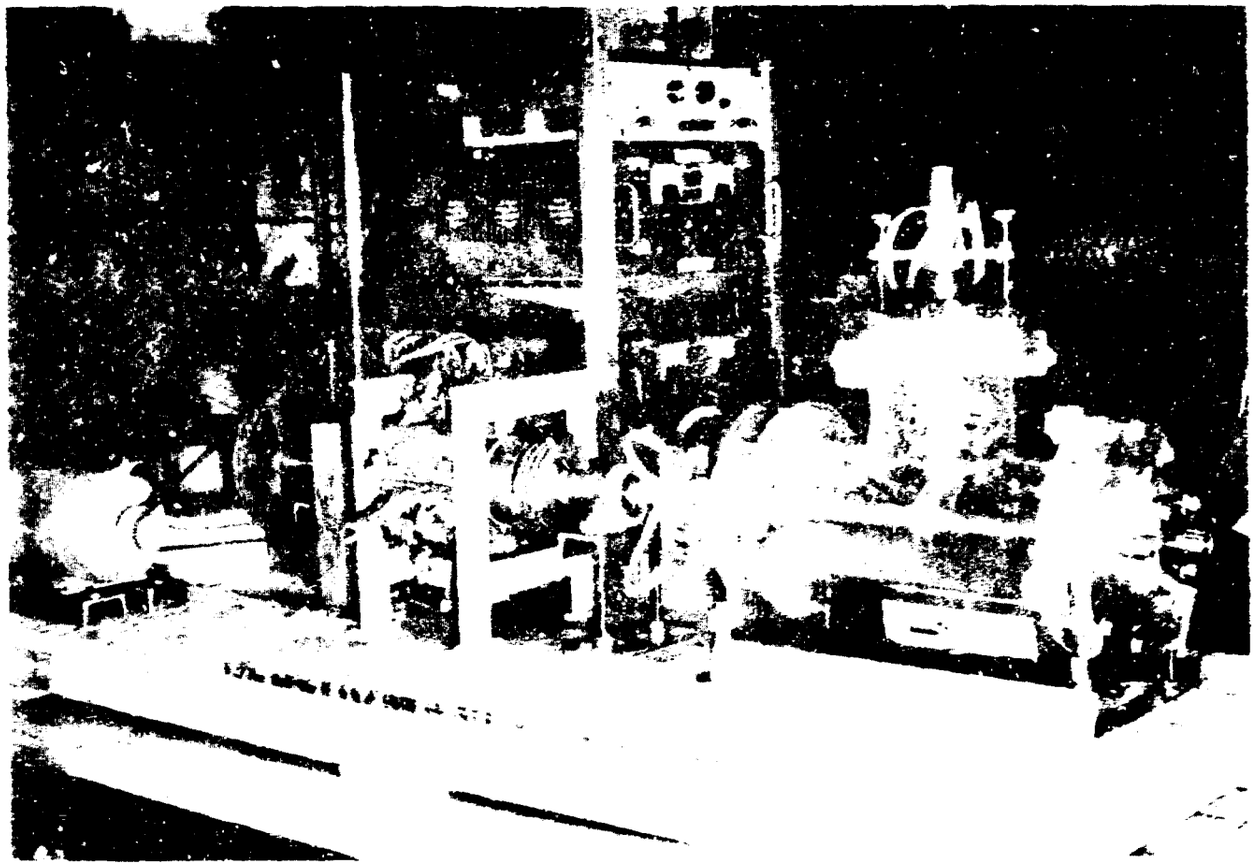

Figure 57. Rotary test apparatus. Visible in the photograph (from left to right) are: 3/4 hp DC motor, drive belt from motor to main shaft, brush holder system for passing current from power supply (visible in background) to rotating main shaft through standard copper-graphite brushes, cooling fins on main shaft, flexible shaft coupling, and inverted glass tee with main shaft, brass collector disc, and vertically mounted test brush holder/collector.

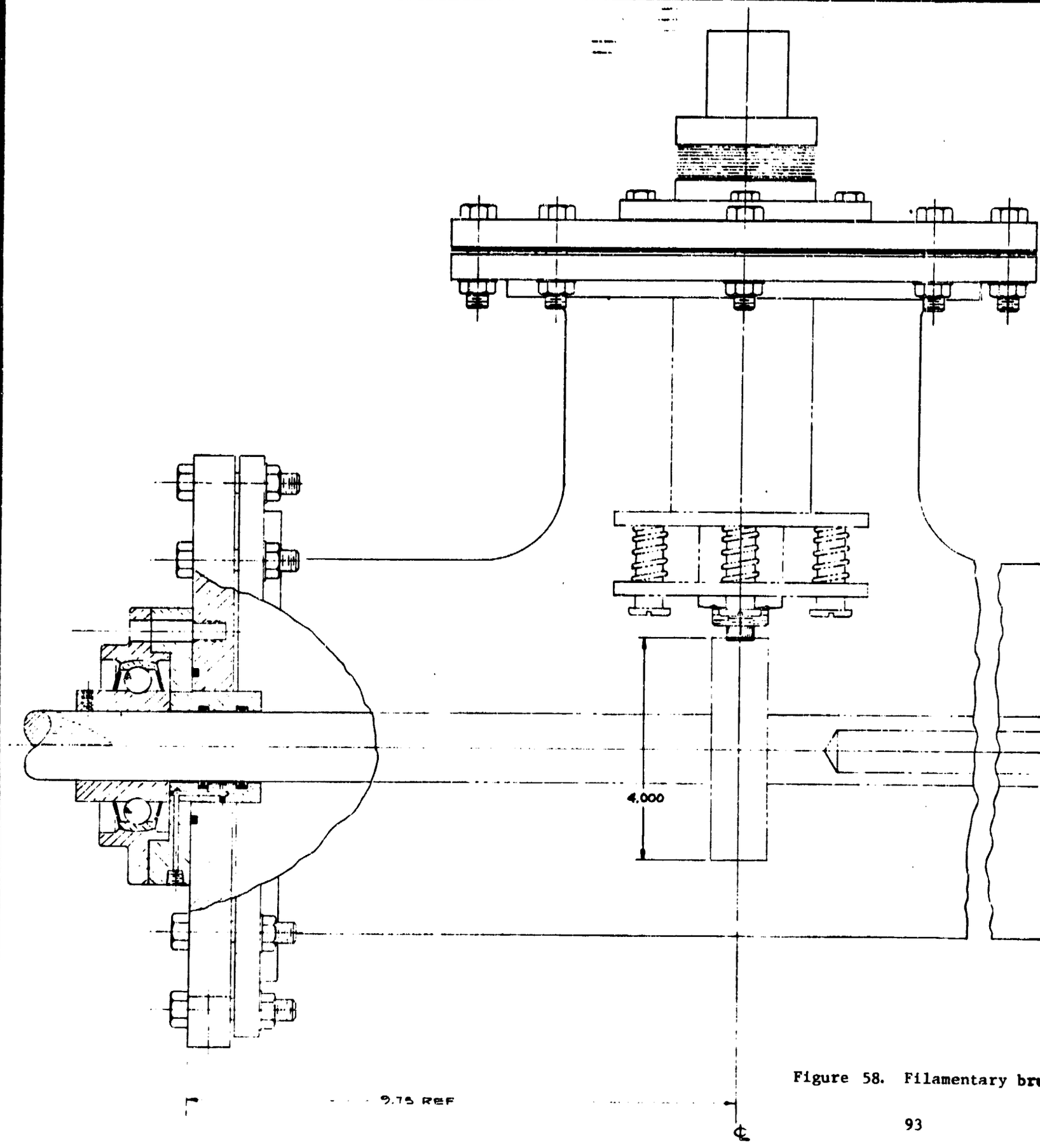

Figure 58. Filamentary br

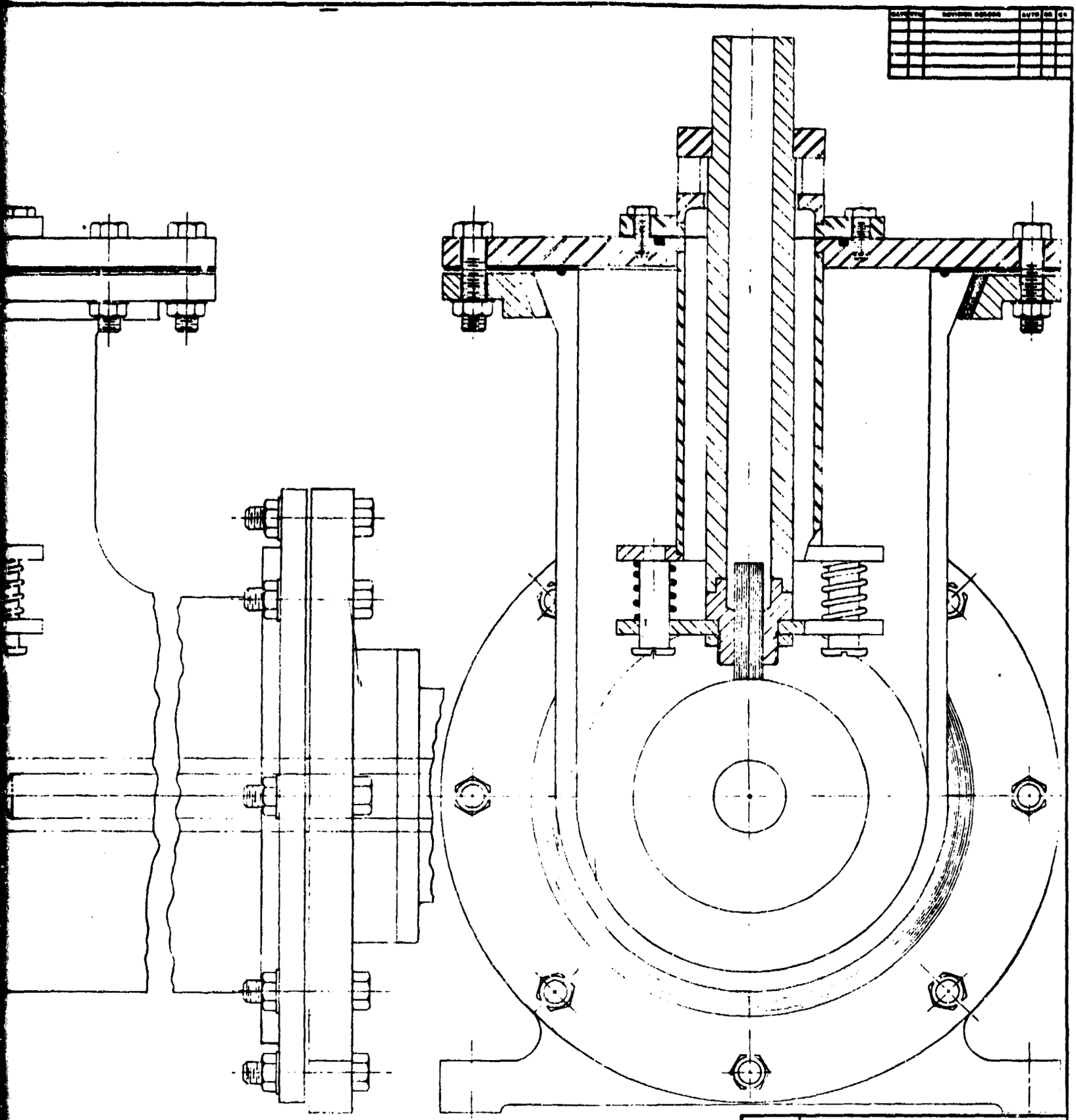

re 58. Filamentary brush test rig assembly.

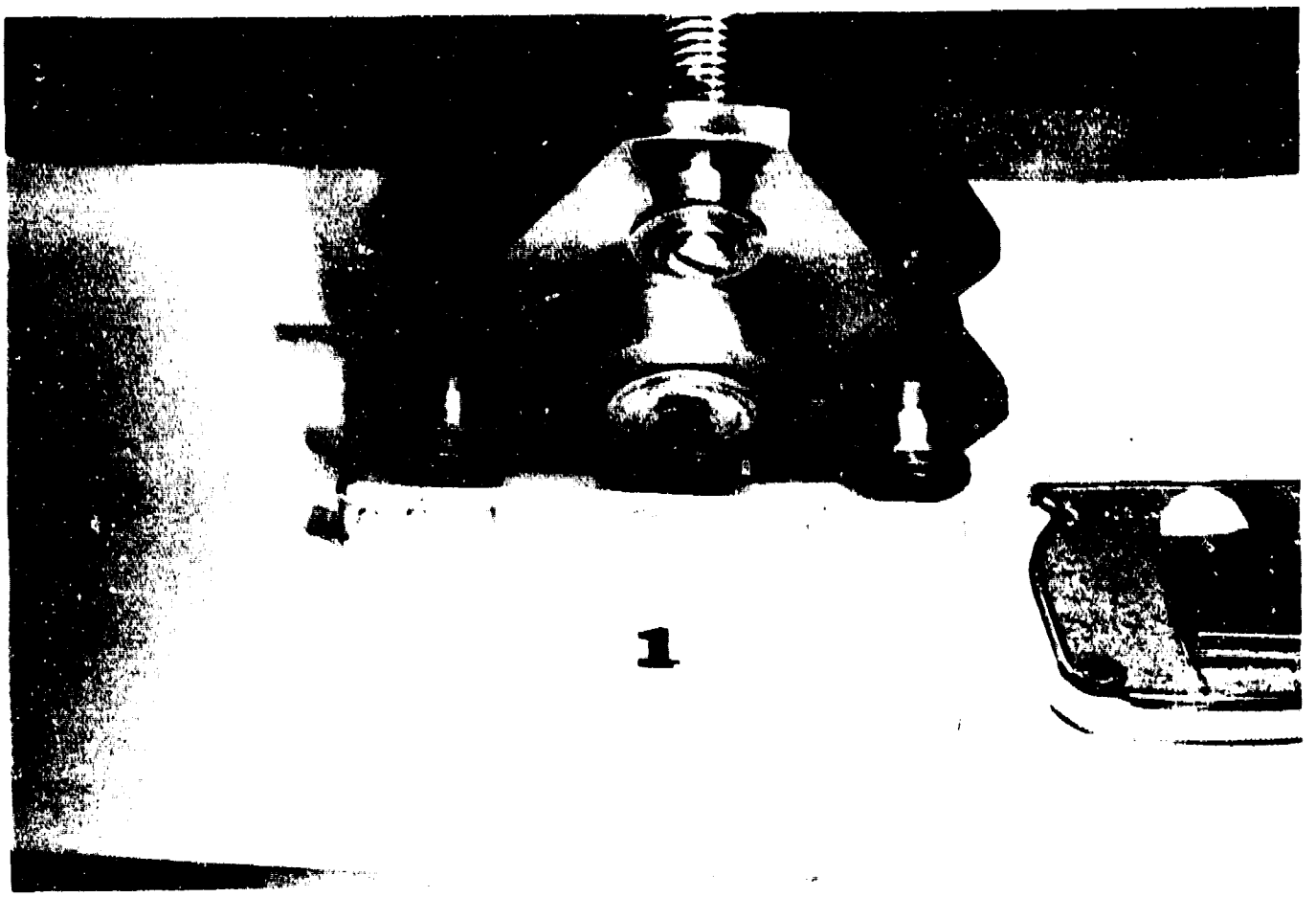

Figure 59. Sample No. 1 for the rotary test apparatus. The brush, shown mounted in its holder, has the following characteristics:

Composition	NbTi filaments in Cu matrix
Ratio, Cu:NbTi	2:1
Size (including Cu)	0.774 cm (0.305 in) dia
Number of filaments	2133
Filament size	0.0097 cm (3.82 mil) dia
Exposed filament length	0.677 cm (0.267 in)

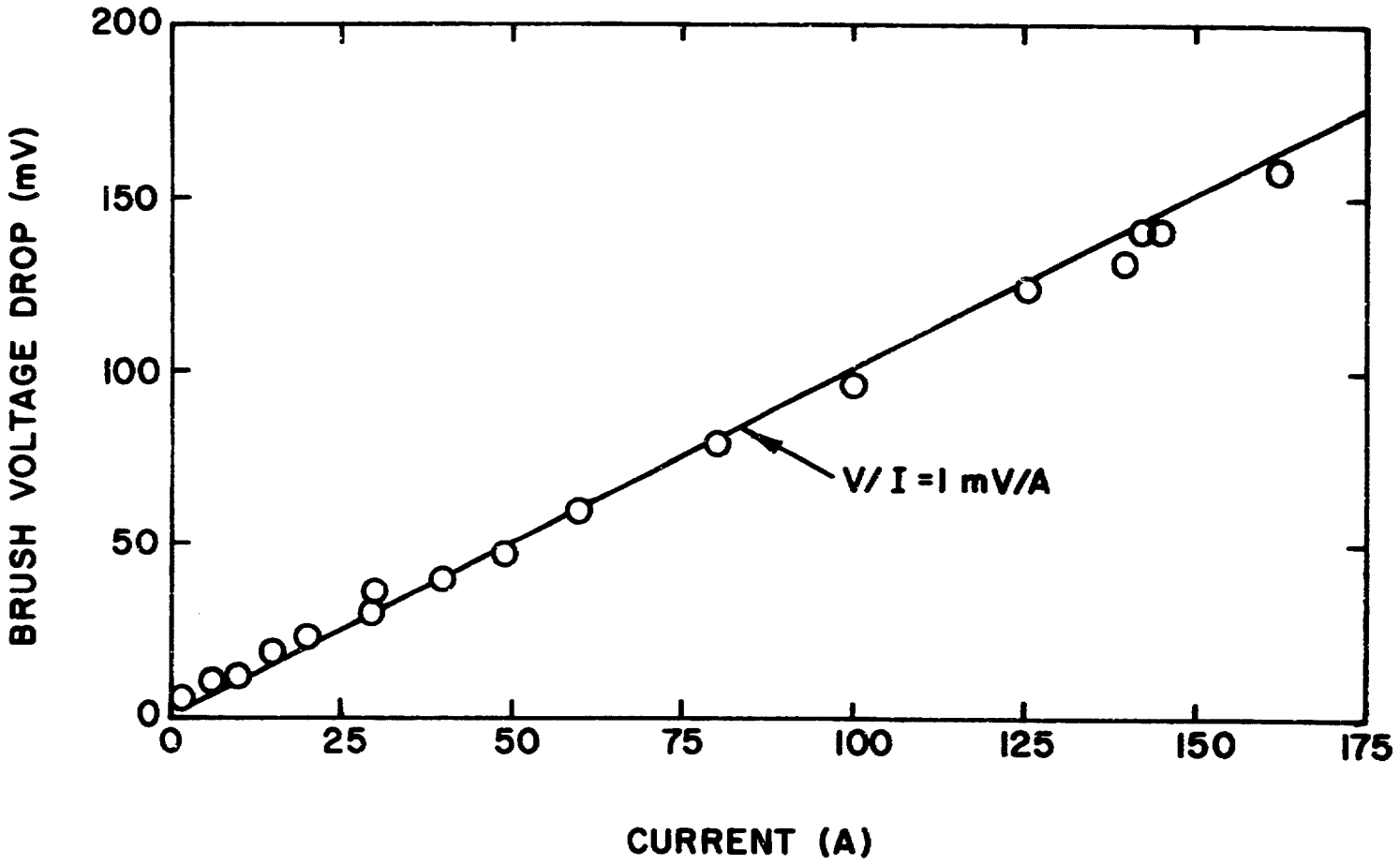

Figure 60. Measured voltage drop across the filamentary brush (Sample No. 1) as a function of the current through the brush for a constant rotational speed of 213 rpm. The straight line V/I = 1 mV/A is included for comparison with the experimental data.

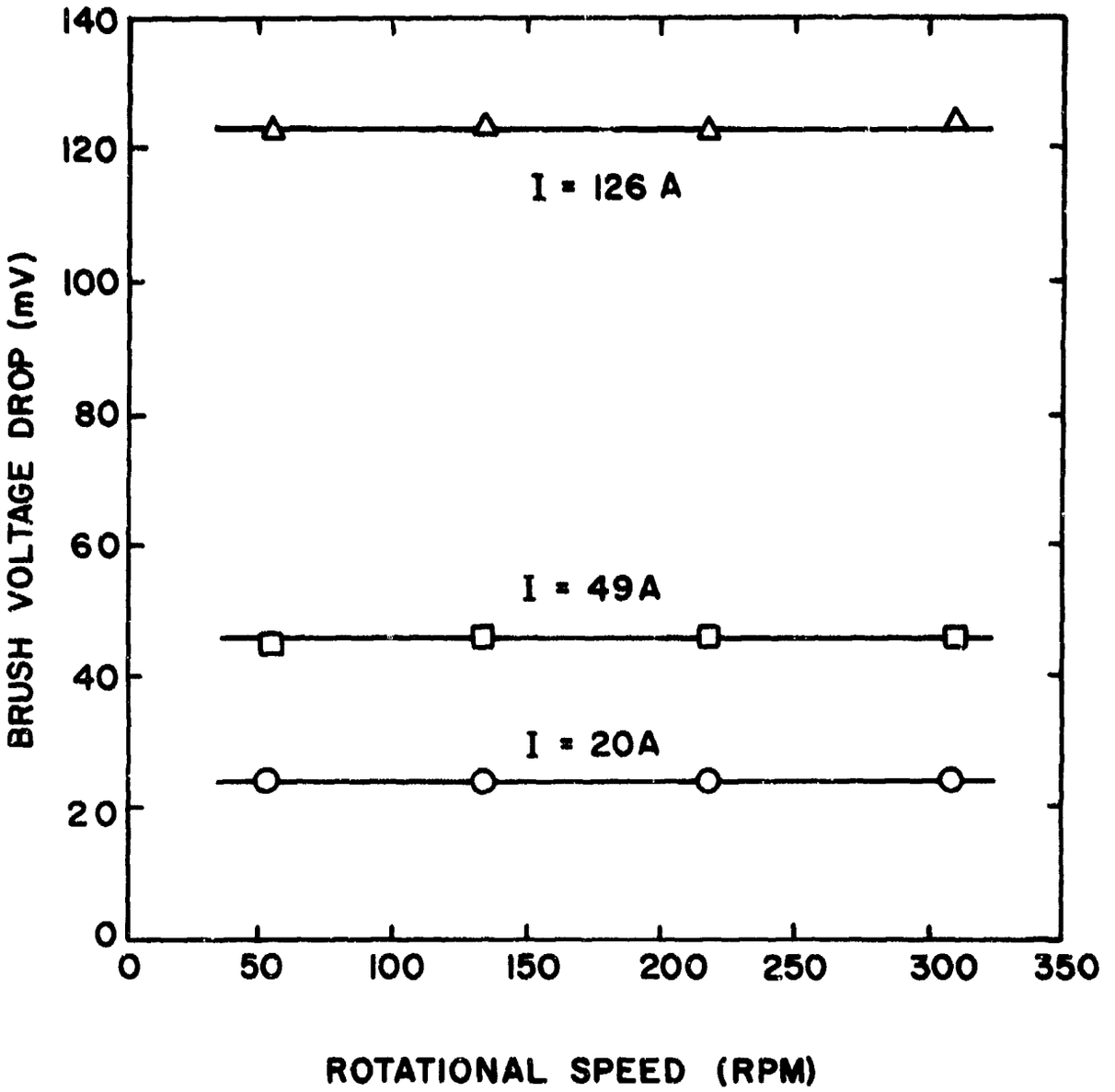

Figure 61. Measured voltage drop across the filamentary brush (Sample No. 1) as a function of the rotational speed of the rotor for various values of current. The straight lines correspond to constant voltage drop for a given current.

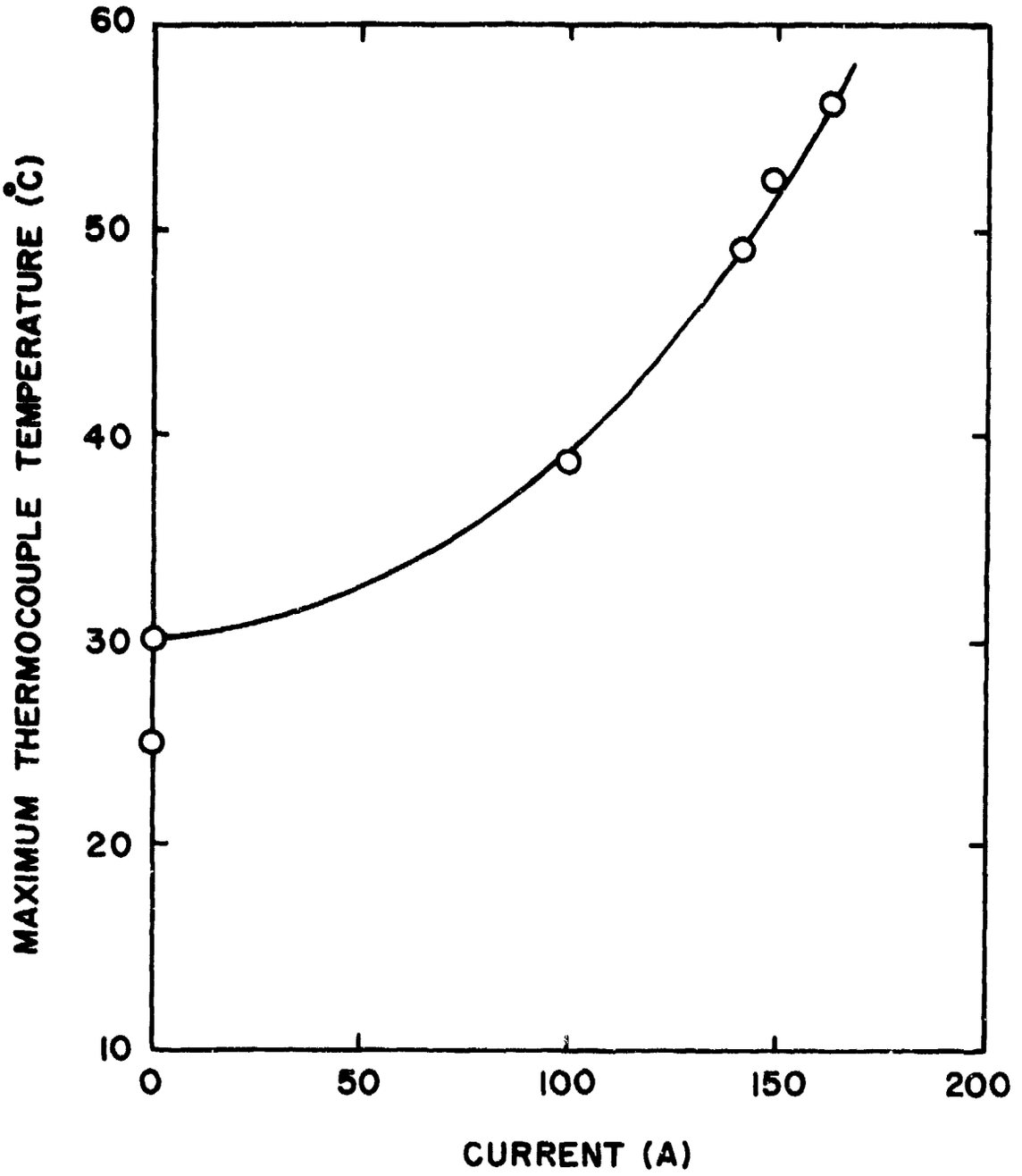

Figure 62. Maximum measured thermocouple temperature as a function of the brush current for Sample No. 1 at a constant rotational speed of 218 rpm. The smooth curve is arbitrary.

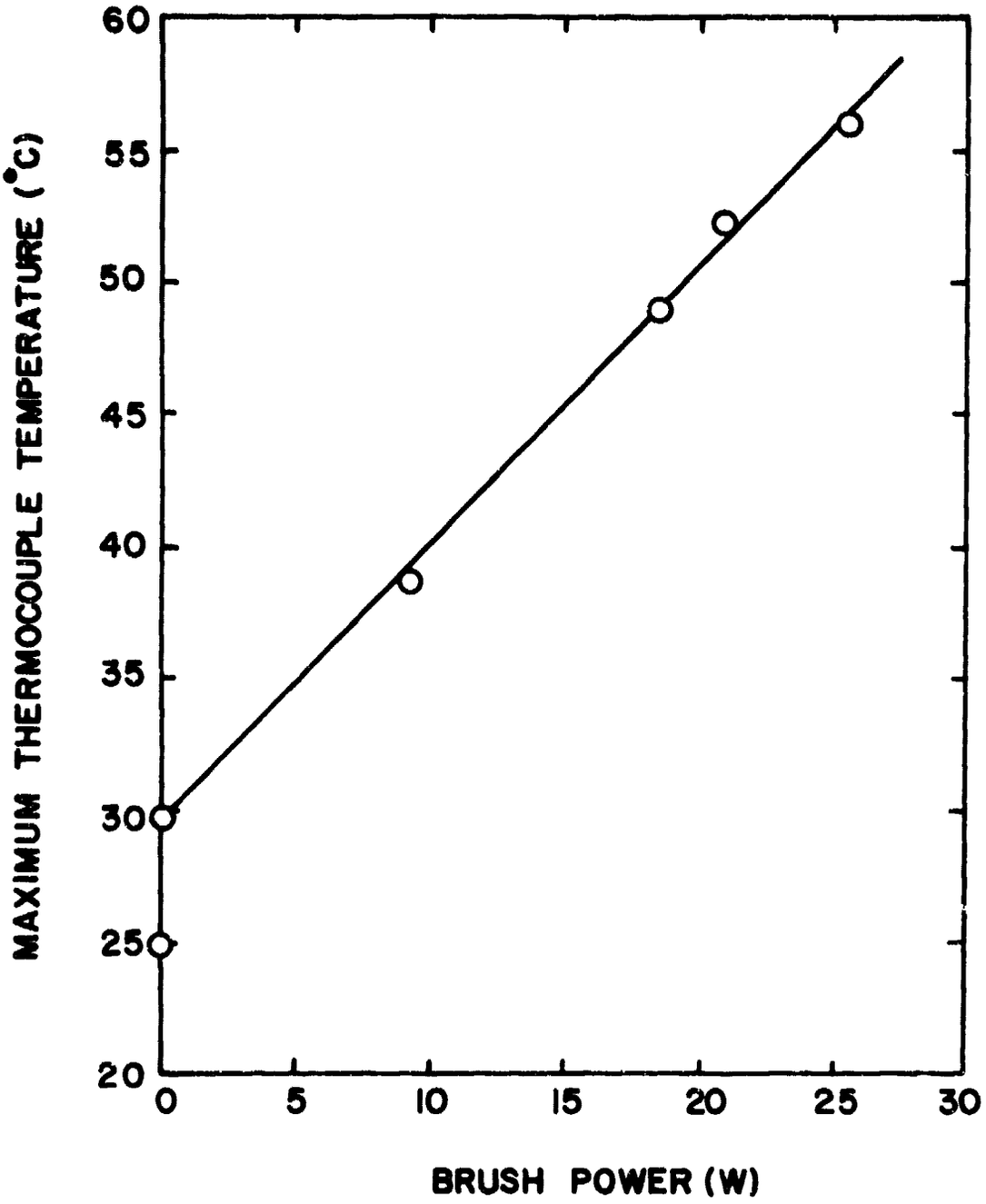

Figure 63. Maximum measured thermocouple temperature as a function of the brush power (defined as current x brush voltage drop) for Sample No. 1 at a constant rotational speed of 218 rpm. The straight line is included to indicate the linear relationship between the temperature and brush power.

The brush described above was fabricated from a single composite conductor. Other configurations included brushes fabricated from several small composite conductors in parallel. An example is Sample No. 7 which was fabricated from seven identical conductors, each of which had the following characteristics: 0.268 cm (0.105 in.) diameter, 0.294 cm (0.1156 in.) average strand length, 2133 filaments, and a 2:1 ratio of copper to superconductor. The brush carried 186 A which corresponds to an overall conductor current density of 473 A/cm^2 (3050 A/in.^{2}), and a filament current density of 1420 A/cm^2 (9160 A/in.^{2}). Figures 64, 65 and 66 summarize the experimental results obtained with this sample. Figure 64 is a plot of the filamentary brush voltage drop as a function of the brush current for a rotational speed of 300 rpm. The straight line indicates a V/I ratio for the brush of 0.64 mΩ. Figure 65 is a plot of the maximum thermocouple temperature as a function of the brush current for a rotational speed of 300 rpm. The difference between room temperature and the zero current temperature corresponds to the temperature increase due to frictional losses. The thermocouple was positioned as close as possible to the base of the brush where the filaments are attached. Figure 66 is a plot of the maximum thermocouple temperature as a function of the filamentary brush power, where the power has been defined as the product of the brush current and brush voltage drop.

A summary of the results of the steady state characteristics of the filamentary brushes is contained in Table X. The samples are listed in the order in which they were tested, from Sample 1 to Sample 7. Only Sample No. 1 of the seven samples was not tested to the limit of its current carrying capabilities. Table X is organized in the following manner: the first section gives the pertinent physical characteristics of the samples; the second gives the electrical characteristics; and the third and final section gives other parameters associated with the performance of the brushes.

The contents of the first section of Table X require little explanation. Samples 5, 6 and 7 were all made up of more than one conductor, as shown in the table. The total conductor area of Sample No. 7 for example, is seven times the area of a single conductor, rather than the overall area that the seven conductors occupied. That is, no attempt was made to include the packing factor of the conductors in each brush, which permits evaluation of the samples on a "per conductor" basis.

The second section of Table X contains the electrical characteristics of the brush samples in terms of their maximum current carrying capabilities. For each maximum continuous current there is a corresponding "run time," as given in the table. A "+" after an entry indicates that that particular sample could have been run longer than the time given. An absence of a "+" indicates that the time given corresponds to the time required for the filamentary brush voltage drop to increase to 1.5 times (arbitrarily selected) its original value at the given current level. The conductor and NbTi current densities conclude this portion of the table. The conductor current densities of Samples No. 3 and 4 are low because of the large ratio of copper to superconductor in these conductors.

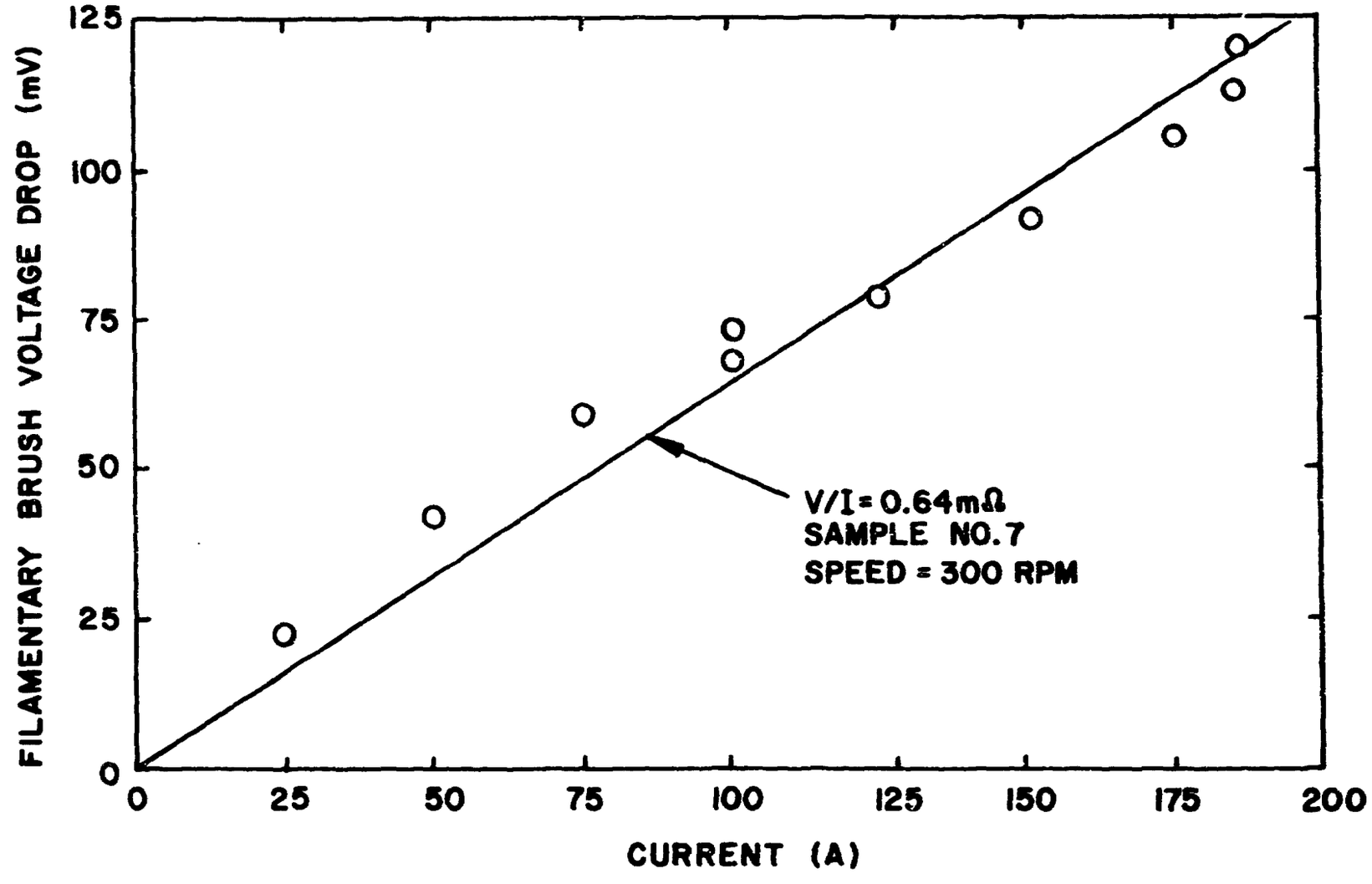

Figure 64. Measured filamentary brush voltage drop as a function of the current for Sample No. 7 at a rotational speed of 300 rpm. The straight line corresponds to a V/I ratio of 0.64 mΩ.

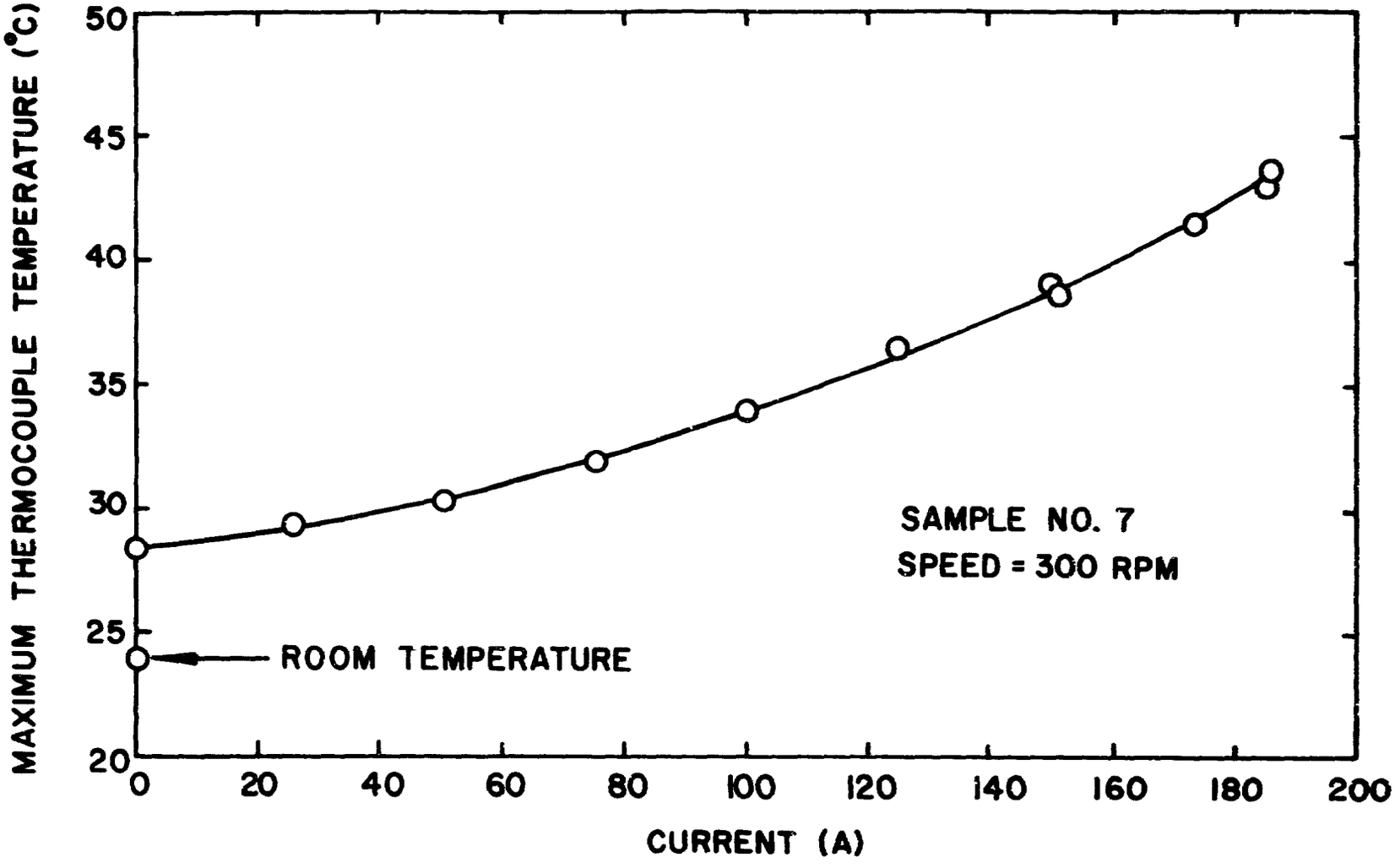

Figure 65. Maximum measured thermocouple temperature as a function of the current for Sample No. 7 at a rotational speed of 300 rpm. The difference between room temperature and the zero current temperature corresponds to the temperature increase due to frictional losses.

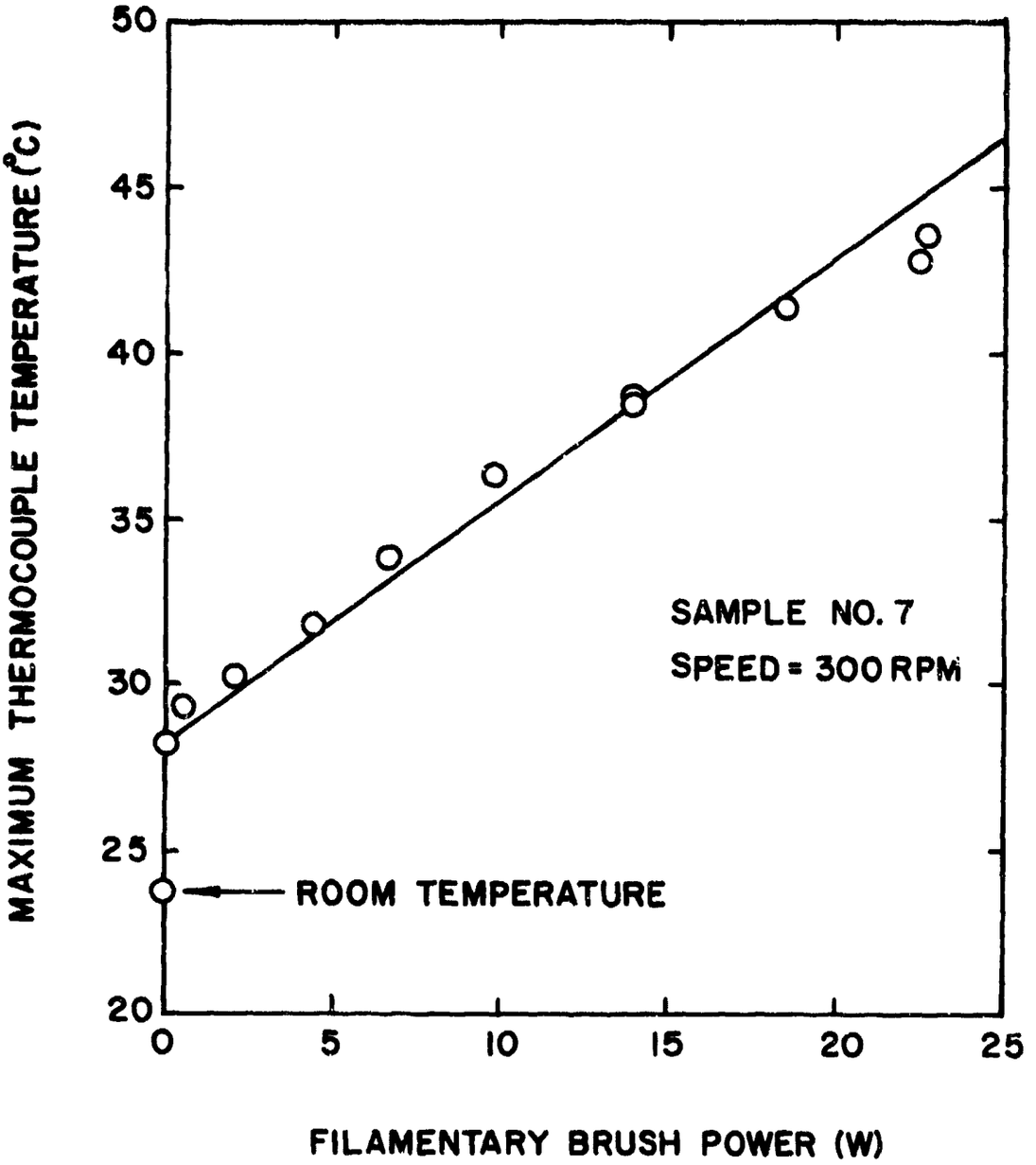

Figure 66. Maximum measured thermocouple temperature as a function of the filamentary brush power for Sample No. 7 at a rotational speed of 300 rpm. The difference between room temperature and the zero power temperature corresponds to the temperature increase due to frictional losses.

Table X.

SUMMARY OF TEST RESULTS:

STEADY STATE CHARACTERISTICS OF FILAMENTARY BRUSHES

Sample number	1	2	3	4	5	6	7
No. conductors in sample	1	1	1	1	3	3	7
No. filaments per conductor	2133	2133	2700	2700	2133	2133	2133
Ratio, Cu:NbTi	2	2	6	6	2	2	2
Conductor size (cm)	.759	.759	.1x.5	.1x.5	.268	.268	.268
(in)	.299 dia	.299 dia	.2x.4 rect	.2x.4 rect	.105 dia	.105 dia	.105 dia
Filament size (cm)	.0095	.0095	.0059	.0059	.0033	.0033	.0033
(mil)	3.73	3.73	2.32	2.32	1.315	1.315	1.315
Filament length (cm)	.965	1.40	.812	.33	.352	.222	.294
(in)	.38	.55	.32	.13	.139	.0876	.1156
Total conductor area (cm^2)	.452	.452	.516	.516	.1682	.1682	.393
(in^2)	.070	.070	.080	.080	.0261	.0261	.0609
NbTi area (cm^2)	.1505	.1505	.0738	.0738	.0561	.0561	.131
(in^2)	.0234	.0234	.0114	.0114	.0087	.0087	.0203
Continuous I_{max} (A)	162.5	175.5	76.	101.	76.5	81.	186.
Run time at I_{max} (min)	40+	15	10.5	69+	20+	21.7	43.5
Conductor j_{max} (A/cm^2)	360	389	147.2	196	454	481	473
(A/in^2)	2320	2500	950	1263	2930	3100	3050
NbTi j_{max} (A/cm^2)	1080	1166	1032	1372	1362	1443	1420
(A/in^2)	6960	7500	6650	8850	8790	9310	9160
Measured R_b (mΩ)	1.0	1.8	4.0	1.2	2.0	1.2	.64
Calculated R_b (mΩ)	1.0	1.45	4.0	1.62	2.0	1.26	.712
ρ_o (10^{-6} Ω cm)	156	156	363	363	319	319	319
$\beta^2 = \rho_o j_{sc}^2 \ell^2 / k$ (K)	1690	4150	2550	1140	733	328	612
Conductor QF ($10^{-8} \Omega m^2$)	4.4	8.38	22.7	6.33	3.37	2.29	2.51
NbTi QF ($10^{-8} \Omega m^2$)	1.46	2.8	3.24	.903	1.124	.763	.838

The third and final section of Table X contains other parameters associated with the performance of the filamentary brushes. R_b is the effective brush resistance, defined as the ratio of the filamentary brush voltage drop to the current. For low values of the current, the brush resistance may be calculated as:

$$R_b = \rho_o \ell / A_{sc}$$

where:

ρ_o = resistivity of the NbTi

ℓ = filament length

A_{sc} = cross-sectional area of the NbTi

This formula was used, along with the measured value of the brush resistance, to "calibrate" the resistivity of the NbTi for the three different conductor types investigated. The next quantity given in the table, β^2, indicates the difference between the maximum filament temperature and the thermocouple readings at the attached end of the filaments (See Appendix II). The final two quantities given in the table are conductor and NbTi quality factors which are defined as the ratio of the filamentary brush voltage drop to the current density (at the maximum continuous current level) in the conductor and NbTi, respectively.

In an attempt to further evaluate the performance of filamentary brushes, additional data was taken. At various current levels, the time required for a 50% increase in the filamentary brush voltage drop was determined. This data is plotted in Figure 67. The two lowest data points on this plot (2 and 3) are the same two points that have the highest value of β^2, as shown in Table X. In addition, at this current level, Sample No. 2 glowed yellow in the central portion of its exposed filaments. This evidence indicates that these two samples were thermally limited by the ohmic heat generated within their strands. That is, these samples had filaments that were too long compared to their cross-sectional areas to conduct away their I^2R losses. Those samples that reached a non-thermal limit (Samples No. 4, 5, 6 and 7), however, have corresponding NbTi current densities at the maximum current levels attained, as shown in Table X. The average of the four NbTi current densities is 1400 A/cm^2 (9030 A/in.^{2}), and all four values lie within ±3% of this average. This evidence indicates that, in order to maintain a stable and low value of contact potential drop from the moving rotor to the stationary filaments, there is a maximum NbTi filament current density that may be tolerated, given by approximately 1400 A/cm^2 (9030 A/in.^{2}).

The above tests were performed with brushes in contact with a continuous rotor. Several tests were also performed on a discontinuous rotor to begin gathering data on filamentary brush characteristics when switching.

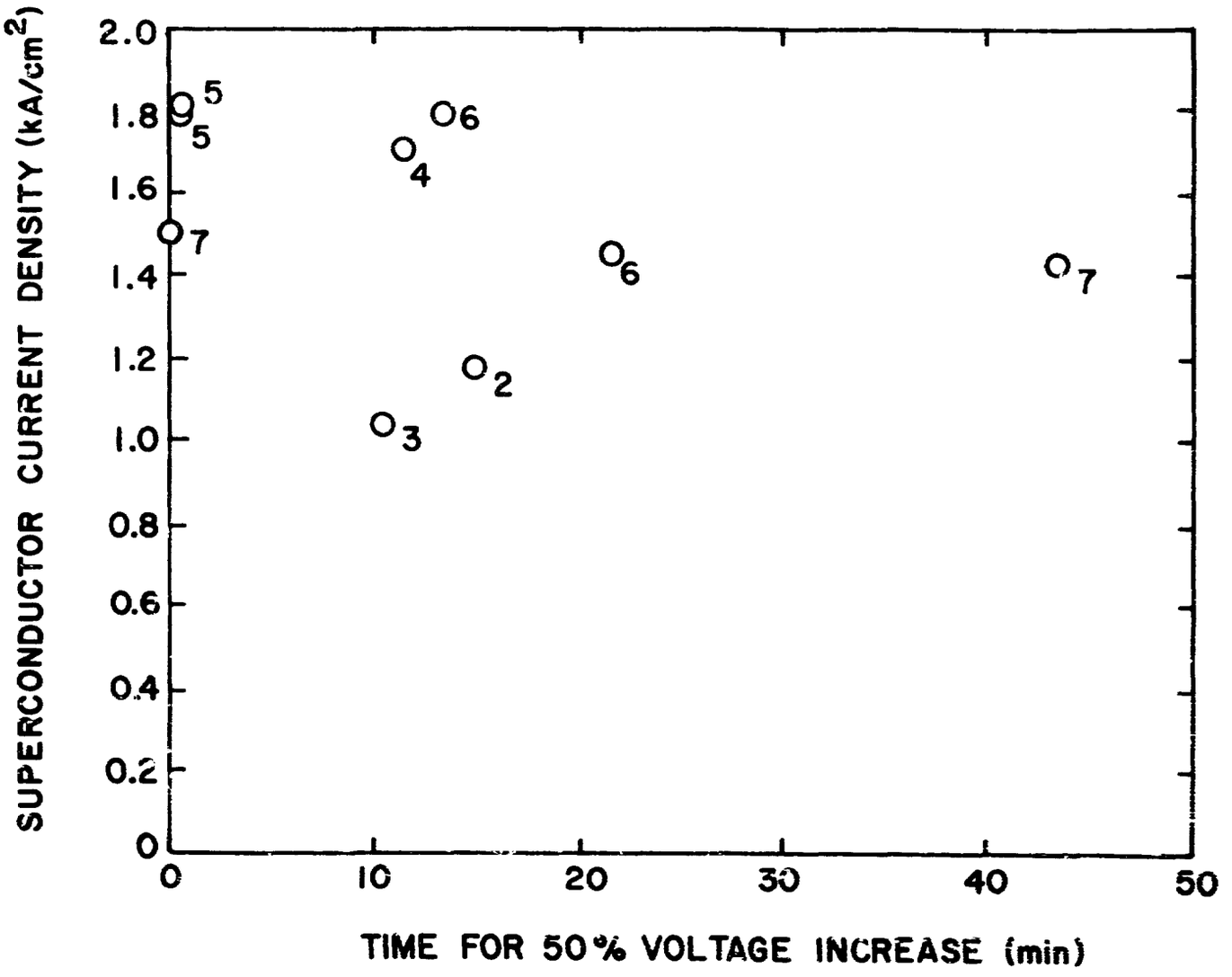

Figure 67. Measured superconductor current density as a function of the time required for a 50% increase in the voltage drop across the filamentary brush. The sample number is included with each data point.

The rotary test apparatus was modified such that a current could be switched by removing portions of the test rotor, as shown in the sketch of Figure 68. This particular configuration was chosen because it presents the brush with a large gap immediately following contact separation. Symmetry was desirable to reduce mechanical balance problems. Results were preliminary in nature. Without an inductive load in the switch circuit, the filamentary brushes were used to switch 150 A at a pulse repetition rate of 5 pps. With an inductive load of 10 mH, the filamentary brushes were used to switch 40 A at a pulse repetition rate of 5 pps, without the aid of an auxiliary arc quench circuit. This does not represent a limitation of the brushes, but the limit of data taken to date.

Looking forward, estimates were made to determine the power supply required to switch 2,000 A at a repetition rate of 10 pps in an inductive circuit. The circuit which was considered is shown in Figure 69. The R represents the load resistor, L the load coil, V the power supply, and R_i the resistance of the power supply, leads, and closed switch. The purpose of the capacitor, C, is to limit the rate of voltage rise across the switch after contact separation. The characteristics of the circuit are basically determined by the ratio of the coil inductance to the parallel combination of the two resistors, $R_p = R R_i/(R + R_i)$. Figure 70 shows results for a final current of 2,000 A using either the field coil or load coil described earlier in this report. Basically, for R_i very small, the L/R_p time constant is long compared to the charge time, very little voltage is lost across R_i, and the current through the coil increases linearly with time. For R_i very large, the L/R_p time constant is short compared to the charge time, the coil charges quickly, and the large supply voltage is required to sustain the large drop across R_i.

Based on the results of Figure 70, it can be seen that for $R_i = 20$ mΩ, a supply voltage of 60 V is required to achieve 2,000 A through a 0.902 mH coil in 50 ms. The requirement for 60 V could easily be met with a set of batteries consequently a test series at the 2000 A level appears reasonable as the next step in brush evaluation.

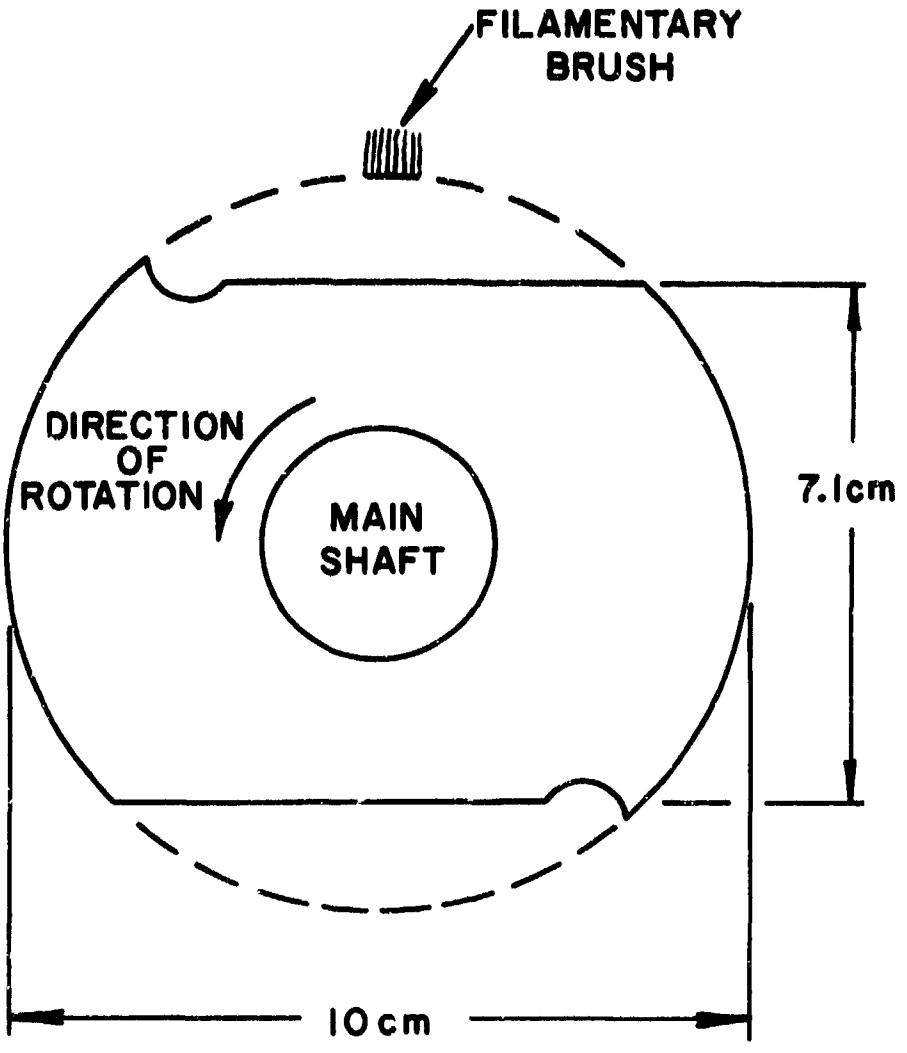

Figure 68 Sketch of the rotor configuration for current interruption with the filamentary brushes. The dashed lines represent the configuration of the rotor before modification.
Scale: ful size.

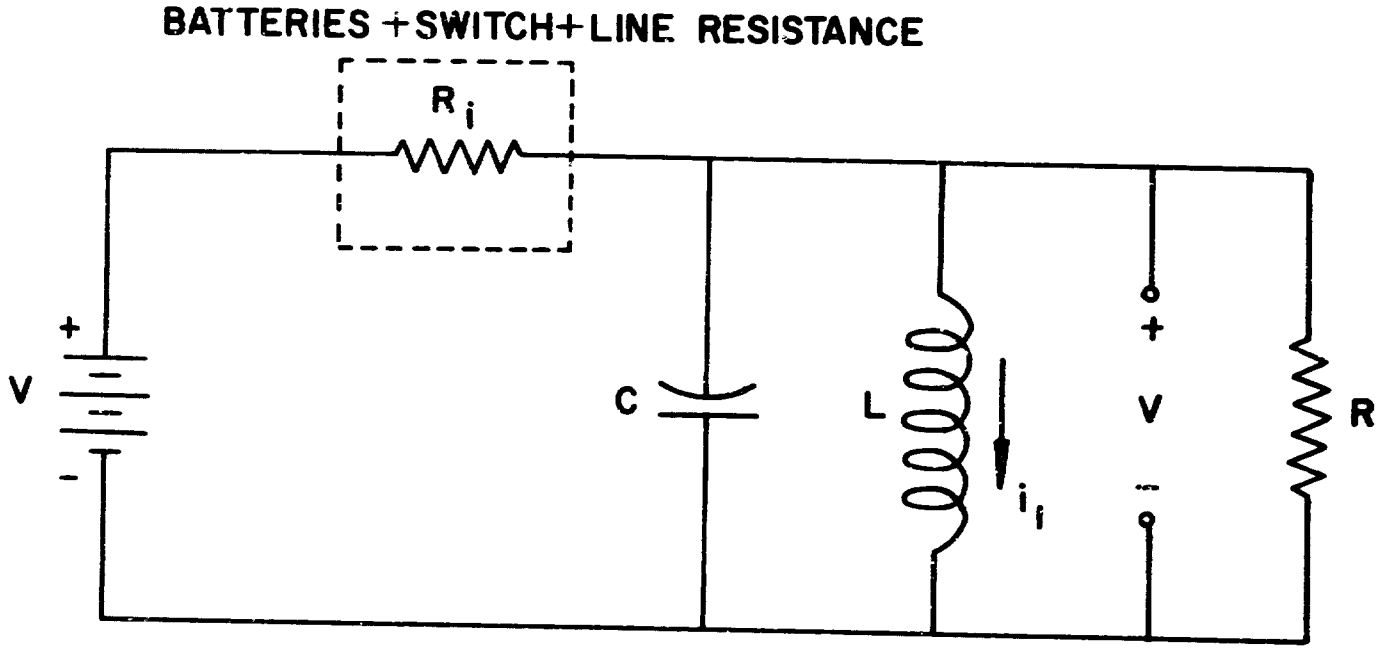

Figure 69. Test circuit diagram to determine parameters necessary for a 2000 A brush test. When the switch is closed, R_i is very low, and the inductor is charged by the voltage supply, V. When the switch opens, R_i becomes infinite and the circuit behaves as a parallel LRC circuit.

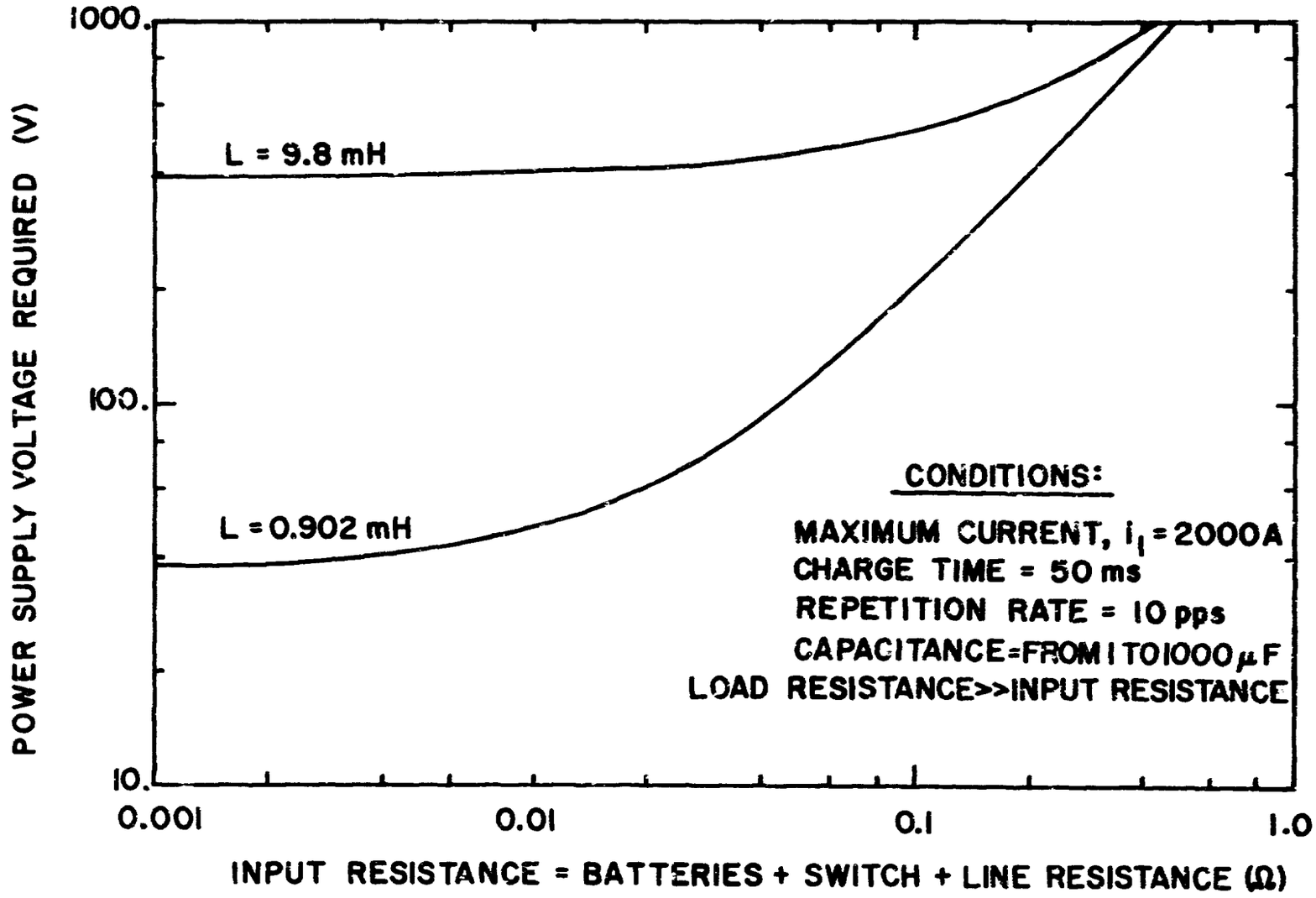

Figure 70. Power supply voltage required to charge the coil (of Figure 59 to 2,000 A in 50 ms as a function of the input resistance for two values of the coil inductance. The load resistance must be very much greater than the input resistance for these curves to be valid.

SECTION V.

SYSTEM INTEGRATION & FUTURE DEVELOPMENT

From an overall systems standpoint, it is technically logical to utilize an applied magnetic field and cryogenic cooling in the switching section of an inductive energy storage system. Cryogens will be available because of their necessity for operation of the energy storage element and the magnetic field is available since it represents the means whereby the inductor stores its energy.

In this section a conceptual design for an integrated energy storage coil, dewar and switching system is presented.

1. SYSTEM INTEGRATION

For the purposes of this section, the switching concept which will be used will be that of a linearly actuated unit with parallel contacts. This will illustrate the means by which the magnetic field from the energy storage coil and the cryogens may be utilized. If a single contact linearly actuated switch or rotary switch with arc chute(s) is(are) developed and found more appropriate, the basic concept for integration will be the same.

In this discussion, the energy storage coil will be assumed to be superconducting. Typically, a one megajoule superconducting solenoid for pulsed energy storage would have the following dimensions:

inside diameter:	0.34 m
outside diameter:	0.41 m
length:	0.24 m
peak flux density:	6.0 W/m^2

The above dimensions indicate the feasibility of mounting several specially designed vacuum interrupters within the bore of the energy storage coil. For the same energy if the peak flux density were lower, the coil would be larger. In the final system design, a trade-off would be performed to determine the optimum configuration. The coil size shown above, together with the configuration about to be discussed, indicates the feasibility of this approach.

For purposes of discussing the integrated system concept, the parallel contact vacuum interrupter configuration was chosen. The final

design may use a rotary switch in a similar fashion. The integrated system is illustrated in Figure 71 which shows three pair of contacts mounted so as to utilize the field produced by the energy storage coil. The latter is superconducting and immersed in liquid helium. The switch and dewar share a common vacuum which is cryo-pumped by the molecular sieve material bonded to the helium container as shown.

The dewar is liquid nitrogen shielded. In addition, the liquid nitrogen is used to heat sink the shield for the molecular sieve and to heat sink the arc vapor condensation shield. A separate liquid nitrogen container is used to heat sink the stationary contacts. The movable contacts are cooled by passing cryogen boiloff through a heat exchanger surrounding the leads. The main features of the integrated system are:

(1) a common vacuum for switch and dewar

(2) shaped contacts to utilize the magnetic field from the energy storage coil

(3) cryovacuum pumping to remove all contaminants including the noble gases

(4) switch losses reduced by reduced temperature operation

(5) switch losses absorbed by cryogen and cryogen boiloff

Several development problems remain in the design and construction of an integrated system, however, the concept appears feasible. Characteristics of subsystems would be intermarried for mutual benefit.

2. FUTURE DEVELOPMENT

a. Filamentary Brush

The large number of applications for a high current density brush system, combined with the preliminary test results obtained in the program form an argument for future development in this area which is overbearing. In the brush tests conducted in this program, current densities in the range of 2000-3000 A/in^2 were attained with filamentary brush voltage drops which are substantially lower than those obtained with conventional brushes operating at their limit of about 150 A/in^2. Potential applications lie in high performance rotating machinery and other devices using sliding contacts such as a rotary switch. Development has barely begun and the need is obvious for extensive fundamental testing to determine the limits of performance in terms of current density, voltage drop, materials, wear, friction and life.

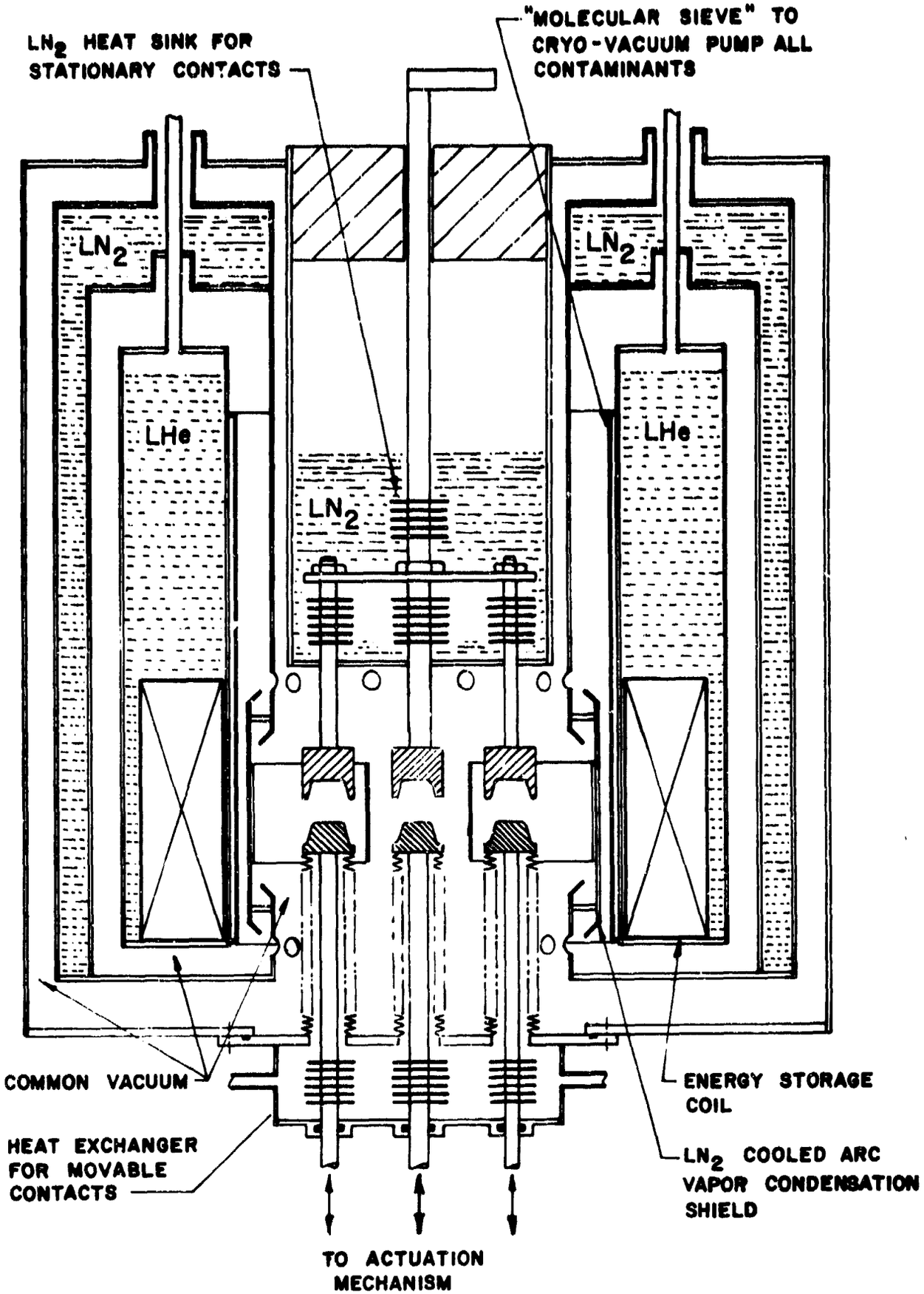

Figure 71. Conceptual sketch of an integrated energy storage coil, linearly actuated switch, and dewar.

FA-1474

b. Rotary Switch

The concept of a rotary device to perform a switching function is particularly promising for future applications because of the potential for achieving high repetition rates. Preliminary results with filamentary brushes indicate that operational current densities may be achieved which will allow compact, lightweight devices to be built.

c. Linearly Actuated Switch

Preliminary estimates indicate that improved performance may be obtained in a linearly actuated vacuum interrupter utilizing cryogenic cooling and an applied magnetic field. Furthermore, operational losses may be substantially reduced if the arc interruption process may be performed on multiple low current arcs in parallel as opposed to a single high current arc (e.g., $\geq$ 20,000 A). A program could be launched using equipment which, for the most part, presently exists. The program would allow the basic effects of cryogenic cooling and applied magnetic field to be evaluated and progress through tests of a single contact unit to the design construction and test of a parallel contact system.

APPENDIX I.

APPLIED MAGNETIC FIELD EFFECTS

Effects which arise due to the interaction of an arc with an applied magnetic field are governed by the Lorentz force:

$$\overline{F} = \overline{J} \times \overline{B}$$

where: $\overline{F}$ = body force per unit volume
$\overline{J}$ = current density
$\overline{B}$ = magnetic flux density

Without loss of generality, the applied field may be projected into components parallel and perpendicular to the arc current and the effect of each considered separately.

The component of applied field which is parallel to the arc yields no effect[2] if the arc is stationary since the "cross" product in the above relationship is zero. If the arc moves in a direction perpendicular to its axis, however, this moving charge constitutes a current which does interract with the axial component of applied field. As shown in Figure 72, the force which results tends to move the arc column in a direction perpendicular to the original motion and to the axial field. This effect arises when the entire arc column moves perpendicular to its axis or when a portion of the arc column moves radially. The latter corresponds to an expanding or contracting column and the net effect of the interaction of an expanding or contracting arc column with an applied field component parallel to the column axis is to initiate rotation.

The component of applied magnetic field which is perpendicular to the arc column interacts directly with the main arc current and causes the arc to move perpendicular to its axis as shown in Figure 73. Figure 74 shows experimentally determined arc velocities plotted as a function of the electrodynamic force per unit length, IB. The data were obtained for arcs in air, but are most likely of the same order for vacuum arcs. As an example, for a current of 2×10^4a and an applied field of 2 W/m^2, the electrodynamic force will be greater than 4×10^4 N/m, hence the velocity may be expected to be 1400 m/sec.

---

[2]This is true in the large scale sense discussed here; the axial field can effect arc stability (e.g.: see O. Morimiya, et. al. "High current Vacuum Arcs Stabilized by Axial Magnetic Fields.") (9)

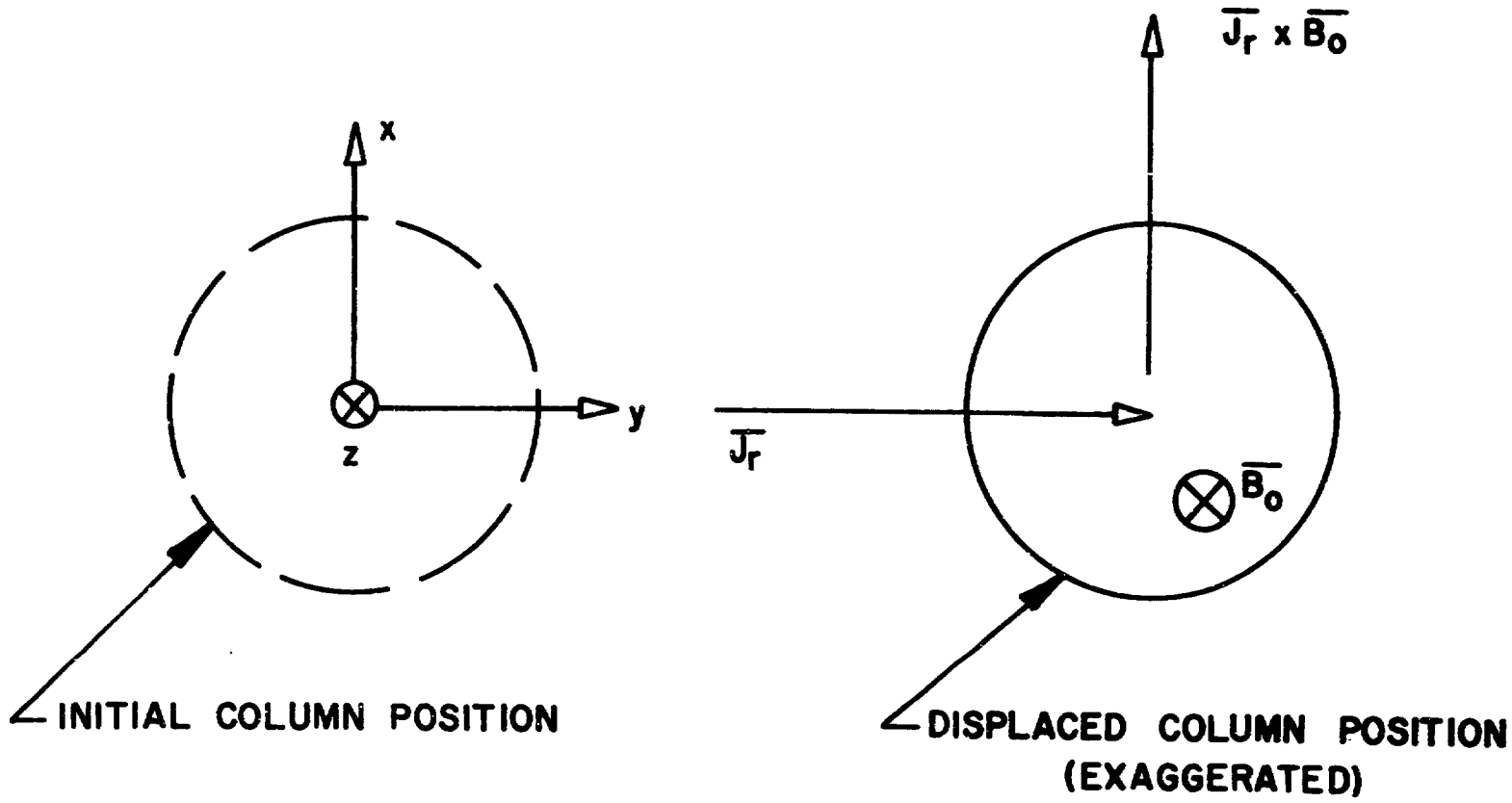

Figure 72. Interaction of a moving arc with a magnetic field parallel to its axis.

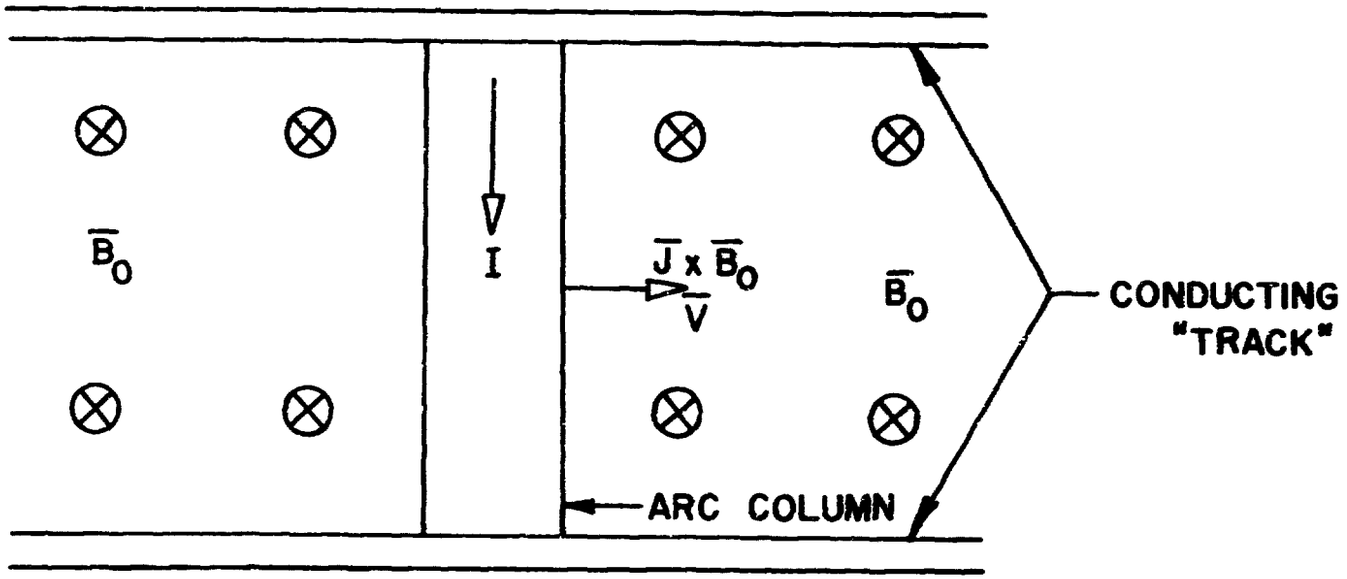

Figure 73. Schematic of arc motion in a transverse applied magnetic field.

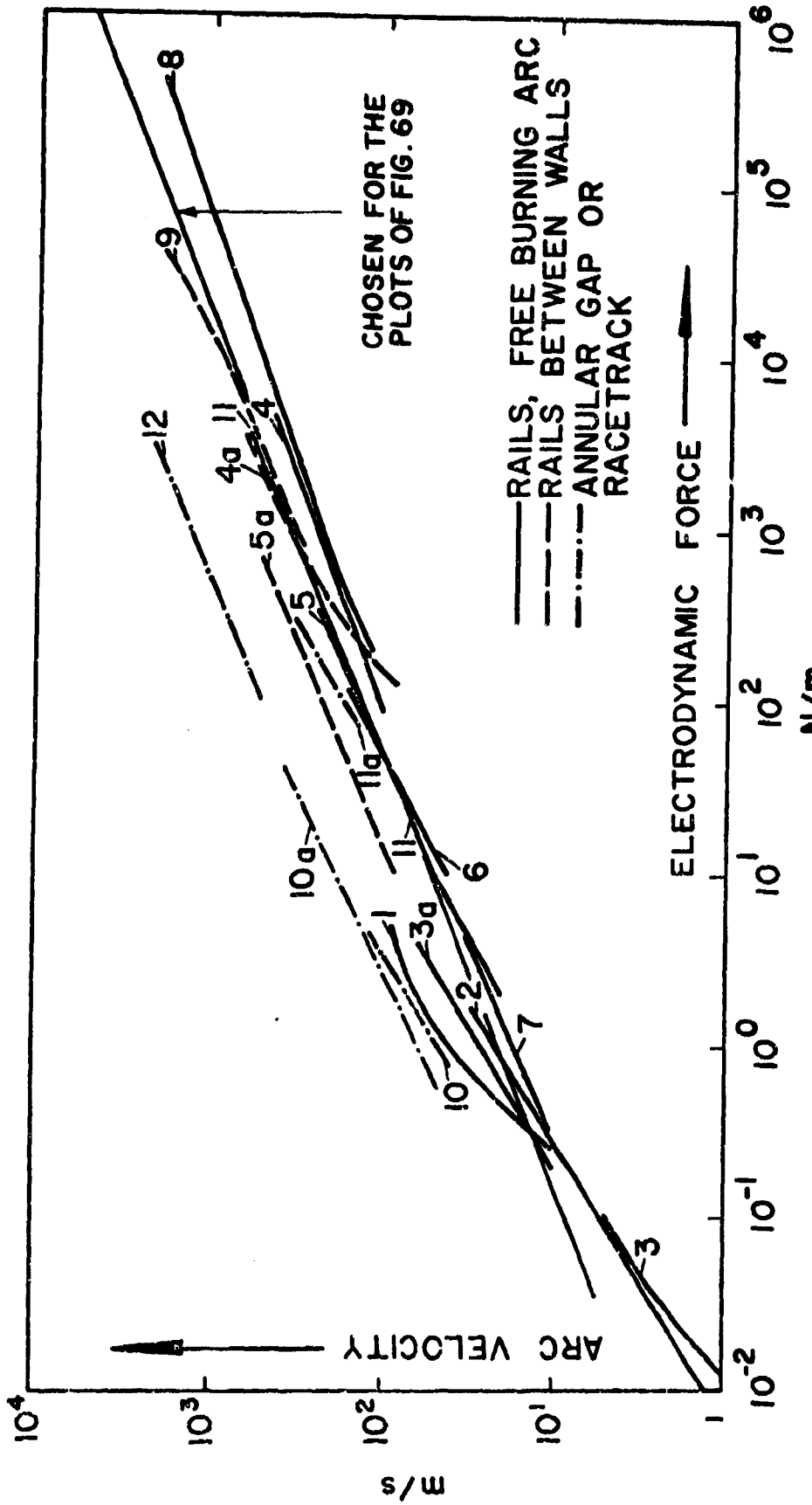

Figure 74. Synopsis of the result of investigation on travelling arcs.(10)

For further clarification, Figure 75 shows the data of Figure 74 plotted in a somewhat different manner: arc velocity (m/sec) versus current (kiloamps) for various values of magnetic flux density (W/m^2). Also included is a scale showing the time required (μ sec) for the arc to travel 10 cm at the average velocity shown. For a current of 2×10^4a and a magnetic flux density of $2W/m^2$, the arc velocity of 1400 m/sec allows 10 cm to be traversed in about 70 μ sec. The magnetic field chosen for this example is a lower limit for the design value of field which may appear in the bore of a solenoidal energy storage system and the indicated speed is also a lower limit if the arc is drawn in vacuum since aerodynamic drag will then be absent. Consequently, higher speeds and, in turn, shorter traversal times may be expected. It should also be noted that the traversal distance of 10 cm was chosen for illustrative purposes only and that shorter distances may suffice in actual application.

The presence of the transverse field as described above helps to extinguish the arc in two ways. First, the motion of the arc in the presence of the field results in a "back emf" which effectively increases the arc resistance. For 2×10^4a and a magnetic flux density of 2 W/m^2, the back emf is of the order of 30 volts for an arc 1 cm long. The second effect arises from the tendency of the transverse field to impede the motion of charged particles parallel to the main axis. The charged particles tend to rotate about the magnetic field lines (assuming no collisions) with a frequency given by $w_c = (qB)/m$ where q is the charge, m is the particle mass and w_c is the so-called cyclotron frequency. From a microscopic standpoint, this shows up as an increase in the arc resistance when the transverse field is present and is shown on Figure 76. As indicated, a transverse field of 2 W/m^2 may be expected to yield a factor of two increase in arc resistance.

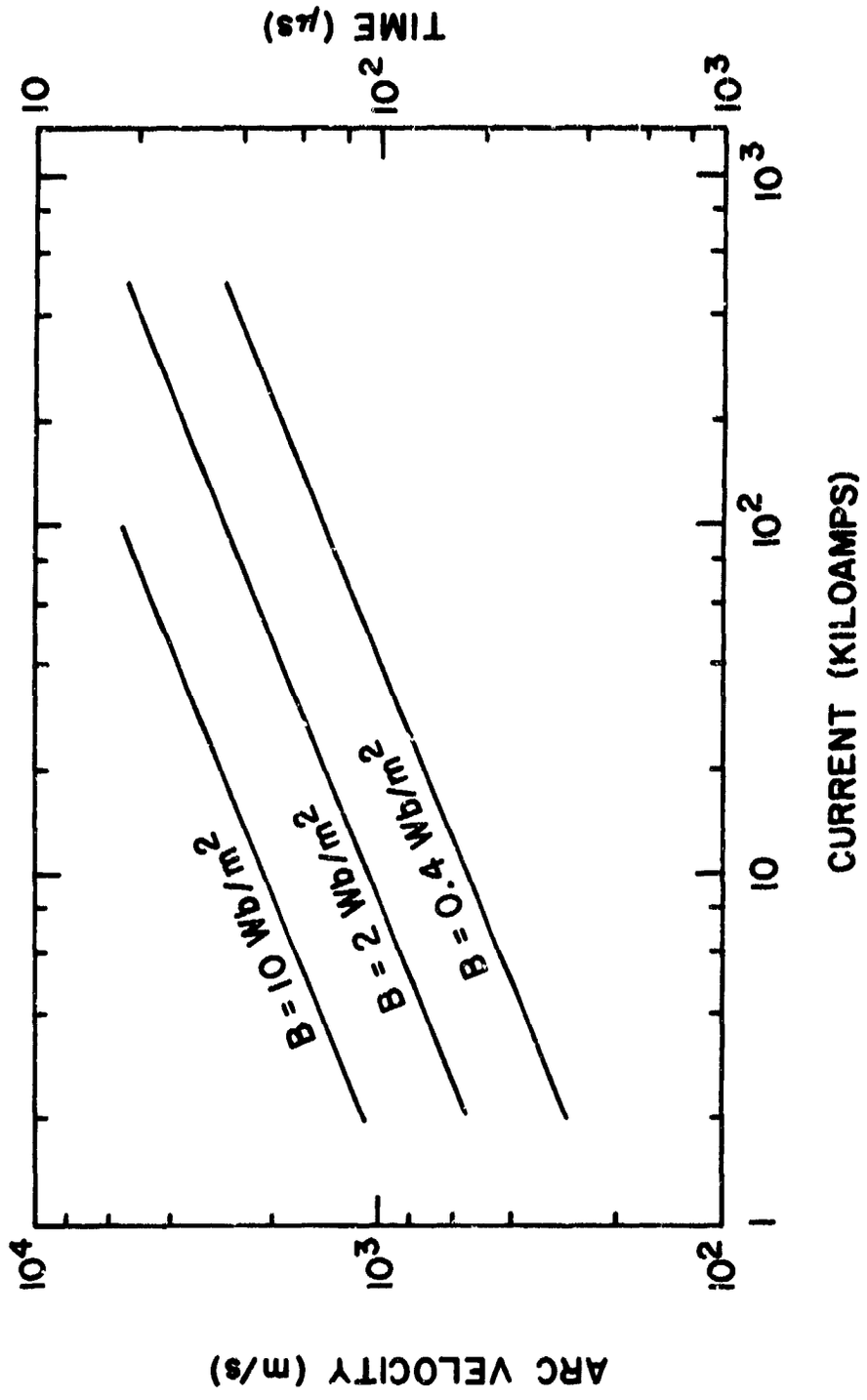

Figure 75. Approximate arc velocity vs. current for various values of flux density. Also shown is the time requried for the arc to travel 10 cm at a particular velocity.

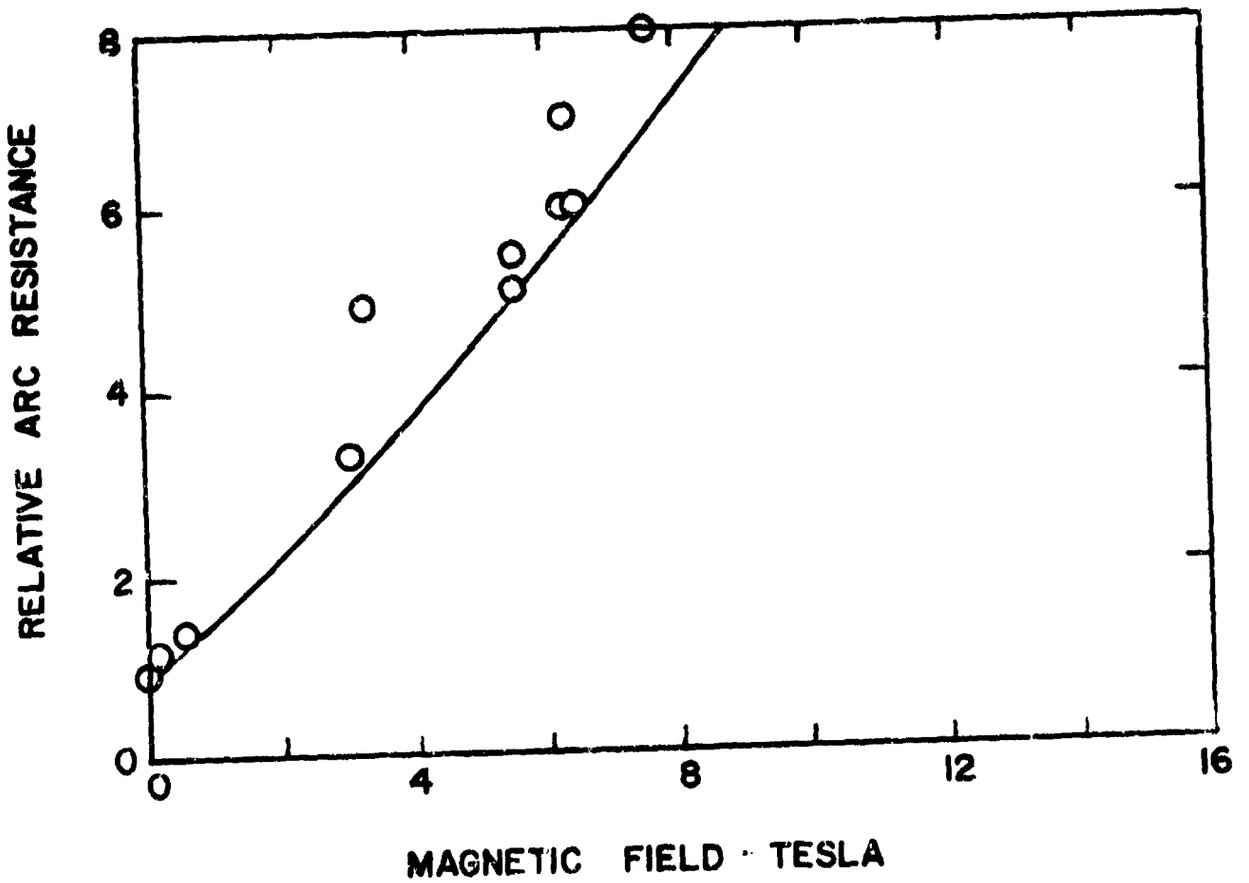

Figure 76. Effect of a transverse magnetic field on arc resistance.

APPENDIX II.

THERMAL ANALYSIS OF A BRUSH FILAMENT

In order to gain insight into the fundamental thermal characteristics of the filamentary brushes, a simplified model was initially chosen for analysis. A single current carrying filament of length ℓ was considered, having a constant resistivity, and constrained to be at a given temperature at each end. The ohmic heat generated within the filament was allowed to escape only by conduction through the filament ends. For the given one dimensional steady state configuration, the governing thermal equation is as follows:

$$d^2T/dx^2 + \rho j^2/k = 0 \qquad (1)$$

where:

T = filament temperature

x = distance from filament end

ρ = filament resistivity

j = filament current density

k = filament thermal conductivity

The above equation may be integrated directly to yield the temperature distribution along the filament. Appropriate boundary conditions (filament end temperatures) may be utilized to evaluate the two integration constants. For the symmetric case of equal end temperatures ($T = T_o$ at $x = 0$ and $x = \ell$), the temperature distribution along the filament is given by the following:

$$T - T_o = (\beta^2/2)\ (x/\ell)\ (1 - x/\ell) \qquad (2)$$

where:

$$\beta^2 = \rho j^2 \ell^2/k \qquad (3)$$

From Equation (2), the location and magnitude of the maximum temperature, T_{max}, may be found to be given by:

$$T_{max} = T_o + \beta^2/8 \quad \text{at} \quad x = \ell/2 \qquad (4)$$

Thus, for this simple case, the maximum filament temperature is directly proportional to the filament resistivity, the square of the filament current density, and the sqaure of the filament length, and inversely proportional to the filament thermal conductivity.

A case very similar to the one discussed above was also analyzed. The same model was used, but with unequal filament end temperatures. That is, the following boundary conditions were chosen: $T = T_o$ at $x = 0$ and $T = T_o + \Delta T$ at $x = \ell$. For this case, the temperature distribution along the filament is given by:

$$T = T_o + (\beta^2/2)\ (x/\ell)\ (1 - x/\ell) + (x/\ell)\Delta T \qquad (5)$$

From the above, it may be determined that the magnitude and location of the maximum temperature are given by:

$$T_{max} = T_o + (\beta^2/8)\ (1 + 2\Delta T/\beta^2)^2$$

$$\text{at}\quad x = (\ell/2)\ (1 + 2\Delta T/\beta^2) \qquad (6)$$

Equations (5) and (6) should be compared with Equations (2) and (4), from which it may be seen that the two cases become identical for $2\Delta T/\beta^2 << 1$.

To carry the analysis a step further, the filament resistivity was allowed to be a function of the local filament temperature; that is, the resistivity was defined as follows:

$$\rho = \rho_o\ [1 + \alpha(T - T_o)] \qquad (7)$$

where ρ_o is the value of the resistivity at a temperature $T = T_o$, and α is the temperature coefficient of resistance. Inserting the above into Equation (1) leads to the following expression for the temperature distribution:

$$d^2T/dx^2 + a^2T + b^2 = 0 \qquad (8)$$

where:

$$a^2 = (\beta^2/\ell^2)\alpha$$

and $$b^2 = (\beta^2/\ell^2)\ (1 - \alpha T_o)$$

where β^2 has been slightly redefined by replacing the ρ in Equation (3) by ρ_o. Using Laplace Transform techniques leads to the following solution: In the "s" domain,

$$T(s) = (sT_o + T_o' - b^2/s)\ /\ (s^2 + a^2) \qquad (9)$$

where T_o is defined as the value of T at $x = 0$, and T_o' is defined as the value of dT/dx at $x = 0$.

Inverting Equation (9) leads to the following solution in real space:

$$T(x) = T_o + (T_o'/a) \sin(ax) - (1 - \cos(ax)) / \alpha \qquad (10)$$

Choosing the boundary conditions allows T_o' to be evaluated. As was stated above, $T = T_o$ at $x = 0$, as may be seen from Equation (10). Choosing the symmetric case of $T = T_o$ at $x = \ell$ leads to the following expression for T_o':

$$T_o' = (a/\alpha) \left[\frac{1 - \cos(a\ell)}{\sin(a\ell)}\right] \qquad (11)$$

Inserting this into Equation (10) yields the following explicit solution for the steady state temperature distribution of a filament which has a temperature dependent resistivity:

$$T(x) = T_o + \left[\frac{1 - \cos(a\ell)}{\alpha \sin(a\ell)}\right] \sin(ax) - (1 - \cos(ax)) / \alpha \qquad (12)$$

Using trigonometric identities, it may be shown that the maximum temperature occurs at a position midway between the filament ends, as would be expected from the symmetry of the problem. That is $T = T_{max}$ at $x = \ell/2$. Substituting this into Equation (12) and simplifying leads to the following expression for the maximum filament temperature:

$$T_{max} = T_o + (1/\alpha) \left[\frac{1}{\cos(a\ell/2)} - 1\right] \qquad (13)$$

A comparison of Equations (4) and (13) is useful. It can be shown that, in the limit of small α, Equation (13) reduces to the following:

$$T_{max} = T_o + (\beta^2/8) (1 + 5\alpha\beta^2/48 + 61\ \alpha^2\beta^4/5760 + \ldots) \qquad (14)$$

Therefore, for $\alpha = 0$, the two expressions are identical, which would be expected from the form of Equation (7).

Using the fact that $a\ell = \beta\sqrt{\alpha}$, it may be seen that the maximum filament temperature as given by Equation (13) is only a function of α, β, and T_o. Further, the maximum filament temperature rise above the the temperature, $T_{max} - T_o$, is dependent only upon α and β. A plot of $T_{max} - T_o$ as a function of β^2 for various values of α is given in Figure 77. A useful comparison of Equations (4) and (13) may be obtained by normalizing the maximum temperature rise given in Equation (13) to $\beta^2/8$. This has been done in Figure 78 in which the normalized maximum temperature has been plotted as a function of β^2 for various values of α. As shown in the figure, the normalized maximum temperature approaches one as α approaches zero. In addition, as can be seen

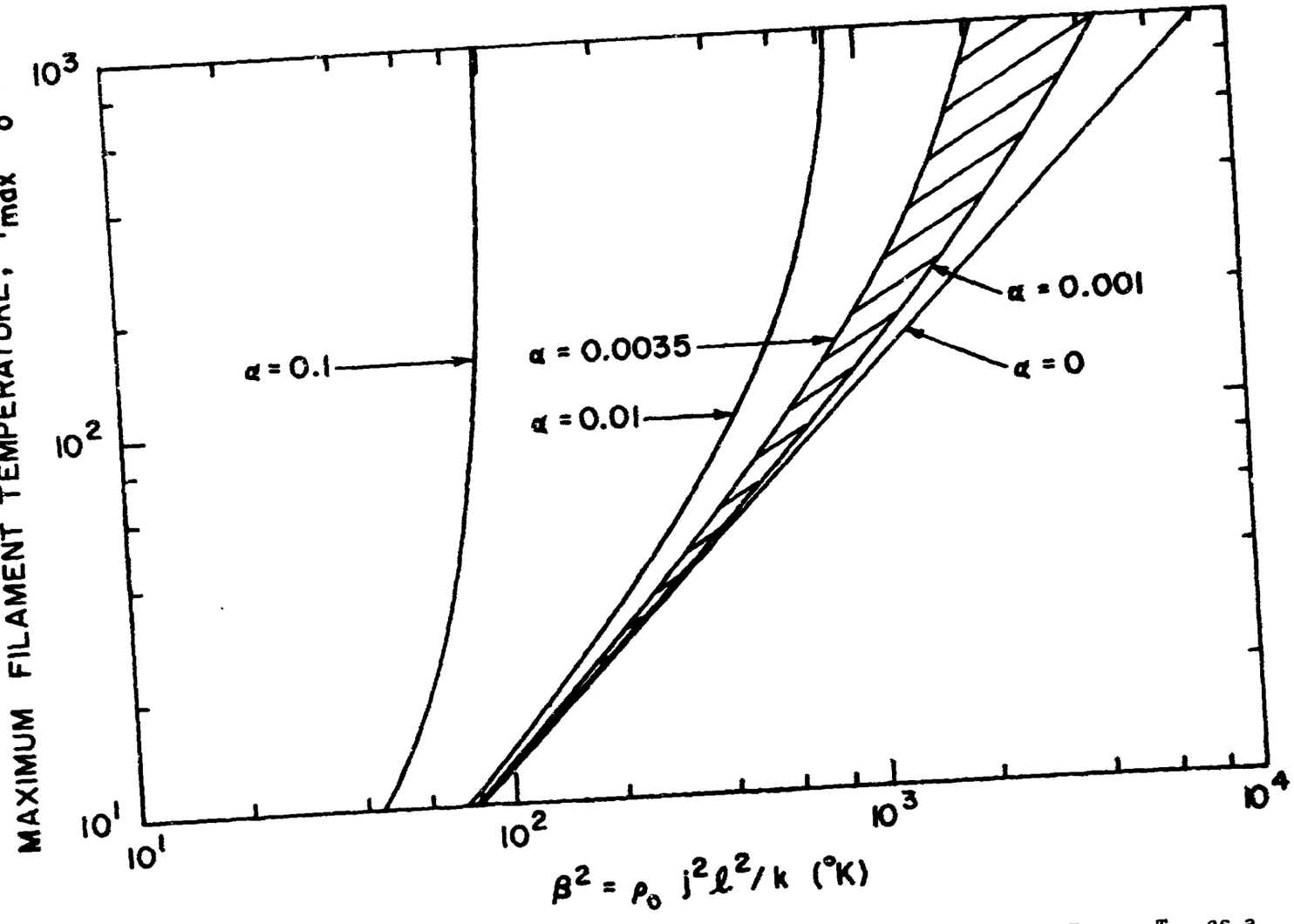

Figure 77. Maximum filament temperature rise above the end temperature, $T_{max} - T_o$, as a function of β^2 for various values of α. The cross hatched area represents typical values of α for the brushes under consideration.

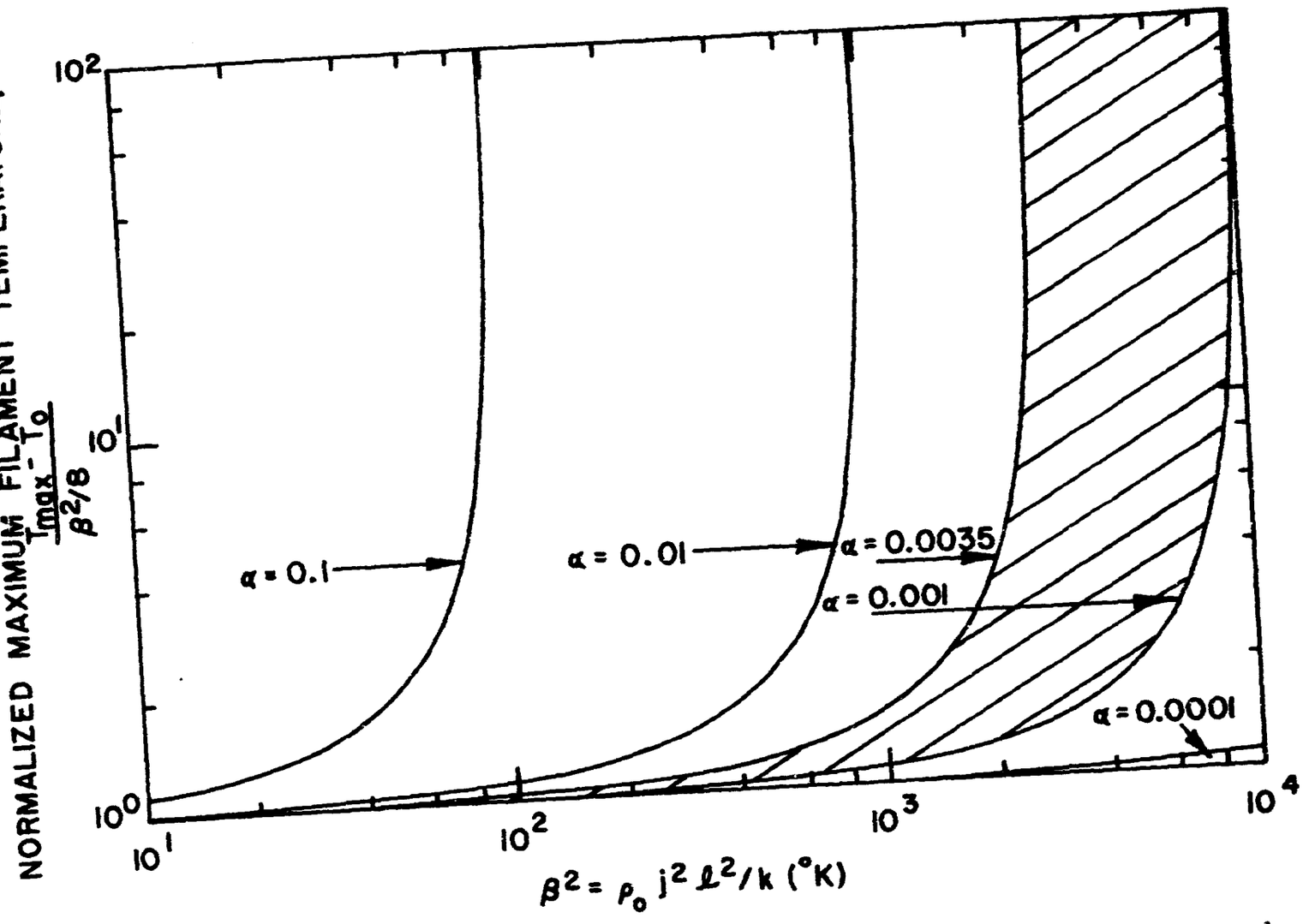

Figure 78. Maximum filament temperature rise above the end temperature, $T_{max} - T_o$, normalized to its value for $\alpha = 0$, as a function of β^2 for various values of α. The cross-hatched area represents typical values for α for the brushes under consideration.

from Equation (13), the maximum temperature becomes infinite for values of $a\ell = \pi = \beta\sqrt{\alpha}$. Thus for a given α, there is a maximum value of β for which the temperature remains finite. Typical values of α for the brushes now under investigation run from approximately 0.0035 to 0.001 K^{-1} for reference temperatures from 300 to 700 K.

The effects of a nonzero α on the shape of the temperature distribution along the filament is also of interest. Figure 79 is a plot of the temperature distribution for a fixed β and various values of α, as given in Equation (12). Because of the symmetry of the distribution about the filament center, only half was plotted. As can be seen from Equation (2), for $\alpha = 0$, the distribution is parabolic. For α small, the deviation from a parabolic shape is not obvious, as shown in Figure 79. In order to accentuate the effects of a nonzero α on the distribution, Figure 80 was generated, in which $\alpha = 0$ and $\alpha = 0.01$ were chosen with a fixed β, and the distributions normalized to their respective maxima. For values of α between 0 and 0.01, the normalized distribution would lie between the two curves shown. Hence, the effects of a nonzero α on the filament temperature distribution are small.

For completeness, the results for the following case will also be included: Unequal filament end temperatures and a temperature dependent resistivity. That is, $T = T_o$ at $x = 0$, $T = T_o + \Delta T$ at $x = \ell$, and $\rho = \rho(T)$ as given by Equation (7). The solution for this case proceeds as in the previous case. The temperature distribution is given by:

$$T(x) = T_o + \left[\Delta T + (1/\alpha)\ (1 - \cos(a\ell))\right]\ \frac{\sin(ax)}{\sin(a\ell)} - (1 - \cos(ax))\ /\ \alpha \tag{15}$$

The maximum temperature is given by:

$$T_{max} = T_o + (1/\alpha)\ \left[\frac{1}{\cos(ax)} - 1\right] \tag{16}$$

where:

$$x = (1/a)\ \arctan\left[\tan(a\ell/2) + \alpha\Delta T/\sin(a\ell)\right] \tag{17}$$

gives the location of the maximum temperature. For $\Delta T = 0$, it can be seen that Equations (15) and (16) reduce identically to Equations (12) and (13), since Equation (17) reduces to $x = \ell/2$. In addition, it may be shown that, in the limit of small α, Equations (15), (16), and (17) reduce identically to Equations (5) and (6).

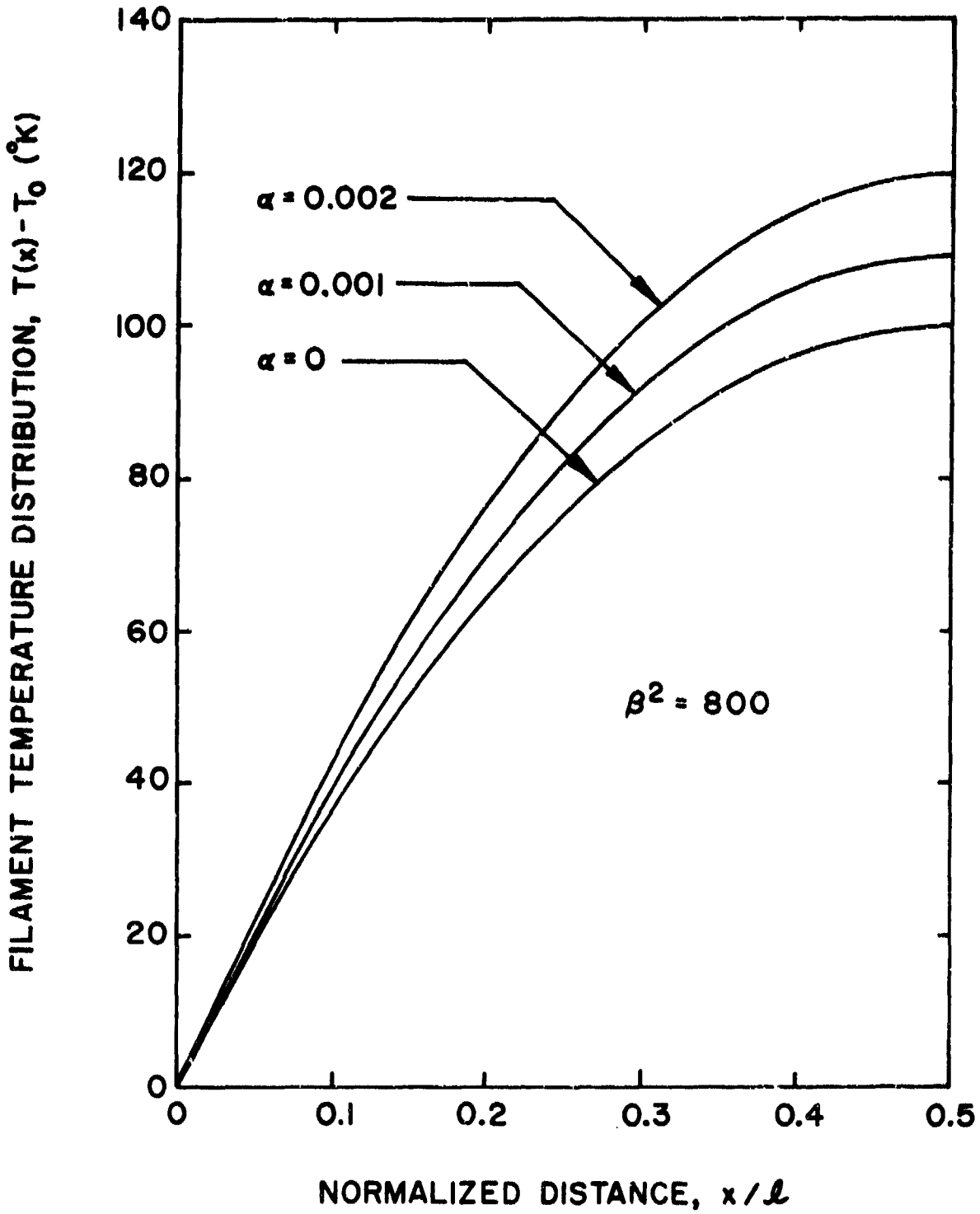

Figure 79. Filament temperature distribution as a function of the normalized distance from the filament end for a fixed value of β and various values of α.

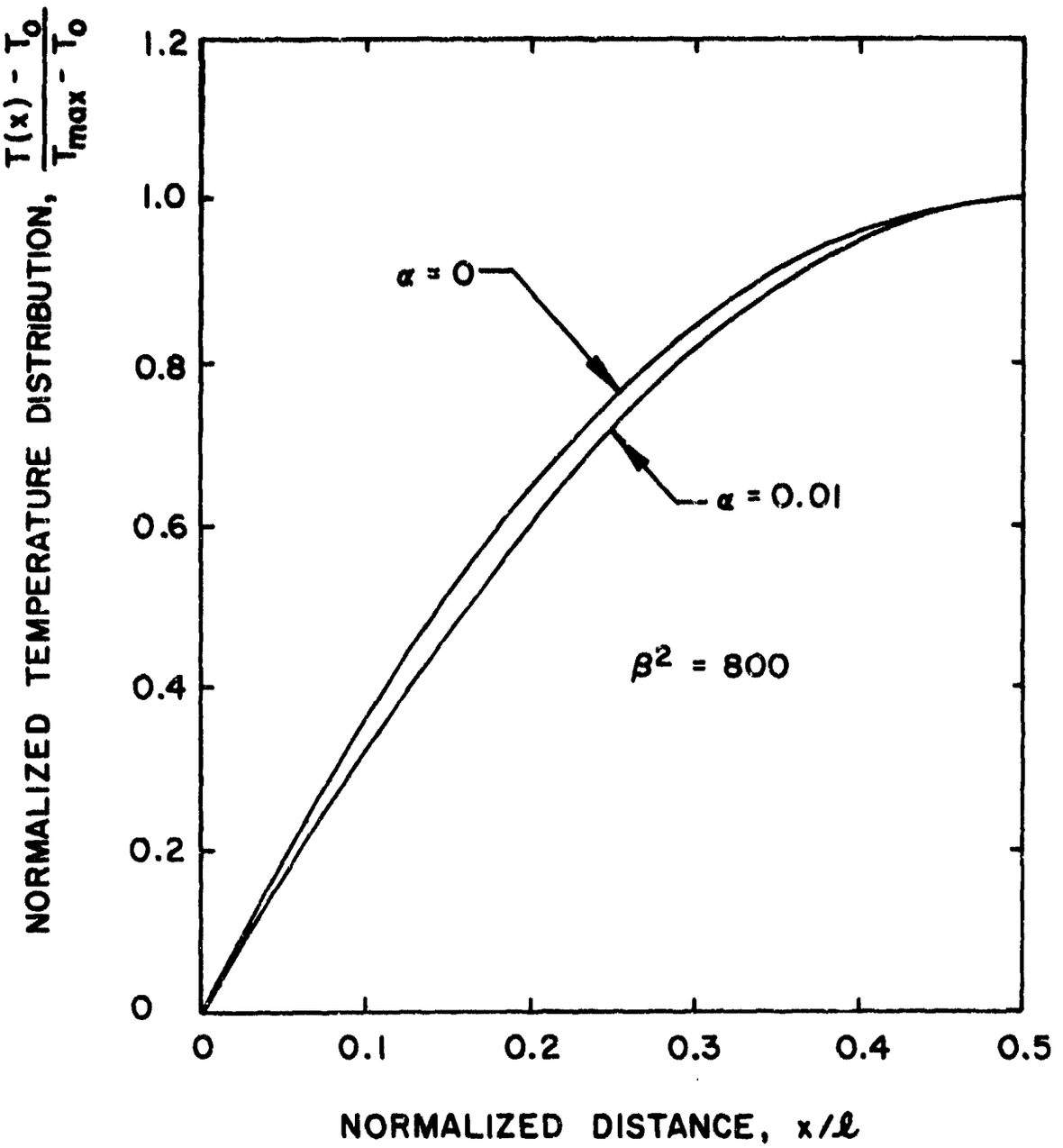

Figure 80. Normalized filament temperature distribution as a function of normalized distance for a fixed value of β and various values of α. Each of the temperature distributions is normalized to its maximum value.

LIST OF REFERENCES

(1) Ross, H. C., "Switching in High Vacuum Environment," I.E.E.E. Trans. on Component Parts, Dec. 1963, p. 155.

(2) Powers, R. J., and Chambers, R. M., "A Clean Cryo-Vacuum System with High Pumping Speeds for All Gas Species," J. of Vac. Sci. & Tech., Vol. 8, No. 1, p. 319.

(3) Stern & Grenier, J. Vac. Sci. & Tech., Vol. 3, No. 6, 1966.

(4) Caldwell, et al, J. Vac. Sci. & Tech., Vol. 2, 1965.

(5) M. P. Reece, "The Vacuum Switch," part 1: Properties of the Vacuum Arc, Proc. IEE, Vol. 110, No. 4, 1963, p. 793.

(6) Carslaw & Jaeger, Conduction of Heat in Solids, Oxford Press, 2nd ed., 1959, p. 269.

(7) Bowden, F. P. & Tabor, D., The Friction & Lubrication of Solids, I., Clarendon Press, 1950.

(8) Holm, R., Electrical Contacts Handbook, Springer-Verlag, 1958.

(9) Morimiya, et. al., "High Current Vacuum Arcs Stabilized by Axial Magnetic Fields," I.E.E.E. PES Winter Meeting, Jan. 1973.

(10) Leber, R., "Arcs in Magnetic Fields," Plasma Arcs and Switching Phenomena, U. of Wisconsin, July 1971.